

**Assessment of PGA Coated Polyimide Microelectrodes as a
Flexible, Implantable Neural Interface for CNS**

BY

DEVANG GANDHI

Bachelor of Science, Electrical Engineering,
Purdue University, West Lafayette, IN USA 1999

THESIS

Submitted as partial fulfillment of requirements
for the degree of Doctor of Philosophy in Bioengineering
in the Graduate College of the
University of Illinois at Chicago, 2012

Chicago, Illinois

Defense Committee:

Patrick J. Rousche, Chair and Advisor
Christos G. Takoudis, Bioengineering, Chemical Engineering
Richard Gemeinhart, Pharmaceuticals
David Wirtshafter, Psychology
David M. Schneeweis, Northwestern University (NUIN)

I dedicate this thesis to Masti Group, our drive to fight against Cancer, to our beloved friend Analp Reshamwala and my sister Payal Pandya.

ACKNOWLEDGEMENT

The author thanks Dr. Patrick Rousche, Dr. Laxman Saggere, Dr. Christos Takoudis, Dr. Winnie Jensen, Dr. Ryan Clament, Ronnie Das, and Hananeh Esmailbeigi for their insightful help in resolving experimentation issues. The author would also like to acknowledge NCF and their staff. The author would like to thank Dr. Terri Chiganos for countless hours of aid during animal surgical procedure.

The author would like to extend his gratitude to the members of the preliminary defense committee Dr. Patrick Rousche, Dr. John Hetling, Dr. Winnie Jensen, Dr. Christos Takoudis, and Dr. David Schneeweis for their insightful advice, and the Thesis defense committee Dr. Patrick Rousche, Dr. Richard Gemeinhart, Dr. Christos Takoudis, Dr. David Schneeweis and Dr. David Wirtshafter for their time and commitment.

Last but not list the author would like to thank Dr. Monika Patel D.O., his best friend Nimisha Salaria, and his family for providing moral support. Lastly, thanks to undergraduate students Ariba Chowdhury, Katie Harrigan and Betty Yang for their assistance with experimentation.

Table of Contents

Chapter 1. Introduction	1
1.1 Background.....	1
1.2 Anatomy and structure of the Human Brain	1
1.3 Functional anatomy of a neuron.....	5
1.4 Studying the Brain.....	6
1.5 Microelectrodes.....	8
Chapter 2. Research Design	24
2.1 Polyimide (PI).....	24
2.2 Poly (glycolic acid) (PGA)	26
2.3 Specific Aims	30
Chapter 3. Methods	32
3.1 Manufacturing and Lithography Protocols.....	32
3.2 PGA Surface coating.....	36
3.3 Electrochemical Analysis	41
3.4.2 Modified Surgical procedure for Survival surgeries.....	44
3.4.3 Euthanasia.....	46
3.4.4 Histology	47
3.4.5 Recording Protocol	51
Chapter 4. Results.....	55
4.1 Manufacturing	55
4.1.1 Autocad.....	55
4.1.2 Mask Processing	58
4.1.3 Lithography.....	61
4.2 Implantation Technique: PGA Surface coating	71
4.3 Electrochemical Analysis	76
4.3.1 Cyclic Voltammetry	76
4.3.2 Electrode Impedence Spectroscopy	83
4.3.3 In-Vivo Electrochemical Analysis	87
4.4 Acute Animal Studies	87
4.4.1 Acute animal Recordings	87
4.4.2 Histology	100
Chapter 5. Discussion.....	110
Reference List.....	117
Appendix A	122
Appendix B	124
Appendix C	126

List of Tables

Table 1: Neural Interface Designs for the CNS. (3, 14, 22-27).....	25
Table 2: Material properties used to construct the model in Ansys.	68

List of Figures

Figure 1: Depicting neuroprosthetic application, showing information exchange between control unit and sensory or cortex interfacial tissue.....	2
Figure 2: (a) Scanning Electron Micrograph of the cranial meninges of a dog. (b) Schemetic diagram of a neuron showing the cell body on the left surrounded by its dendritic harbor, showing several input synaptic terminals. The arrows indicate the direction of signal/information conduction. The longer extension from the cell body extending rightward towards another cell body is the schematic representation of an axon covered with myelination sheath. The action potential is initiated at the based of the axon on the cell body and travels down the axon towards the axon terminal. Once the action potential reaches the terminal local graded potentials are induces at each of its output synaptic terminals. (Nolte, J. 1988).....	4
Figure 3: (a) Utah Intracortical Electrode Array. 100 electrodes array made using photolithography and etching technique on to a Silicon substrate (b) Explanted array with moderate encapsulation (thickness about 250 mm). (Rousche & Norman 1999)	14
Figure 4: Silicon based three shank 12-site recording probe developed at Michigan (Wise et al. 2004)	16
Figure 5: A six-site, three-shaft device with an “S”-curve for strain relief engineered directly into the cable (scale bar lower left = 1.5 mm.) (Rousche et al. 2001).....	19
Figure 6: 3D flexible probe array after folding. The recording pads are vertically aligned. (Suzuki et al. 2003)	22
Figure 7: (a) An imide group is composed of nitrogen bound with two C-O pairs and R group. (b) The crosslink between the nitrogen atoms forms the polyimide chain.	27
Figure 8: a) AutoCAD layout of 16 devices that can be produced during a single batch processing. b) Enlarged two shaft device C) Dimensions of a two-shaft device showing 40um x 40um contact sites, 10um wide trace lines and two shafts measuring 156um.	33
Figure 9: Schematic of the steps involved in the fabrication process. Process starts with bare silicon wafer (top left row) and ends with lifted devices (bottom right row).....	34
Figure 10: Two shaft device-connector assembly successfully manufactured and a close up view showing ‘ground’ shaft and electrode site shaft.....	37

Figure 11: Illustration of back coating of PGA on a Polyimide device. The contact site is left uncovered.	38
Figure 12: Displacement force measurement setup to measure the peak force withstood by the device before buckling.	40
Figure 13: Three lead electrochemical test setup.	42
Figure 14: A craniotomy exposing left auditory cortex, indicated by a red circle. Two shafts electrode is resting on the surface before insertion, indicated by black arrow. Red box indicates the four working contact sites.	45
Figure 15: A Typical layout of implants done during histology studies. (I) marks the sites of injury where a device was implanted and then removed. (PI) marks the sites where polyimide devices were implanted. (X) marks the sites where test devices, Polyimide or PGA coated devices, were implanted.	48
Figure 16: Outline of steps performed to compute cell densities. (a) Original picture capture under microscope. (b) Red filtered, high contrast image. (c) Image displaying detected cells, cell count displayed in the title. (d) Image displaying cell density, mean cell density displayed in the title.	50
Figure 17: (a) Mean GFAP expressions (grey levels) are computed from the grey scale image of a GFAP stained tissue section and plotted along the x-axis. Darker regions in the image correspond to higher GFAP staining and therefore higher glial fiber expression. The peaks in the grey scale profile correspond to the darker grey regions. (b) Peak GFAP expression is computed as peak deviation from the base line and GFAP expression width is computed as the distance from the onset of deviation from the baseline to the Peak GFAP expression. The orange boxes represent the device location.	52
Figure 18: TDT recording setup used for electrophysiological recording (a). Typical PSTH generated using NEX software (b). Sample unit activity recorded and displayed by TDT (inset).	54
Figure 19: AutoCAD design of the masks manufactured in NCF facility. (a-b) Close up of shafts and connector modules. (c-d) AutoCAD models of a two shaft devices with and without top polyimide layer.	56
Figure 20: Processed polyimide layers masks. (a) Electrode tip patterned incorrectly. (b) Electrode tip, angular tip design was chosen to induce maximum pressure at the point of insertion. (c) Polyimide layer 1 for two shaft devices. (d) Polyimide layer 2 for two shaft devices. (e) Measurement of 40x40um via and contact site openings. (f) Multishaft device, polyimide layer 2.	59

Figure 21: Processed metal layer masks. (a) 20x20 um contact site. (b) 40x40 um contact site. (c) Three shafts contact array with local reference in the bottom shaft. (d) Typical mask alignment markers. (e) Traces near connector pads. (f) Traces connecting contact sites to stem traces.	60
Figure 22: Issues encountered during device processing (a) Miss aligned polyimide layers due to improper alignment markers (b) Metal fails to etch uniformly, especially between traces as seen in (c). (d) Traces fail to adhere to polyimide surface. (e) Traces peel off near corners. (f) Traces disappears near via due to shadowing effect.....	Error! Bookmark not defined.
Figure 23: Metal traces reproduced on wafer and sheet of PI surfaces. (a) Traces reproduced on wafer itself. (b-d) Metal traces reproduced on polyimide sheets after pre-curing, polyimide.....	64
Figure 24: a) Typical profile of layers 1 and 2 (super imposed graphically) of the patterned polyimide shaft. b) Optical profile of a shaft surface shows the curvature of the first layer of a device. c) Surface profile through a contact site. d) Optical profile around vias.....	65
Figure 25: Temperature profile across the cross sectional view of first layer of a polyimide device (polyimide layer is outlined with white rectangular box in the center of the image) resting on 1mm thick silicon wafer. The 95°C heat temperature source was applied to the base of the silicon wafer. The temperature across the cross section shows similar but inverted profile in comparison to the measured surface profiles. Scale-bar range is from 0°C to 95°C. (a) Heat profile at 0.4sec after the onset of the heat source. Temperature displayed in the image is between 5°C and 15°C. (b) Heat profile at 2.6sec after the onset of the heat source. Temperature displayed in the image is between 65°C and 75°C.	67
Figure 26: (a) A device in comparison to a penny. (b) Two shaft polyimide device, similar to the ones used in histology studies. (c) Tip of a shaft, the first layer of a device. (d) Via in the first layer of the polyimide device. (e) First layer of a four shaft device. (f) A shaft of two shaft device measuring 145um wide.	69
Figure 27: a) A complete two shafts device. b) Four contact sites interspaced with via (image digitally stitched). c) Metal traces leading to the connector pad. d) A close up of a 40x40um contact site.	70
Figure 28 (a-b): a) Mean line widths along the shaft of devices respective of their location (n=16). b) Mean line width across the stem connecting the electrodes to the connector respective of their location (n=16).....	72-72
Figure 28 (c-d): a) Mean line widths along the shaft of devices respective of their location (n=16). b) Mean line width across the stem connecting the electrodes to the connector respective of their location (n=16).....	72-72

Figure 29: (a) PGA coated final device compared with US nickel (left). Uncoated device (center). Close up of the coated fork (right). (b) Uncoated device showing exposed contact sites (left). PGA Coated device showing exposed contact sites. You can also see air bubbles within the PGA coating.....	74
Figure 30: (a) A SEM image of a typical single sided coat of the device along the fork length. (b) Close up view of the tip of the device showing backslash coat of the tip. (c) Close up view of the shaft showing exposed contact sites and vias with back coated PGA seen in between two fork shafts. (d) Another sample of the exposed contact sites and vias.....	77
Figure 31: (a) Typical force relaxation curves obtain by displacing the device 1mm perpendicular to weighing surface. (b) Peak forces generated for the coated and uncoated polyimide devices PGA coated devices produce 10 times larger peak forces then uncoated devices. Re-coating PGA restores the mechanical strength by 50% of the original. (n=28, no coating; n=15, 1 st coat; n=25, recoat).....	78
Figure 32: Percent Degradation of 1mmx1mmx1mm cubes of PGA over the period of 7 days	79
Figure 33: (a) pH change of a 1mm x 1mm x 1mm PGA in PBS solution over the period of 7 days, measured once daily. (b) pH changes of PGA coated devices in PBS over the period of 6 hours. The PBS saline was changed after each measurement to simulate perfusion.	80
Figure 34: 10 scans of cyclic voltammetry performed on (a) Site 01 (b) Site 02 (c) Site 03 (d) Site 04 (e) Ground Strip (f) Dummy Site of a polyimide device	81
Figure 35: Comparison of CV performed on a dummy site of a device from previous figure (a) and a device without metal traces (b)	84
Figure 36: Comparative mean (10 scans each) CV plots of Gold wire (green) and a PI device site (blue). The CV curve for the device is left shifted as compared to the gold	85
Figure 37: Nyquist and Bode plots of four different sites on four individual devices.	86
Figure 38: Bode plots showing comparison between gold wire and a site on a PI device. The wires lower impedance was to its larger surface area.	88
Figure 39 (a-b): Slight increase in impedance was observed for all the channels for In-Vivo measurements. Also, an increase in phase angle near DC and decrease in phase angle near as was observed for all the channels. (a) Site 01 (b) Site 02: no in-vivo signal was recorded	89-88

Figure 39 (c-d): Slight increase in impedance was observed for all the channels for In-Vivo measurements. Also, an increase in phase angle near DC and decrease in phase angle near as was observed for all the channels. (a) Site 01 (b) Site 02: no in-vivo signal was recorded	89-88
Figure 40: Mean CV curves for (a) Site 01 (b) Site 03 (c) Site 04 prior to implant (Green), during implant (Red) and post implant (Blue)	91
Figure 41: For site 02 five scans of CV were performed prior to implant (a), site 2 provided no signal during implant. During 3 rd scan of the five scans post implant site to started to measure signal again (b) and five more scans were performed to verify the CV (c).....	92
Figure 42: Typical signals recorded from the cortex using the PI devices. Traces from three of the channels recorded simultaneously is shown in the middle frame, the third channel is enlarged in the top frame. The bottom two frames show typical capture action potentials.	93
Figure 43: (a) Raster plots of a channel shown in figure 29. (b) PSTH of the same channel, with 99% confidence interval indicated by green lines.	95
Figure 44: Baseline recording performed simultaneously on four individual channels of a two shaft device.....	96
Figure 45: PSTHs generated using click stimuli present over a period of 40min.	97
Figure 46: PSTHs vs. time of the same signal as in figure 32, indicates a stable interface.....	98
Figure 47: Similar study performed on another animal to establish short term interface stability, here the animal had suffered sever blood loss during surgery.....	99
Figure 48: PSTHs vs. amplitude plot, showing increase in response with increase in stimulus amplitude. Frequency was fixed at 2 Khz.	101
Figure 49: PSTHs vs. frequencies shows that strongest responses were recorded for stimuli with frequencies between 1 Khz to 3 Khz. Amplitude was fixed at 100db.....	102
Figure 50: Comparative results of healthy tissue with implanted tissue. 248 cells were computed in healthy tissue and 217 cells were computed in the implanted tissue. (a and b) Original images capture under microscope. (c and d) Cell densities with mean cell densities displayed in respective titles	104
Figure 51 (a-d): H&E stained images of the tissue and the implant sectioned at various depths keeping the implanted device (orange) in place and	

preserving the device-tissue interface. (a-d) Uncoated polyimide devices show minimal encapsulation and cell density variation. 105-104

Figure 51 (e-h): H&E stained images of the tissue and the implant sectioned at various depths keeping the implanted device (orange) in place and preserving the device-tissue interface. (a-d) Uncoated polyimide devices show minimal encapsulation and cell density variation. 105-104

Figure 52 (a-d): GFAP stained images of the tissue and the implant sectioned at various depths keeping the implanted device (orange) in place preserving the device-tissue interface. (a-d) Uncoated polyimide devices show minimal encapsulation and cell density variation. 107-106

Figure 52 (e-h): GFAP stained images of the tissue and the implant sectioned at various depths keeping the implanted device (orange) in place preserving the device-tissue interface. (a-d) Uncoated polyimide devices show minimal encapsulation and cell density variation. 107-106

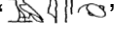
Figure 53: GFAP stains appear as darker gray levels in the black and white images. Peak gray intensity near the implant edge is taken and the intensity and width is computed across the samples (n=5). (a) Peak GFAP levels. (b) Distance from the implant edge to the approximated smallest increase from the mean GFAP expression. 109

ABSTRACT

Neuroprosthetic devices have been suggested as part of a Brain Machine Interface (BMI) intended to restore functionality in humans affected with various sensory or motor function losses. The longevity of such implantable devices is increasingly becoming a limiting factor in successfully developing and delivering neuroprosthetic systems suitable for clinical use. One factor implicated in the long-term failure of implanted devices is the relative rigidity of the devices with respect to the softer mechanical property of the human brain. To alleviate these concerns, polymer-based devices have been suggested as an alternative to more traditional, silicon-based micromachined devices. The objective of this research is to develop such polyimide based electrode array suitable for the specific application of restoring hearing in deaf patients. The work on the manufacturing, electrochemical evaluation, acute animal recording and implantation techniques of the polyimide-based flexible recording electrodes, designed for rat auditory cortex, is discussed. Specifically, application of poly (glycolic acid) (PGA) to temporarily enhance the device stiffness of the flexible polyimide devices is discussed in the scope of the thesis. The temporary enhancement of the device stiffness is to minimize the brain damage during the insertion of the device into the brain.

CHAPTER 1.INTRODUCTION

1.1 BACKGROUND

The hieroglyphic symbols ‘’ represent the earliest known reference to the brain (1). Written during the 17th century B.C., a body of Egyptian records, known as “The Edwin Smith Surgical Papyrus,” describes the treatment of two patients with multiple skull fracture referencing the brain eight times. Since then our understanding of the brain has increased tremendously. Figure 1 illustrates the next frontier of our understanding of the brain and our attempts to communicate with it. These communication channels, with different functional and physical parts of the brain, are called Brain Machine Interfaces (BMI). One such BMI application is considered in this thesis. The premise of this thesis is to design and characterize implantable microelectrode-brain interface for application of auditory prosthesis based on our current, functional and anatomical understanding of the brain.

1.2 ANATOMY AND STRUCTURE OF THE HUMAN BRAIN

The brain consists of the left and right hemispheres, each of which can be further divided by anatomical distinction. The main anatomical regions include the frontal, parietal, occipital and temporal lobes. Although functionally distinct, the hemispheres remain connected by a central concentration of axonal tracts called corpus callosum, allowing for information exchange and coordination between corresponding contralateral regions. The parenchyma of the brain is grossly classified as white or gray matter, according to the relative concentration of axons versus dendrites/cell bodies. White and gray matter can be easily distinguished by gross examination of coronal brain



Figure 1: Depicting neuroprosthetic application, showing information exchange between control unit and sensory or cortex interfacing tissue.

slices as well as histological examination of cell content. The white matter is composed of fibers called axons leading away from the neuron cell bodies. The characteristic white color comes from the adipose-laden myelin sheaths encompassing the axons, forming an electric insulation that allows for rapid conduction with minimal energy expenditure. In contrast, gray matter is composed of the cell bodies called somas. The outermost region of the brain comprised of six highly ordered gray matter layers called cerebral cortex. The cortical surface is protected by three layers of tissue called meninges. From the cortical surface outward, the meninges are comprised of the delicate pia mater, the highly vascular arachnoid membrane, and the relatively thick dura mater. The pia mater is attached directly to the cortical surface and follows the multiple involutions characteristic of the adult cortex. Beyond the pia, the arachnoid and arachnoid trabecula (inner arachnoid layer attached to pia mater) delineates a potential space known as the subarachnoid space. All larger-bore arterial vessels course through the subarachnoid space before branching and penetrating the brain parenchyma proper. The outer arachnoid layer adheres directly to the dura mater. The most substantial of the meninges, is the dura mater. The dense, inelastic dura is comprised of two continuous layers, the periosteal layer (attached to the skull) and meningeal layer (attached to the arachnoid layer). Scanning Electron Micrograph of a slice through the dog skull depicting the normal organization of the cranial meninges is shown in Figure 2a (2). Several regions of the skull are covered by two major muscle groups, the temporalis (situated over the lateral aspect of the cranium, above and anterior to the temporal lobe) and the frontalis (located directly over the frontal lobe).

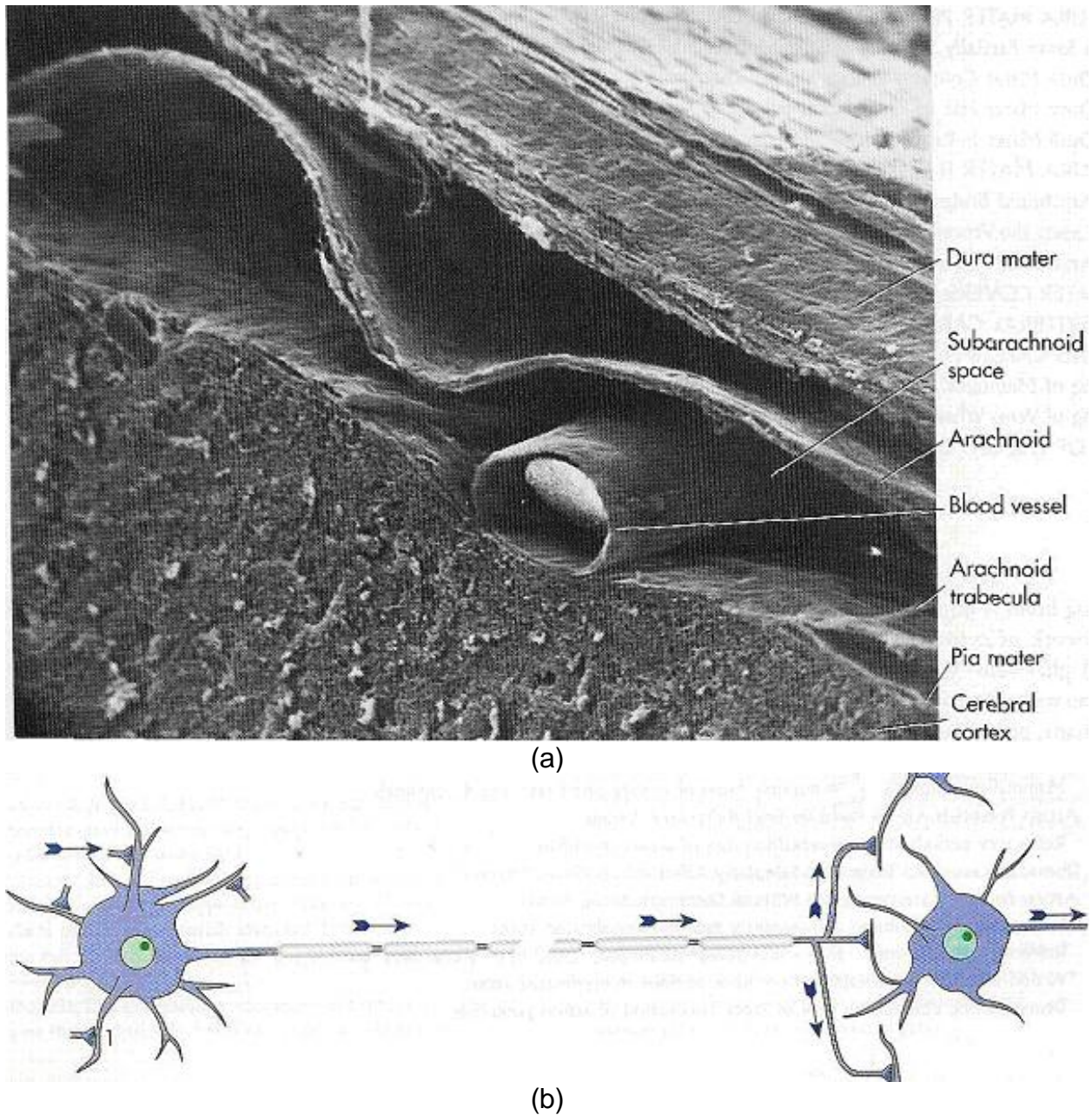


Figure 2: (a) Scanning Electron Micrograph of the cranial meninges of a dog. (b) Schematic diagram of a neuron showing the cell body on the left surrounded by its dendritic harbor, showing several input synaptic terminals. The arrows indicate the direction of signal/information conduction. The longer extension from the cell body extending rightward towards another cell body is the schematic representation of an axon covered with myelination sheath. The action potential is initiated at the base of the axon on the cell body and travels down the axon towards the axon terminal. Once the action potential reaches the terminal local graded potentials are induced at each of its output synaptic terminals (Nolte, J. 1988).

The large majority of the cells in the brain are glial cells providing support, protection and nutrition to the primary cells of the brain. Among several types of glial cells, astrocytes play a predominant role in forming the blood brain barrier by selectively permitting nutrient exchange while preventing toxins and various pathogens from invading the brain tissue proper. They also play a major role in regulating the chemical profile of the extracellular environment. The oligodendrocytes wrap around axons forming myelin sheaths. Although not as numerous as glial cells, the main function of the brain is carried out by neurons. Neurons are electrically excitable cells capable of receiving and transmitting information using electrical impulses. Neurons connect to each other via synapses; the synaptic terminal is, formed by the terminal end of one axon and a dendrite of another neuron (Figure 2b). Such connections form the basis for large and complex neuronal networks spanning across the lobes and hemispheres. Neurons are responsible for processing and transmitting sensory information and producing a perception, thought, memory or an action (1-3, 3).

1.3 FUNCTIONAL ANATOMY OF A NEURON

Neurons produce action potentials by regulating ionic concentration across its lipid-protein based cell membrane and by generating ionic currents through the protein channels down the ionic concentration gradient. The semi permeable membrane separates the intercellular space from extracellular space and maintains a resting intercellular potential of -65 mV with respect to the extracellular space. The membrane is electrically polarizable, the property which allows one to stimulate them using microelectrodes. The potential values are primarily regulated using Na^+ and K^+ ions. The neurons uses two types of signaling mechanisms, a graded local potentials, which

are compared and summed as an input from the surrounding neurons, by the receiving neuron's dendritic body, and spike like action potentials to convey messages across a larger distances. The graded potentials are mainly found near the synaptic junctions where axonal terminals meet with dendrites. The graded potentials can be excitatory (positive going) or inhibitory (negative going) and are only several millivolts in amplitude. Action potentials or spikes amplitude, on the other hand, is around 100 mV. A summed graded potential from the dendritic harbor spreads passively along the cell body towards a region at the base of the cell's axon called trigger zone. The trigger zone is densely populated with voltage gated Na^+ and K^+ ionic protein channels. Once the potential across the membrane of the trigger zone reaches a threshold potential of approximately -55 mV the voltage gated ionic channels in the trigger zone are activated. These channels in turn produces a Na^+ and K^+ ionic flux through each individual channels. The summed potential generated by these channels produces an upswing of voltage to approximately 40 mV, which returns back to its base line value of -65 mV over a period of 1-2 msec. This rapid depolarization and repolarization of the membrane is termed as a spike or an action potential. The spike is then propagated down the axon in similar manner via other voltage gated ionic channels distributed along the axon (Figure 2b). Furthermore, once the action potential is fired, the involved channels enters refractory period for another 1 to 2 msec. This ensures that the spike only travels in primary direction down the length of the axon towards the synaptic terminal.

1.4 STUDYING THE BRAIN

A thorough understanding of basic neurophysiology is necessary to design a device to interact with the individual cells and complex systems of the human brain. The field of

neural engineering combines engineering design principles and basic physiology to aid patients with neurologic deficits and create tools to further our understanding of perception, action, learning and memory. Such tools are designed to interact with an ensemble of hundreds to thousands of cells as in the case of MRI imaging, or with a single cell, as in the case of invasive implantable micro-electrodes.

Through extensive work by Hodgkin and Huxley in 1952, we have gained an excellent insight into the molecular dynamics of individual nerve cells (neurons) during initiation and propagation of action potentials (electrical signal) (4). The action potentials are electrical impulses transmitting perceptual as well as motor actions information, through a network of more than 100 billion individual nerve cells (4). Using modern imaging technology, we can now monitor the electrical activity of the human brain as it processes sensory information and devises a plan or a motor output. Despite the wealth of knowledge, it remains a mystery as to how the sequence of action potentials translates into a sensory perception or a precise motor action involving the orchestrated contraction and relaxation of several different muscle groups. Recording from individual neurons is necessary to understand the complex network dynamics of dense neuron populations. In order to interact with these networks of neurons for understanding the information processing and transmission we may need a high density interface that can interact with as many single cells within a network as possible. This view of interfacing with neuronal network may also be necessary in aiding sensory or motor function deficits in a patient. Extracortical imaging and stimulation technologies lack the resolution necessary for monitoring or inputting information at a single cell level, thus necessitating invasive implantable technology with high channel density.

1.5 MICROELECTRODES

Since the initial applications of single microelectrode, a large body of knowledge has been accumulated about the function and physiology of the mammalian brain and specifically the organization of the cerebral cortex. The scientists in neuroprosthetic field are studying the possibility of microelectrode interfacing directly with CNS in an attempt to input information at the cellular level. This is hoped to allow rehabilitation of certain cases of blindness, deafness or paralysis (5, 6). The current trend is to monitor and/or stimulate interconnected groups of neurons as a system in non-anaesthetized, awake and behaving animal. From initial experimentation, it was quickly understood that one must increase the density of the microelectrodes to understand the specifics of the interconnection between the cortical neuronal cells. Microfabrication techniques have been used to develop microelectrode technology since the early seventies. Microfabrication technology was initially developed by the semiconductor industry for microelectronics applications such as microprocessors and gating devices. The same semiconductor material namely silicon and silicon dioxide were used to create the first batch-fabricated microelectrodes. A study by Edel et al. confirmed that silicon and silicon dioxide are biologically inert, i.e. they neither enhance nor hinder cellular growth (7). Many researchers have since successfully monitored the interaction between groups of neurons and silicon-based devices. Furthermore, intracortical microstimulation (ICMS) has shown to require 3 to 4 orders of magnitude less charge than surface stimulation. These types of results have encouraged development of ICMS arrays to be used in neuroprosthetic systems for blind or deaf, or for basic research studies such as cortical mapping. Many groups feel that it would be ideal to have every

single neuron within, per say, visual cortex be interfaced with an individual electrode, even though, such electrode density is far from reality for today's technology. Yet, bringing a step closer to this ideal electrode density is the semiconductor technologies. First semiconductor based multiple electrode array was created in 1975 by Wise and Angel. Despite the modest design of the first single shaft microelectrode, the modern intracortical implantable device boasts multiple electrodes/recording sites, biologically active coating and on-board signal processing circuitry (8). Continuing evidence of reliable and stable long-term implantable electrode resulting from modern electrode designing and building techniques is very promising for the realization of clinically useful cortical prostheses. Although years of research have produced substantial improvement of the fabrication techniques and device design, commercially-available electrodes available today have yet to demonstrate the long-term stability necessary for clinical use.

The surface property of the electrode and specifically its interaction with surrounding cells ultimately determines the quality of the interface and plays a very crucial role in in-vivo experiments. As described later, in the case of Utah electrode, the bare electrode was rejected by the neural tissue and hence resulted in minimal or no recording. Post experiment craniotomy showed that the electrodes were pushed out from the cortical region. Other studies have indicated that they lose their electrical connectivity over period of time even though the device was embedded inside the cortical tissue. Micromachined prosthetic devices are nevertheless important devices for functional stimulation as well as recording. Possible applications range from aiding blind and deaf as mentioned earlier or understanding and mapping of cortical region to their functions

using techniques such as multisite recording. Very little is known about how neuronal interaction occurs between different regions and layers of the brains, and multisite, simultaneous single neuron recordings may provide insight to such complex mechanisms. Such multisite recordings are crucial, since the simplest of behaviors depends upon parallel and sequential activities coordinated between different regions of the brain. First introduced in 1926 by Adrian, the single electrode recording technique aims at sampling the activity of one neuron at a time. The groundwork for a cortical neuroprosthetic device based on stimulation of multiple sites in the cerebral cortex was first established by two groups of investigators nearly three decades ago. The stimulation of the surface of the human visual cortex using arrays of small platinum electrodes has generated localized perceptions of light known as phosphenes (9, 10). Such results have encouraged researchers that simultaneous, multisite neuronal recordings can be applied to better understand large-scale brain processes.

The history of multichannel devices is divided into three generations of electrode technology. The first devices consisted of a single shaft wire electrode, conferring excellent signal-to-noise ratio and mechanical flexibility. Second generation devices consisted of multiple-site electrode arrays typically built from a single substrate, allowing for high electrode density and precise machining. The current generation of devices employs bioactive coatings to improve surface chemistry and intimate interface to neuron connection. Despite technological improvements, problems such as device longevity, biocompatibility and data clarity persist.

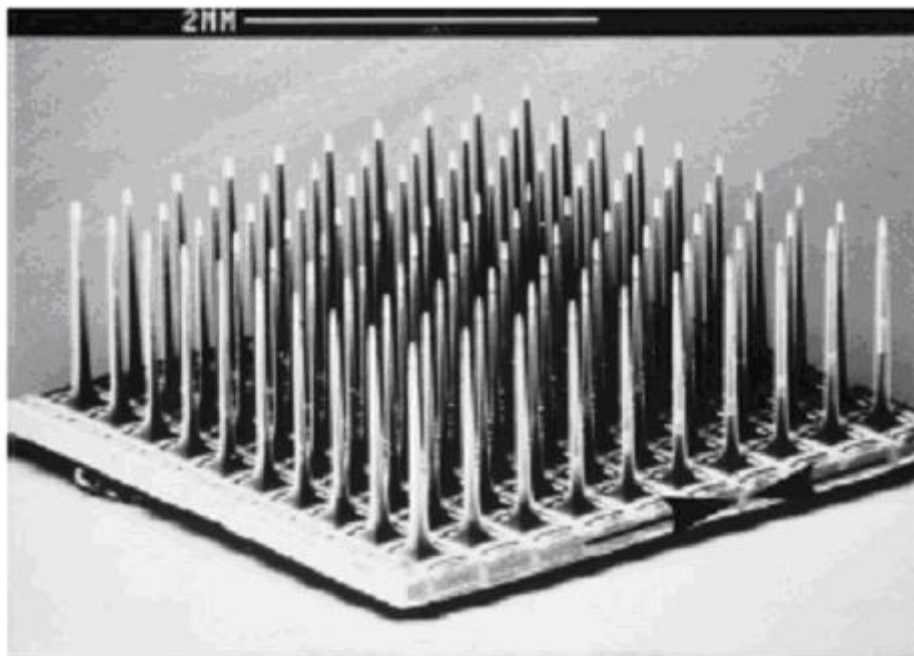
Bioactive nerve growth factors (NGF) coated single channel devices direct neurite growth toward the recording sites, thus improving the SNR 5-10 times and device

stability compared to uncoated devices (11). Yet researchers believe that we must be able to monitor and if necessary stimulate the neurons in many locations and layers simultaneously to ultimately provide a reasonable clinical benefit to patients with complex sensory deficits (12). It is well known that the most simple of tasks requires the coordinated function of many levels in the brain. To study this phenomenon single microwire electrodes are assembled into an array of different geometries. Ideal microwire spacing for typical row-column geometry is 100 μm - 250 μm , with maximum of 48 microwires implanted into the animal. This type of electrode allowed simultaneous recording from the trigeminal ganglion (Vg), principle (PrV) and spinal (SpV) nuclei of the brain stem complex, the ventral posterior medial (VPM) nucleus of the thalamus and the primary somatosensory (SI) cortex. The average signal to noise ratio was calculated to be around 3.7. The analog signals were captured for offline analysis. This approach allowed reconstruction of the parallel flow of sensory information across several subcortical and cortical relays of the rat trigeminal somatosensory system. It was shown that by stimulating different whiskers produced unique spatiotemporal patterns (different magnitude and time latencies to identify individual whiskers) of sensory responses from the same ensemble of 30 neurons in the SI cortex. They also showed that their methods recorded stable signal over long period of time. The post stimulus time histogram (PSTH) was very consistent over a period of 2 months in some rats and at least for 1 month in majority of the experiments. Furthermore, even after 30 days, 85% of the microwires yield recordable single neurons. During the entire 30 days period the number of neurons isolated per microelectrode also remain very constant averaging 2-3 per electrode. Moreover, by using the same approach to record from

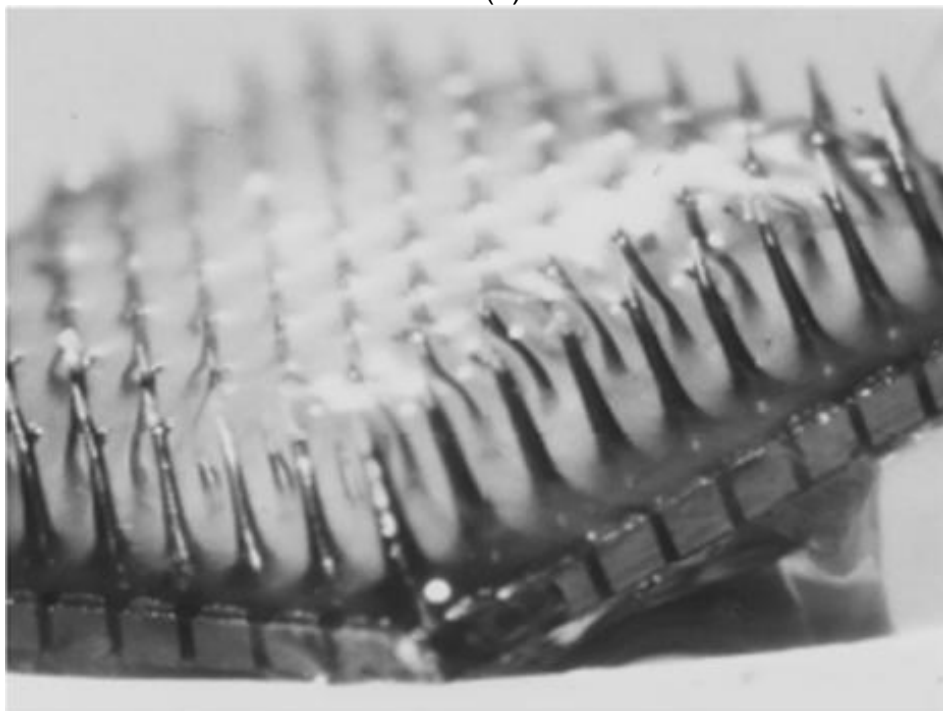
cortical neurons in primates, viable recording of 50-70 single units were maintained for 8-15 months. This technique provided stable recordings of concurrent extracellular activity of up to 100 single neurons were obtained, dispersed along the entire rat neuro-axis, with time resolution of 250us.

The studies described above confirmed batch fabrication that of the larger and denser arrays will improve functional performance by ensuring accurate and reproducible manufacturing. Researchers, therefore, turned to microfabrication techniques. Since neurons are typically organized in columns, researchers at the University of Utah theorized that a single electrode per column would suffice to interface with input neurons, typically located in layer IV of the cortex. The device must also withstand the micromotions of the brain despite be affixed to the dura and skull (5). Work also has been done to improve the surface chemistry by creating an electrode interface that yields a stronger and more intimate connection with the neuron. The goal of the surface modification approach is to reduce or prevent the growth of nonconductive tissue material which impedes the electrode interface in chronic implants. Electrospinning nanometer-diameter filaments of protein/polymer onto the electrode have shown enhanced attachment and growth of the cells on the probe in vivo and vitro environment (13). Subsequently, the stability of UIEA and the tissue response following chronic implantation was studied to optimize the long-term viability of the recording interface. A monolithic substrate of silicon was acid-etched to give a 1 mm x 1 mm array of 100 electrodes, as shown in Figure 3a. Each probe or shaft is isolated by glass as dielectric barrier with inter-electrode spacing of 400 μm . 50 μm - 100 μm length at tips of the electrodes were coated with Pt, Ti, and W. The non-metalized portion of

the shaft and the substrate were insulated with polyimide and in later studies in some cases with Parylene-C. There was no observed correlation between the electrode impedance and its viability reported. A clear trend of impedance decrease 6 months post implant was observed and was attributed to possible degradation of the insulator material. Furthermore, the background activity significantly fluctuated over time. Such variance was attributed to possible displacement of the electrode as fibroblast cells began encapsulating the electrode, expelling the electrode from the cortex (see Figure 3b). Histological examination after extracting the electrode confirmed the hypothesis that glial-mediated encapsulation did produce movement of the electrode tip, contributing to the loss of signal viability observed over time. The tissue tracks of cause by the electrode shafts were observed for less than half of the implants. The analysis of most of the tracks however showed minimal damage to the neuronal tissue near or surrounding the electrode. It was concluded that it may be necessary to manufacture an array with unique properties specific to the anatomical subtleties of the intended region of implantation to minimize insertion damage. Following the functional study on the UIEA, studies on those electrodes application in aiding deaf or blind were done in an awake, unrestrained animal. The stability of the electrode for over 115 days or 25 stimulations was shown by recording SNR to be similar values. Although the Utah Intracortical Electrode Array was originally designed to act as the interface for a



(a)



(b)

Figure 3: (a) Utah Intracortical Electrode Array. 100 electrodes array made using photolithography and etching technique on to a Silicon substrate. (b) Explanted array with moderate encapsulation of 250 nm thickness (Rousche & Norman 1999).

neuroprosthetic system to aid the blind, it could be used for any other similar ICMS applications of the CNS.

Another group at the forefront of micro-machined neural interface technology is situated in Michigan (8, 14). Michigan researcher remains the only group to successfully demonstrate viable recordings for up to one year from a silicon based chronic implant (See table I). Even though the devices are made from silicon, researchers hypothesize that by removing sharp edges (other than the insertion tips) reduces insertion damage and prevents inflammatory cells from adhering to the surface. Additionally, meticulous surgical protocol is claimed to have helped attain the 1 year long recording. Fabrication of the Michigan device begins with a 1 mm thick silicon wafer. Thermal oxide is grown and patterned, following a boron diffusion step. This allows for boron etch stop technique to be used in shaping the smooth exterior surface of their device. Subsequent steps deposit and pattern alternating layers of dielectrics and conductors. Finally contact sites are formed by depositing gold pads. A typical three-shaft, 12-channel device is shown in Figure 4.

To improve biocompatibility necessary for long term implants, many researchers have begun to investigate modification of surface chemistry. Cui et al. stated that surface modification is needed to the electrode sites in order to improve the information exchange at the electrode-tissue interface (13). An ideal electrode site would provide an intimate contact with the tissue, give enhanced charge transport and provide neuronal growth factor to attract neurons and its processes.

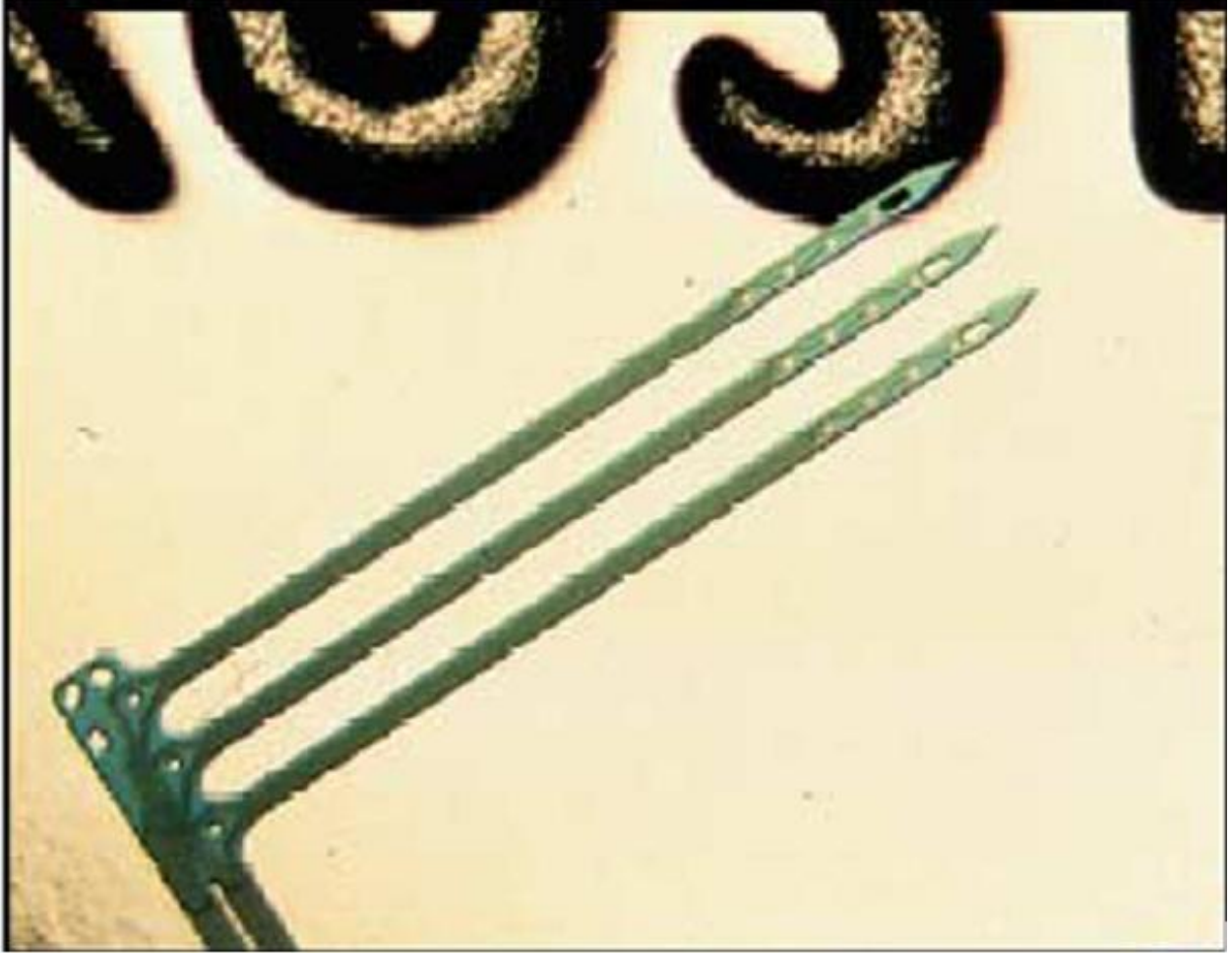


Figure 4: Silicon based three shank 12-site recording probe developed at Michigan (Wise et al. 2004)

One approach uses electrochemical deposition of the conductive polymer polypyrrole (PPy) in combination with bioactive species onto microelectrode sites. Due to its electrical conductivity, PPy is an attractive candidate for such application. Another study showed the electrically conductive polymer, oxidized polypyrrole, may also be a suitable material for *in vitro* nerve cell culture and *in vivo* implantation (9). Based on oxidation mechanism of PPy, bioactive species such as DNA, proteins, NGF etc. have been patterned onto electrode sites together with PPy. Using electrochemical polymerization, PPy combined with peptides and synthetic protein polymer (genetically engineered protein that contains the cell binding peptide sequence RGD) were precisely deposited specifically onto the active site without covering the nonfunctional area of the electrode. Previously discussed Michigan electrodes with four active sites of deposited gold per shaft and 4 shafts per device were used. The amount of PPy/bioactive material deposited onto the electrode was controlled by the amount of charged passed during the deposition. FTIR was performed on the electrode to characterize the composition of the polypyrrole/biomolecule. The results confirmed the presence of the protein polymer and PPy in the coating. SEM micrograph showed that PPy/SLPF formed finger like structure that grew longer and thicker with more material deposition and eventually collapsing into a densely packed smooth surface. Impedance spectroscopy indicated that after being coated with PPy/biomolecule, the electrode impedance decreased by 1-2 orders of magnitude. This was accounted for by increase in surface area due to the finger like conformation of the deposits and the polymers higher conductivity. At higher frequencies above 10 KHz the gold electrode impedance does drop below the impedance of the coated electrode. Nevertheless the PPy coated electrode had lower

impedance magnitude around 1KHz, which is the mid-range for the relevant frequencies of most biological signal. The gold electrode impedance showed a steep straight line over range of frequencies, typical of capacitive component, whereas after coating the slope dropped to 1 closely resembling the Warburg frequency dependent impedance on mass transfer of ions to the interface. More fingers like structure of the deposit gave the lowest impedance compared to the densely packed structure as well as small amount of PPy/SLPF coating. In vivo and in vitro studies showed promising results. Based on their results, the group theorized that, it may also be possible to engineer neural network systems in vitro conditions which could be put into the living system as a neural prosthesis, but chronic stability of such devices is yet to be shown.

The electrodes discussed thus far have tried to overcome some of the problems, namely multisite stimulation and recording, and biocompatibility. Mechanical resistance to brain-dura and micro-stress, however, still remain significant problems. The Arizona group studied polyimide-based electrode to optimize the mechanical properties of intracortical electrodes. Arizona polyimide electrodes are made from gold metal contact pads and traces sandwiched between mechanically flexible, insulating polyimide substrate (Figure 5). Its surface chemistry is readily modifiable to allow for bioactive surface modification. Polyimide material is proven biocompatible, thus an excellent choice for neuroprosthetic applications (11, 15). A photolithographic method was used to pattern polyimide and metal layers in planar structure over the sacrificial silicon/silicon dioxide substrate.

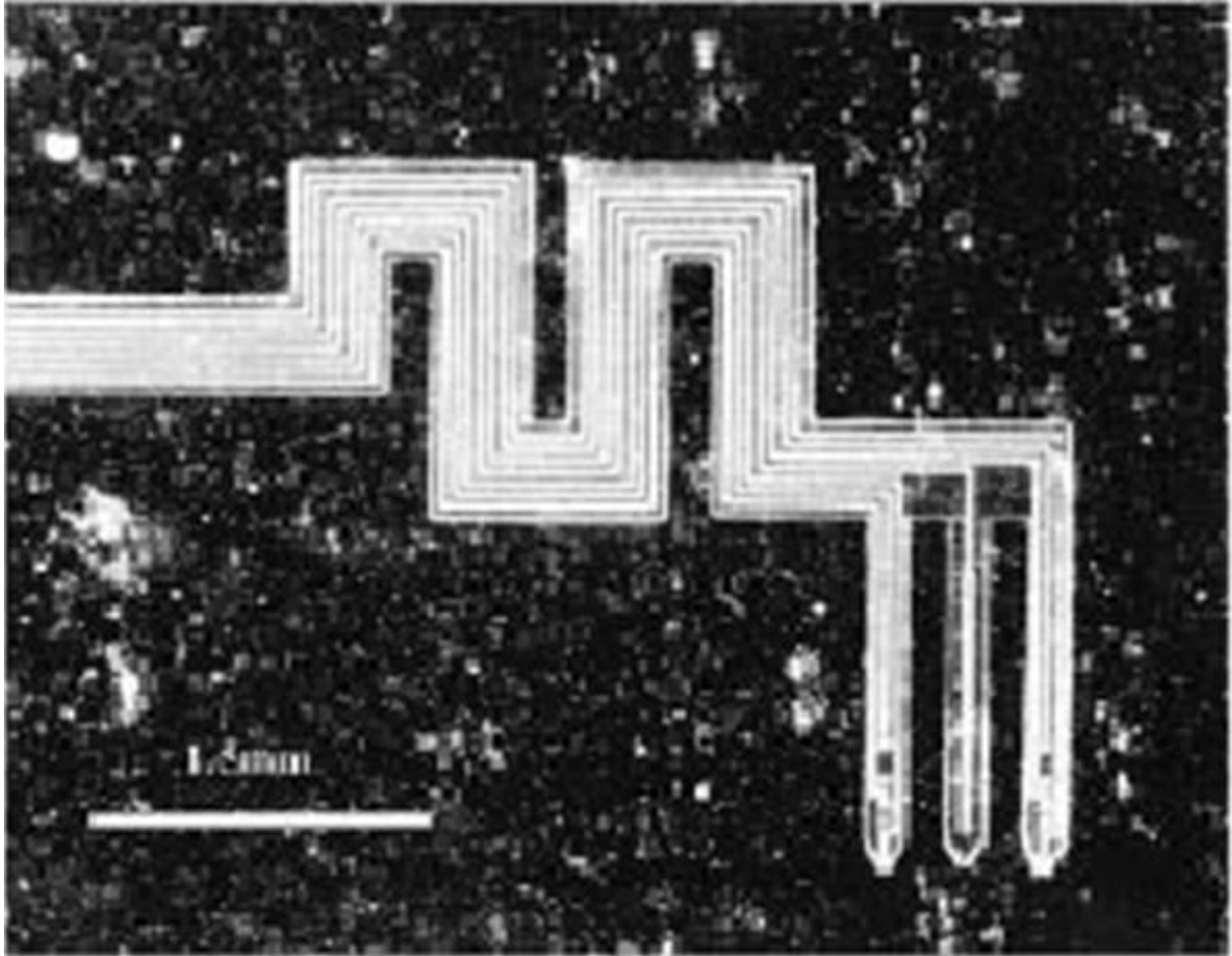


Figure 5: A six-site, three-shaft device with an “S”-curve for strain relief engineered directly into the cable (scale bar lower left = 1.5 mm.) (Rousche et al. 2001)

Cytotoxicity test on completed structures revealed no significant cytotoxicity among the device material. Average initial impedance at the standard frequency of 1 KHz was 1837 k Ω , the impedance drastically decreased to 355 k Ω in after two days of soaking into a saline solution. The drop in impedance was attributed to the polyimide layer not bonding completely, allowing the water vapor to pass directly through the structure. Later structures, where the bottom polyimide was not cured completely before laying down the top layer resulted in stronger, more complete bonding between the layers and eliminated water seepage as described above. The devices were implanted into rat somatosensory cortex and impedance measurements obtained at 1 kHz revealed average electrode impedance of 190 k Ω . Mechanical testing showed a modulus of elasticity of 2.8 GPa and a mean buckling force of 0.00362 N. They also showed that flexing the device with varying loads does not induce mechanical breakdown of the conductive traces of electrode sites. Lastly they commented that bioactive components can be incorporated into the polyimide surface through simple adhesion or through covalent bonding. The drawback encountered here was that polyimide electrodes were too flexible due to very small buckling force; even traditional methods to insert the electrode, through the dura and even pia, were unsuccessful. Therefore, after folding open the dura, incisions of the same geometry as of the shaft were made and then the shafts of the electrode were inserted through it. Recordings were performed in anaesthetized and awake animals.

Takeuchi et al. also developed their own array of polyimide based microelectrodes for the purpose of cortical recording (16-18). More specifically, they developed a technique to stiffen the shaft by inserting nickel in between layers of polyimide. It is

uncertain, whether they had considered toxicity related with nickel as part of the implant material. Nevertheless, they showed that introducing this nickel back plating increases the young modulus of the device nearly 100 fold to 176 GPa. This places their device among the category of silicon devices with respect to stiffness. The group does not comment devices application under chronic conditions, but claims that the material still retains lateral flexibility and is more likely to conform along with micromotion of the surrounding tissue as compared to conventional silicon devices. Figure 6 shows an image of their final product.

Jian Tan et al established the biocompatibility of polyimide while studying motility of neutrophils on polyimide surfaces having different geometries (19). The cell motility greatly depends on the surface's chemical property which promotes or impede adherence and its physical property such as porosity. They compare the behavior of neutrophils on different polyimide with flat glass surface (control). They used "Photosensitive Polyimide (PSPI)". This photosensitive nature of this particular type of polyimide simplifies few steps in its processing as will be discussed under Lithography. The three types of surfaces they explored are PI pillars, PI holes and flat PI surface. The attachment of cells to the glass surface and pillars were similar compared to the flat PI surface and surface with holes. The cells attached them self with many micro-extensions, which is some cases, were attached at the top of the pillars. On the other hand the cells were more spherical shaped with many extensions reaching out in the case of flat PI surface and PI-holes surface. The migration of the cells was hindered in the case of pillars, whereas was enhanced in the PI-holes scenario.

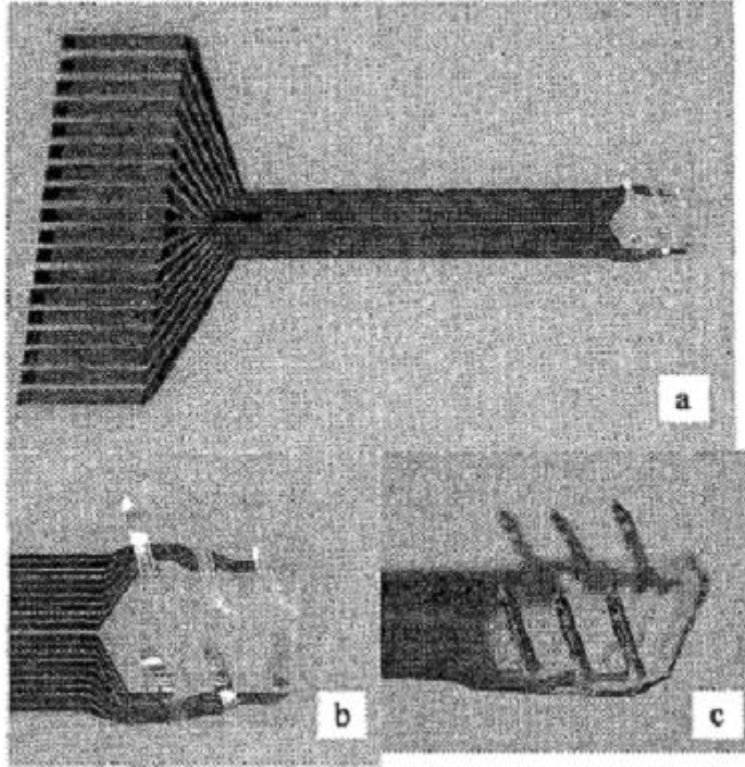


Figure 6: 3D flexible probe array after folding. The recording pads are vertically aligned (Suzuki et al. 2003).

The flat PI showed similar moderate motility as the glass surface. They showed that the neutrophils adhere to glass and pillars but not to the flat PI and PI-holes surfaces. They concluded that PI with its chemical and heat resistive property is very suitable material for bio-device application. Such study shows that we are a step closer to making these devices to reduce inflammatory response. Kanno et al performed a study on polyimide for its application in membrane oxygenators for “semi-permanent lung replacement”. As we have seen so far the contact of the material triggers a cascade of events leading to the inflammatory response and resulting into and isolation of the device. Not only isolation of the device but neutrophils releasing reactive ion species during frustrated phagocytes cause a lot of local tissue damage. This group synthesized their own fluorinated polyimide using chemical imidization with very low polydispersity index. Using this high molecular weight polyimide they tested “protein adsorption, neutrophils adhesion and activation and complement activation.” They stated that complement activation was primarily done via alternative pathway. They concluded that the protein adsorption was very dependent on the curing temperature, with greatest adsorption at 50 °C and smallest at 250 °C. Similarly the amount of neutrophils adhered to the PI cured at 50 °C was much higher than the one cured at 250 °C. They measured the amount of O_2 released by neutrophils to estimate its activation. The neutrophils activation was minimal at 250 °C curing temperature. Their study also suggested that PI cured at higher temperatures (150 °C and 250 °C) showed suppression of complement activation via alternative pathway.

CHAPTER 2. RESEARCH DESIGN

2.1 POLYIMIDE (PI)

Polyimide has been a very promising polymer in many biomedical applications. Due to its lithography friendly properties and excellent insulation property, it has gained a great popularity in neural prosthesis. Literature as well as our preliminary results shows polyimide to be a biocompatible material (3, 15, 20, and 21). Once in contact with a biological tissue polyimide did not leech toxins or any other byproducts. Our studies exploit polyimide's mechanical flexibility to create gold neural recording electrodes. As discussed in background section, in past rigid neural electrodes has not achieved success under chronic conditions. It is hypothesized that rigid nature causes damage to the brain tissue during micromotions of the surrounding tissue. This damage in turn causes an immune response to isolate the electrode material from the tissue. As per young's modulus values listed in Table 1, polyimide's young's modulus is 25 to 100 times lower than that of other materials used for electrodes; and furthermore, it is much closer to matching the young's modulus of the brain. Due to the mentioned flexibility of polyimide it is hoped that it can withstand the micromotions forces and bend along with the brain, increasing its chronic functionality. Furthermore, polyimide's surface chemistry can be easily changed and hence it can very readily be made into a bioactive material, for example by coating it with nerve growth factor. A study also showed that with increase in curing temperature of polyimide, its hydrophobicity increases and therefore reduces the adhesion of leukocytes responsible to fight against foreign body (15). Therefore, polyimide's biocompatibility, its mechanical property and the ease with which it can be processed and shaped makes it very relevant material.

Material	Young's Modulus (GPa)	PI	Success Rate
Silicon	120-170	Normann	~3 years
Microwire (W)	400	Nicolelis	~6 weeks
Silicon	120-170	Kipke	~1 year
Polyimide	4	Rousche	-
Brain Tissue	0.067	-	-

Table 1: Neural Interface Designs for the CNS (3, 14, 22-27).

It is apparent from the name that polyimide is a polymer made with imides (Figure 7). Polyimides are heat and chemical resistant polymers. As mentioned earlier polyimides are used as insulating material in electronics and semiconductor industries. The polyimides are generally chains of imides as most polymers are, but it's the cross-linkage between these chains which gives them the properties mentioned.

Despite all the benefits of polyimide, it is often very difficult to implant the mechanically soft polyimide device through the overlaying dura and pia matter of the brain. Usual surgical techniques for almost all the devices discussed in the introduction requires a small incision in the dural layer. The incision in the dural layer is relatively easily done and with minimal damage. But due to the high density blood vessel density in the pia matter layer, it is often preferred to prevent making any incision in the layer beside the incision due to the insertion tract. To implant polyimide in such matter it is often required to use some form of assisting tool that is removed once implanted.

2.2 POLY (GLYCOLIC ACID) (PGA)

To overcome the implantation issues several techniques, including surface coating as well instrumentation, has been explored by several groups. The reasons for implant techniques are two fold; one is to minimize insertion damage and two to easily and precisely implant a device, specifically in the case of polymer technology. Suzuki et al. used microfluidic channels to initially strengthen the insertion shaft and then, once implanted, to infuse bioactive and inflammatory agents (17, 28). Suzuki et al. and Fofonof et al. used Parylene-c as the base material instead of polyimide, which is structurally stronger and is biocompatible (16, 17, and 29). Rousche and Normann used

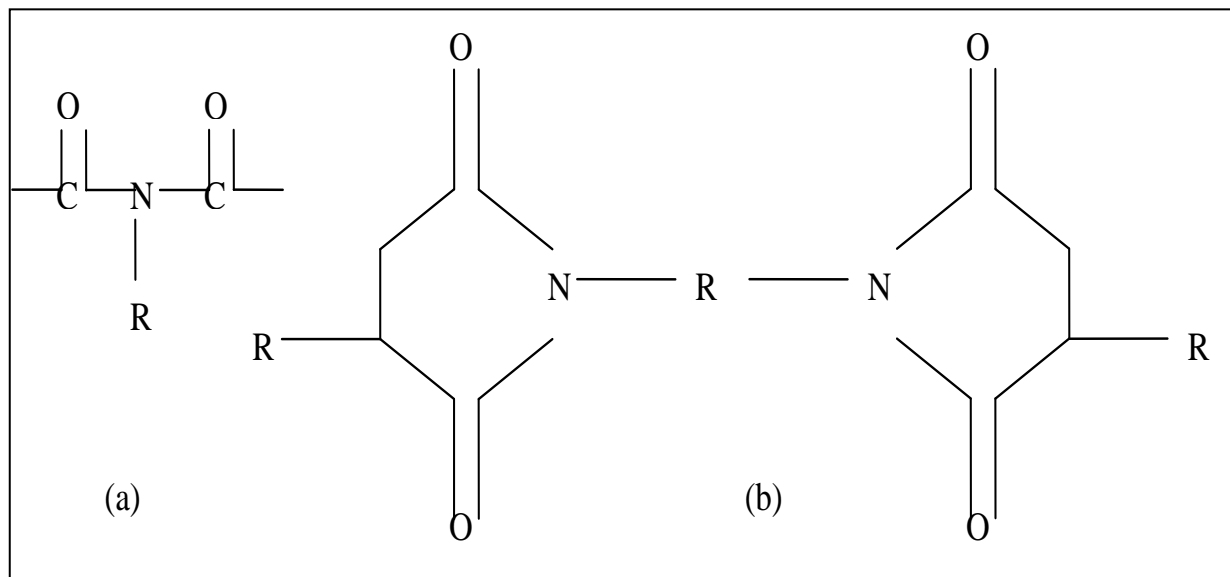


Figure 7: (a) An imide group is composed of nitrogen bound with two C-O pairs and R group. (b) The crosslink between the nitrogen atoms forms the polyimide chain.

pneumatic insertion device to insert multi-shaft silicon array at fast speed to minimize bleeding and damage due to compressive forces on the surface of the brain (5). Wise et al. also made their silicon based devices with smoother edges to minimize the tissue damage both during and after insertion (8). We chose poly (glycolic acid) (PGA) coating as a technique to temporarily enhance the shaft stiffness. Aside from us, Muthuswamy et al. recently published the use of PGA and PEG for surface coating their wire electrodes to improve their structural strength during insertion (30, 31). PGA has been used in dissolvable surgical sutures, nerve guidance channels, absorbable screws and artificial cartilage (32-37). It's biocompatibility as well as neurocompatibility has been well established by several groups, including Muthuswamy and Stahelin (31, 33). Several properties of PGA made it an ideal candidate for this purpose. PGA has a glass transition temperature of approximately 35 °C, which makes it structurally stiff at room temperature and undergoes glass transition once implanted, making it softer (38, 39). It is also biodegradable and completely degrades over the period of several weeks (33). Using Euler's equation (Eq. 1), Rousche et al. showed that polyimide with Young's modulus (E) of 2.8 GPa has critical buckling load of 2.5 mN (11, 40). Using the same formula we computed PGA's critical buckling load of 6.25 mN, 2.5 times greater.

$$P_{cr} = \frac{\pi^2 * E * I_m}{L^2} \quad (\text{Eq. 1})$$

I_m is the moment of inertia and L is the length along which the force is applied. PGA's Young's modulus was taken to be 7.0 GPa (37, 38). Lastly, once implanted PGA undergoes hydrolytic cleavage as it degrades losing half its strength in two weeks, and 100% in four weeks (41-43). The PGA is completely reabsorbed in 4-6 weeks post implant (44). The degradability of PGA using hydrolytic cleavage also makes it very

difficult to process. PGA is obtained is powdered, monomer form and is not soluble material. Melt process polymerizes it and allows one to coat the devices. It is therefore also very difficult to control the coating parameters for PGA.

Aside from the benefits of the implant materials, their biocompatibility must also be accessed. Several groups have shown that assessing GFAP expression is an excellent indication of implants biocompatibility in cortical tissue. Shain, Normann-Rousche and Belamkonda has studied gliosis and GFAP expression surrounding silicon implants, showing GFAP expression extending 130 μm - 150 μm from the edge of the implant (6, 22, 23, 45-47). Bellamkonda et al. showed that Dexamethasone coating reduces the gliosis around the silicon devices to the distance of 100 μm at 1 week post implant. Such numerical analysis of GFAP expression for implanted polyimide and PGA coated devices has not been performed yet. Furthermore, the flexibility of polyimide based devices allowed us to slice through the implanted devices preserving the tissue-device interface and for the first time, the preserved interface is histologically studied.

2.3 SPECIFIC AIMS

Specific Aim I: Manufacturing and functional verification of HD-4000 polyimide based implantable devices as a neural interface in auditory cortex.

Several authors have tried using different types of polyimide polymer to devise a neural interface, yet none has addressed tissue-device interfacial properties or device implantation mechanics. Here we aim to establish another polyimide device manufacturing protocol with HD-4000 photodefinable polyimide polymer. This is a commonly used polymer for its insulation property and its low moisture transmission and retention properties. Furthermore, its photodefinable property allows simplification in clean room processing protocol.

Specific Aim II: Surface coating of poly (glycolic acid) (PGA) to temporarily enhance the material stiffness to allow insertion without removal of pia layer.

The flexible polyimide devices make a potentially excellent tissue device interface while closely matching the mechanical impedance to that of the brain tissue. But the same flexibility of the material raises problems during implantation. The devices are extremely difficult to insert into the cortical tissue, especially through the over laying pia layer, without causing severe damage to the cortical tissue and the pia layer. An incision and partial removal of the pia layer is a must, in order to implant the devices. As a solution to temporarily enhance the mechanical stiffness of the implantable shaft we propose to use poly (glycolic acid) coating on the back side of the polyimide devices. The larger Young's modulus of the PGA coating improves the strength of the polyimide

device 3 fold. Furthermore, the biodegradable nature of the PGA coating will cause the device to regain its flexibility over the period of 2-4 weeks.

Specific Aim III: Characterize tissue response over the period of two weeks to uncoated polyimide devices as well as PGA coated devices.

Despite, many groups manufacturing the polymer based devices very little work has been done to establish histological assessment of flexible devices. Here we aim to perform analytical-histological studies of PGA coated and uncoated polyimide devices to access its benefits in terms of tissue immune response, such as gliosis. We will do so by showing reduction in gliosis and, therefore, reduction in glial encapsulation around the electrodes. The data obtained here will be compared to the numbers published in the literature for the silicon based devices.

CHAPTER 3. METHODS

3.1 MANUFACTURING AND LITHOGRAPHY PROTOCOLS

Flexible, polyimide-based devices are fabricated using the standard lithography techniques used in the microelectronics. Photo-definable polyimide (HD-4000), purchased from HD-Microsystems, is used to provide the base structure. A chromium metal/electrode layer is patterned in the initial devices. Subsequent devices (used for electrochemical analysis and animal studies) are created using the more biocompatible metal of gold.

Devices are created in the Nanofabrication Core Facility (NCF) at the University of Illinois at Chicago. Fabrication process begins by using AutoCAD to designing a schematic layout of the devices for each layer of the lithography process. In Figure 8a, a typical layout for single and multi-shaft electrodes is shown. Here the devices are oriented in a radial configuration to reduce the shadowing effect from the walls of the devices and improve uniformity in the coating of the photoresist. A design of a two shaft device is also illustrated in Figure 8b. All the shafts for single- and multi-shafted devices have the same dimensions as illustrated for a two-shaft device in Figure 8c. The typical material makeup of a polyimide electrode is a 0.1 μm thick metal layer sandwiched in between two layers of polyimide ($\sim 10\text{ }\mu\text{m}$ each) resulting in a 20 μm thick device.

The overall fabrication process is outlined in Figure 9. A silicon wafer is cleaned using Piranha solution (3:1 $\text{H}_2\text{SO}_4\text{:H}_2\text{O}_2$) and oxidized for 15 minutes in an oxidation furnace, resulting in $\sim 1000\text{ }\text{\AA}$ of uniform silicon dioxide (SiO_2) film (Figure 9a-b). Polyimide is

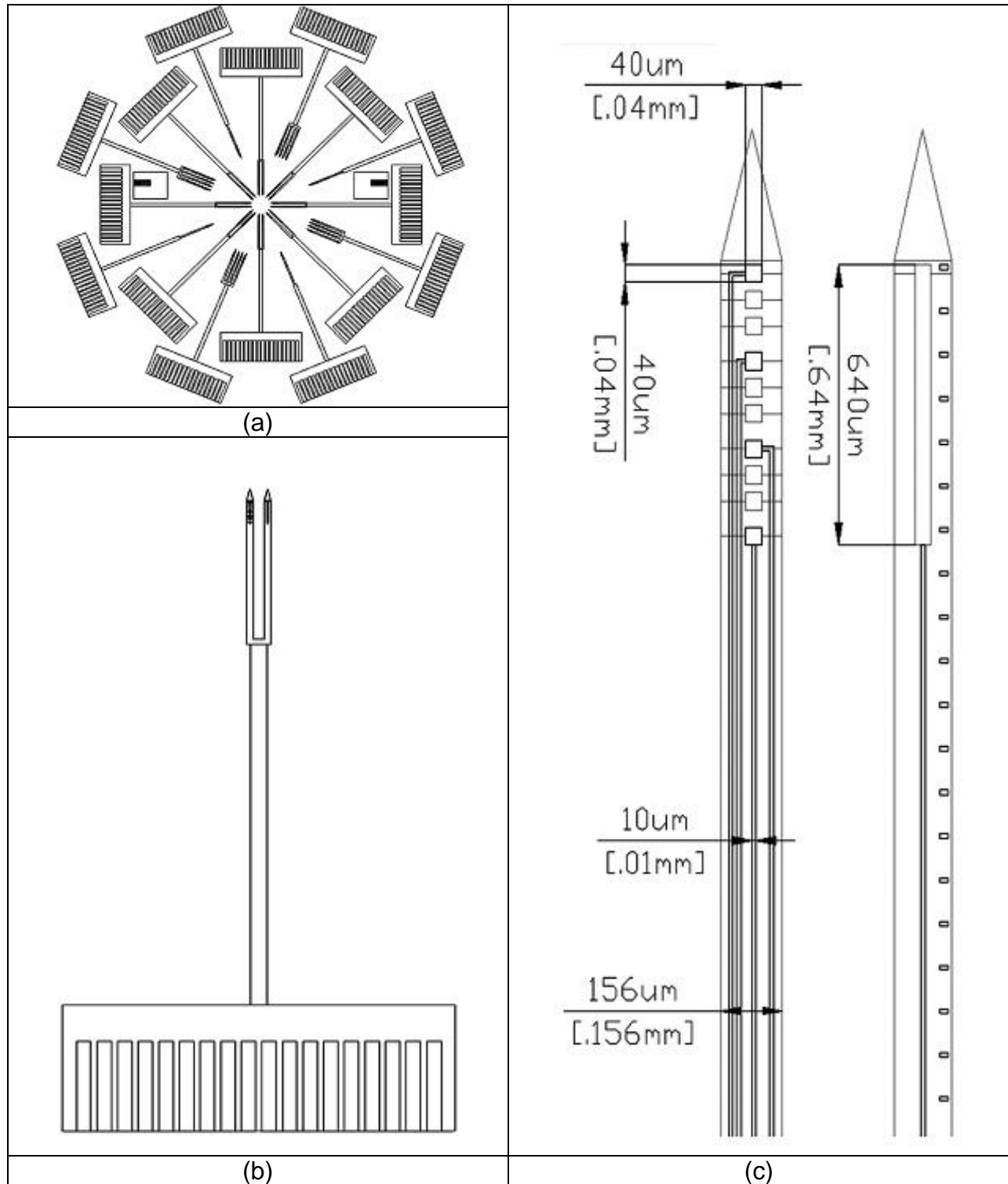


Figure 8: a) AutoCAD layout of 16 devices that can be produced during a single batch processing. b) Enlarged two shaft devices. c) Dimensions of a two-shaft device showing 40 μm x 40 μm contact sites, 10 μm wide trace lines and two shafts measuring 156 μm .

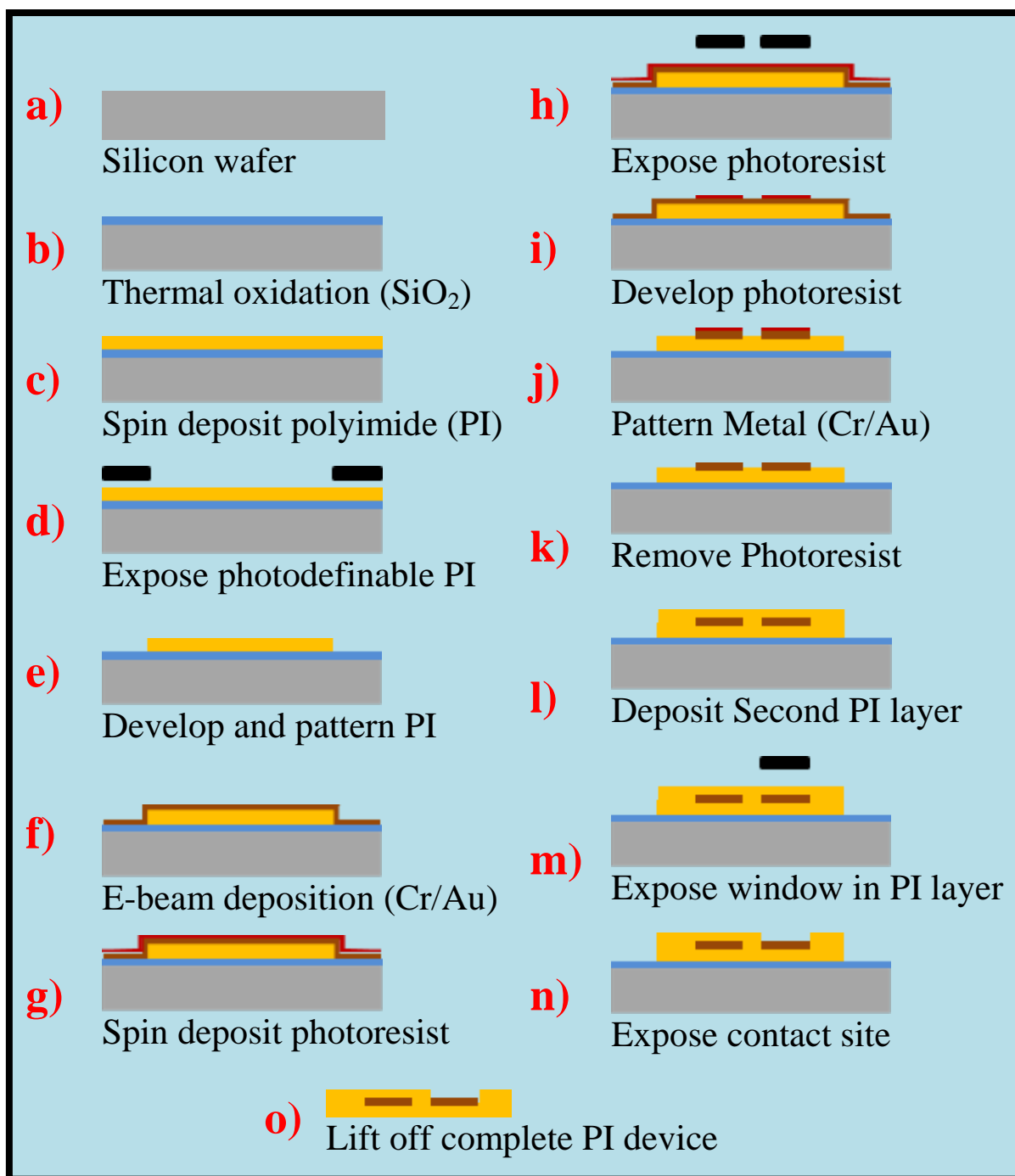


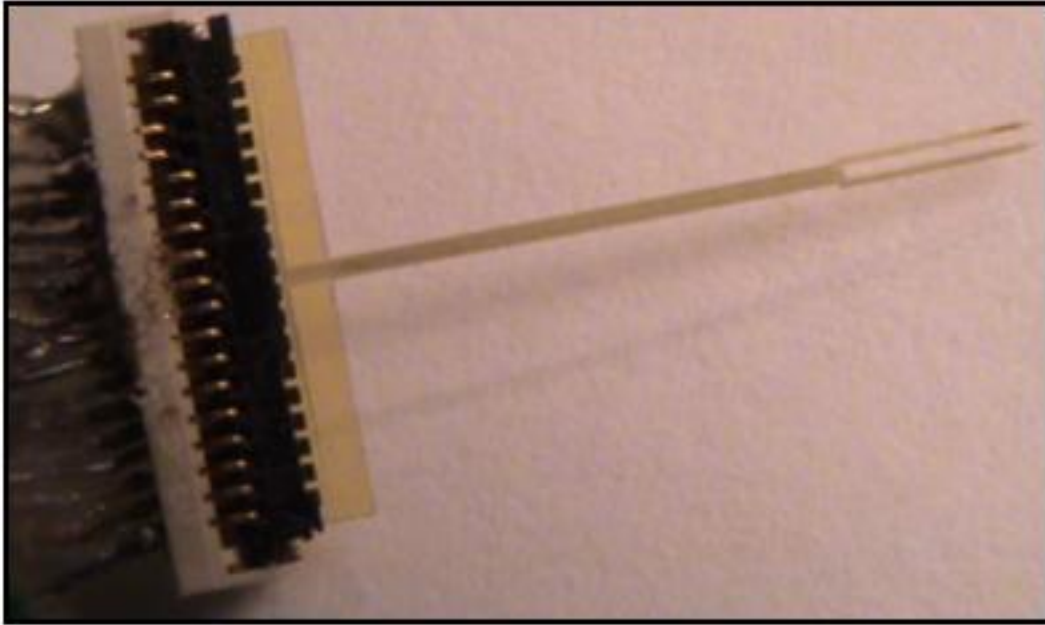
Figure 9: Schematic of the steps involved in the fabrication process. Process starts with bare silicon wafer (top left row) and ends with lifted devices (bottom right row).

spun onto the wafer at 1500 rpm for 60 seconds to obtain a uniform coating for the first (bottom) layer of the device (Figure 9c). The entire substrate is then baked at 85 °C and 95 °C for 100 seconds each to evaporate the solvents from the polyimide and begin the polymerization process. The polyimide-coated substrate is placed beneath the layer 1 mask and exposed under UV light (365 nm). This creates free radicals in the substrate over the regions where the mask allows light to penetrate and react with the polyimide (Figure 9d). The exposed polyimide becomes insoluble in the subsequent polyimide developer and rinse (PA-400D and PA-400R, HD-Microsystems). The polyimide substrate is then baked at 85 °C and 95 °C for 100 seconds each. The substrate is then developed for 4 minutes and rinsed until all of the unexposed polyimide is dissolved away in developer and rinse baths (Figure 9e). The bottom layer of polyimide is then cured at 375 °C for 1 hour. The substrate is exposed to oxygen plasma using Reactive Ion Etching (RIE), to clean the surface of polyimide debris and also to improve the surface adhesion properties. A 2000 Å thick layer of chromium or gold metal is evaporated and deposited onto the patterned polyimide coated wafer (Figure 9f). S1818 photoresist is then spun on at 1500 rpm and patterned to create a protective layer over the metal surface using the mask for layer 2 in a similar manner as the polyimide process described (Figure 9g-i). The chromium or gold-coated substrate is submerged into their respective etchants and etched from the entire wafer except for the region protected by the photoresist S1818 (Figure 9j). Following this step, the protected photoresist is stripped off, exposing the metal traces (Figure 9k). Lastly, the final layer of polyimide is processed in a similar manner as the initial layer of polyimide; exposing 40x40 µm metal contact sites (Figure 9l-n). The entire wafer is placed in a

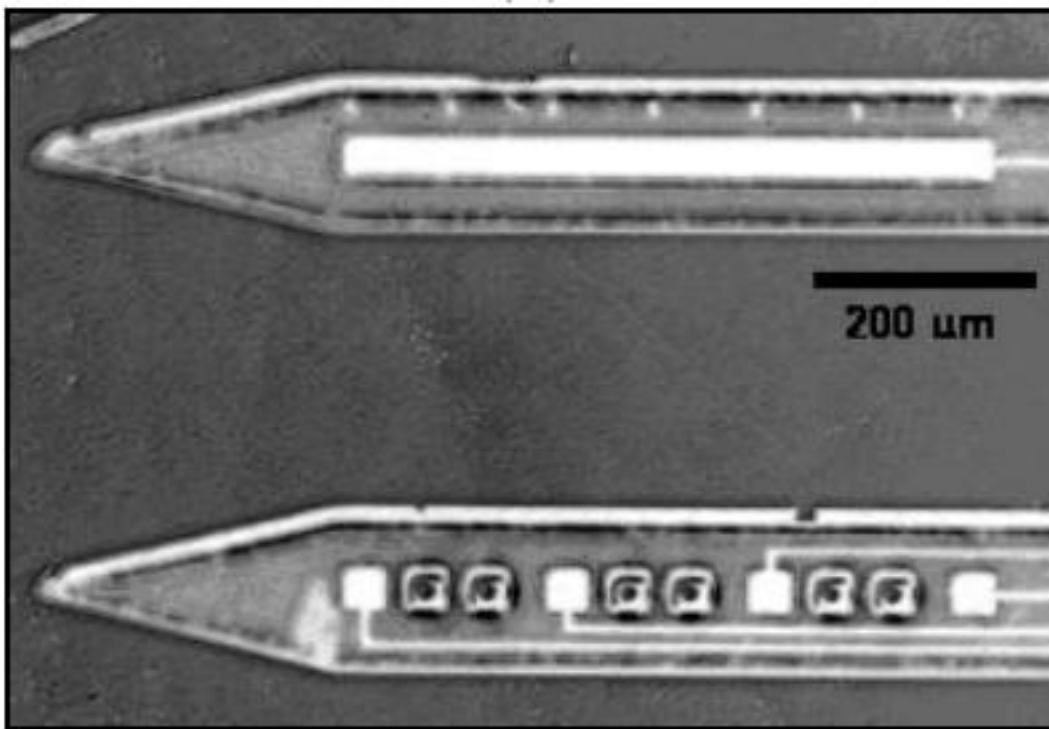
bake oven at 375 °C for 1 hour. The bake cures the polyimide layers, completing the polymerization process and infusing the two layers of polyimide and sandwiching the metal. The entire substrate is further submerged into HF for 3 minutes - 5 minutes to etch away the SiO₂ film and for individual device release (Figure 9o). Devices are then rinsed with deionized water and mounted onto a flip-lock connector (Hirose-FH19, FPC-FFC, 18-pin gold lead) as shown in Figure 10a. A close up view of a two-shaft fabricated device is shown in Figure 10b. Top shaft shows 640 µm long local reference electrode and bottom shaft shows 40 µm x 40 µm electrode sites. Refer to appendix A for a detailed outline of the protocol.

3.2 PGA SURFACE COATING

To temporarily enhance the mechanical stiffness of the devices during insertion, devices are dipcoated on one side with poly (glycolic acid) (PGA). A puddle of PGA is created by melting one teaspoon of powdered form of PGA, DuPont – DU00824, is scooped and placed on a temperature controlled hotplate. The hotplate is adjusted to 210 °C, the melting point of PGA. Due denature temperature of PGA at 250 °C, the hotplate temperature is precisely controlled at the melting point of PGA. The devices are swiped across the surface of the melted PGA, without breaking the puddle's surface tension, assuring one sided coating of PGA as shown in the sketch (Figure 11a). The single sided coating of the device is verified using SEM as well as by comparing electrode impedance spectroscopy (EIS) analysis of the device's contact sites before and after the coating. PGA coating is limited only to the backside of fork of the device leaving the stem and rested of the device un-altered. A small, 3 mm x 10 mm,



(a)



(b)

Figure 10: Two shaft device-connector assembly successfully manufactured and a close up view showing 'ground' shaft and electrode site shaft.

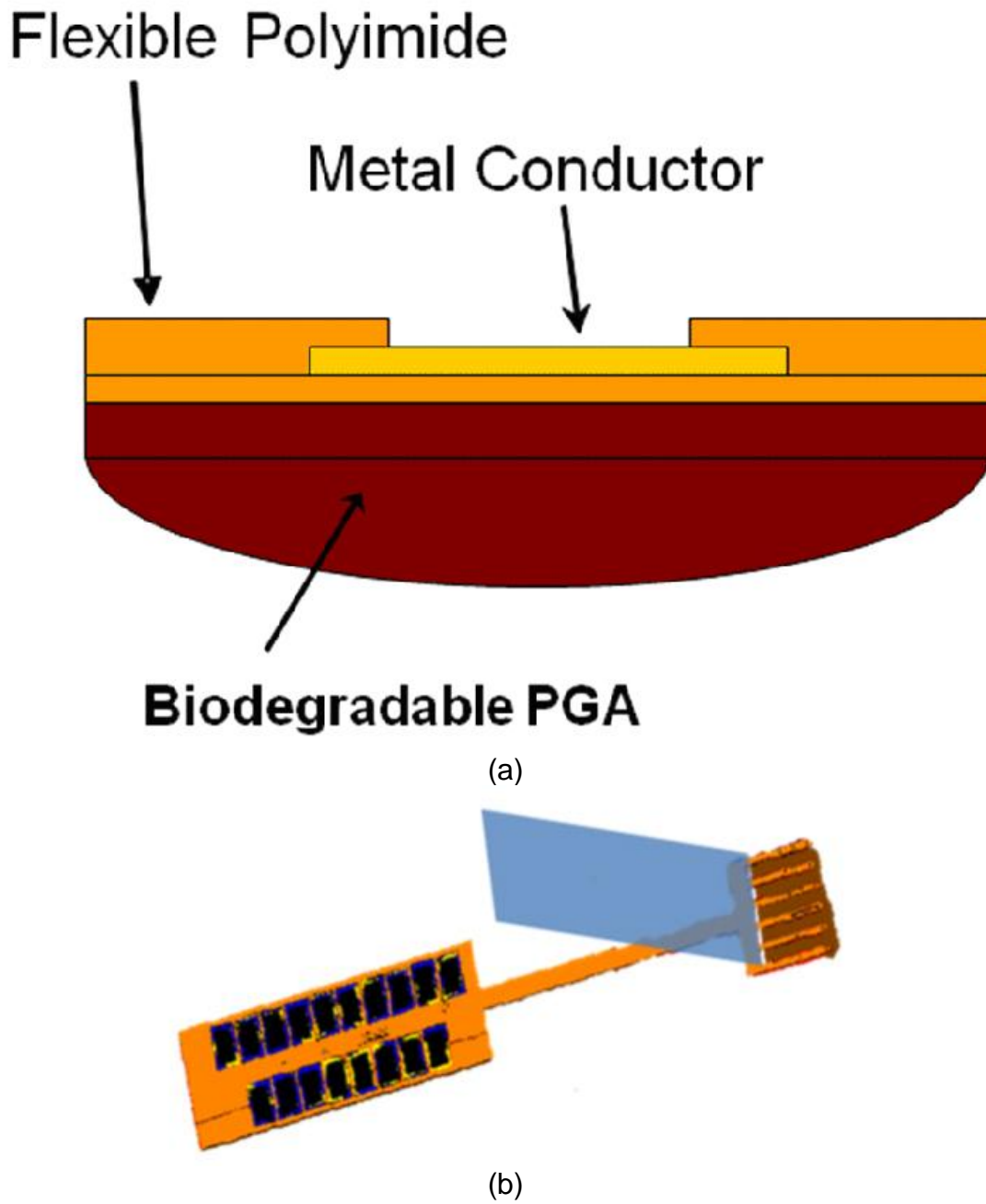


Figure 11: Illustration of back coating of PGA on a polyimide device. The contact site is left uncovered.

rectangular piece of plastic is then attached at the base of the fork to anchor the device for insertion and manipulation (Figure 11b).

The devices buckling strength test is performed to characterize the increase in the strength of the device. Peak displacement force withstood by device, before buckling, is measured using apparatus shown in Figure 12. The weight balance with 0.1mg precision is set for continuous recording at 5Hz. The tip of the device is adjusted to just above the surface of the weight balance using micromanipulator. After 5 seconds of base line recording, the device is displaced 1 mm onto the face of the weight balance in 1sec. Force (N) is computed offline by multiplying the weight measured with the gravitational acceleration constant g (9.8 m/s). The peak of the Force-displacement curve is taken as the buckling force of the device.

Aside from the enhanced mechanical strength from PGA coating, it is also important to access the degradation period of the PGA coating. The amount of PGA coating applied on the device, using the method discussed here, was very minute and had degraded completely over the period of 6 hours. It was difficult to measure the weight of the coating and the degradation rate of the coated amount; therefore two sets of experiments are devised as outlined below:

Experiment 1: PGA cubes, 1 mm x 1 mm x1 mm were used to measure degradation rate and pH change over the period of 7 days. The cubes, weighing approximately $27.8 \text{ mg} \pm 3.8$, were placed in 35 different test tubes with phosphate buffered saline (PBS). The test tubes were stored at 35 °C. The cubes were allowed to degrade via hydrolytic cleavage. 5 test tubes each were open on subsequent days over the course of 7 days. The pH of the solution (PBS + PGA) was measured. The solution

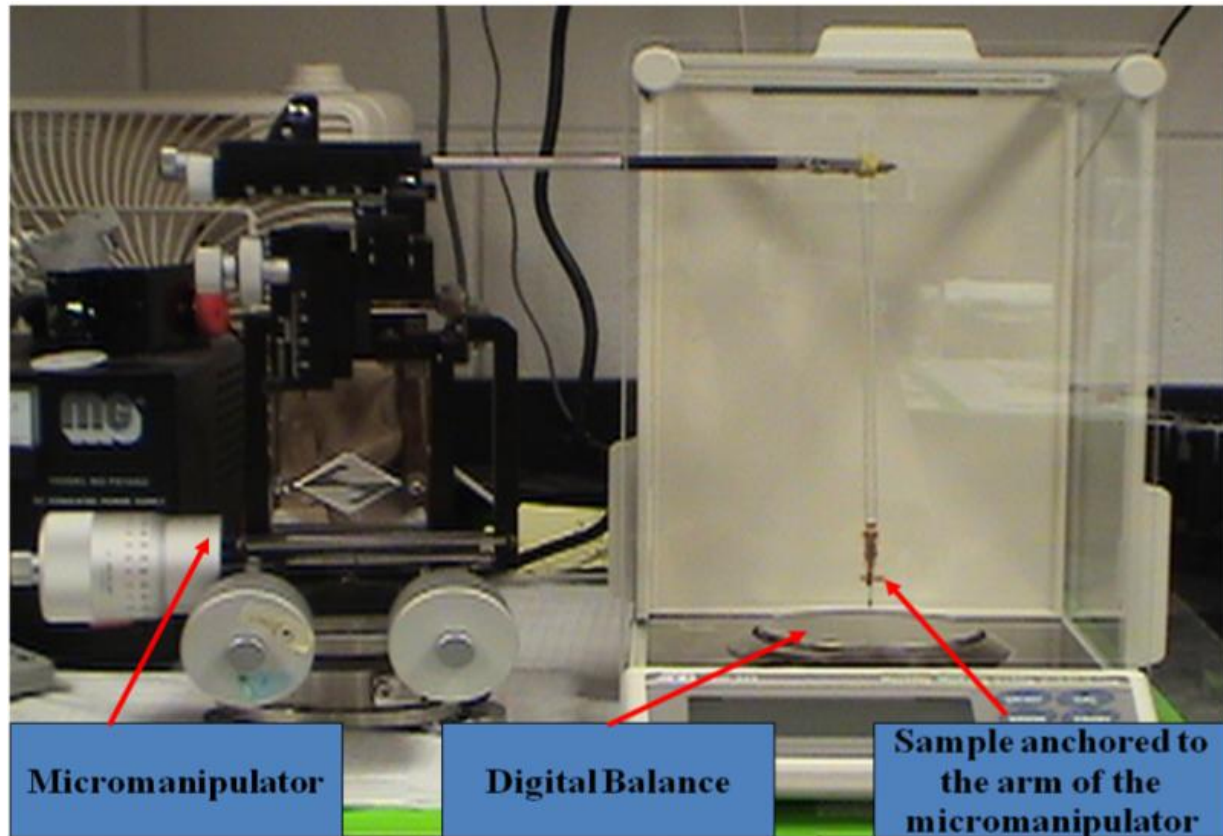


Figure 12: Displacement force measurement setup to measure the peak force withstood by the device before buckling.

was carefully discarded without allowing any solid pieces of PGA to drain away. The remaining PGA contents were then emptied, dried at 150 °C and weighed. There was no saline change done in the remainder of the test tubes, ignoring the effects of perfusion.

Experiment 2: Twelve PGA coated devices were placed in 12 test tubes with PBS. The pH measurements were made every 10 minutes - 20 minutes for first 2 hours and then at every hour until pH returned to 7.4. Saline change, to mimic perfusion, was done after each measurement. Any visible solid pieces were not allowed to drain away.

3.3 ELECTROCHEMICAL ANALYSIS

An electrochemical testing machine (Autolab[®] PGSTAT30, Brinkmann Instruments), a standard 3-electrode electrochemical setup in a Faraday cage is used to quantify electrical characteristics of the microelectrodes. A silver/silver chloride reference electrode and platinum wire counter electrode are used to test the electrode under consideration (the working electrode). Cyclic voltammetric and electronic impedance spectroscopic data/measurements that quantify electrode performance are obtained through analysis using Autolab[®] and a custom-written program in Matlab[®].

Cyclic voltammetry is conducted from -1 V to 1 V as well as from -0.6 V to 0.8 V (the water window). A scan rate of 50 mV/s and a step potential of 0.00045 V best elicited electrochemical reactions upon the metal surface. Impedance spectroscopy is conducted with a frequency range of 1Hz to 10000 Hz with a 25 nA p-p current. CV and EIS data is processed using custom written Matlab programs. Figure 13 illustrates the electrochemical setup.

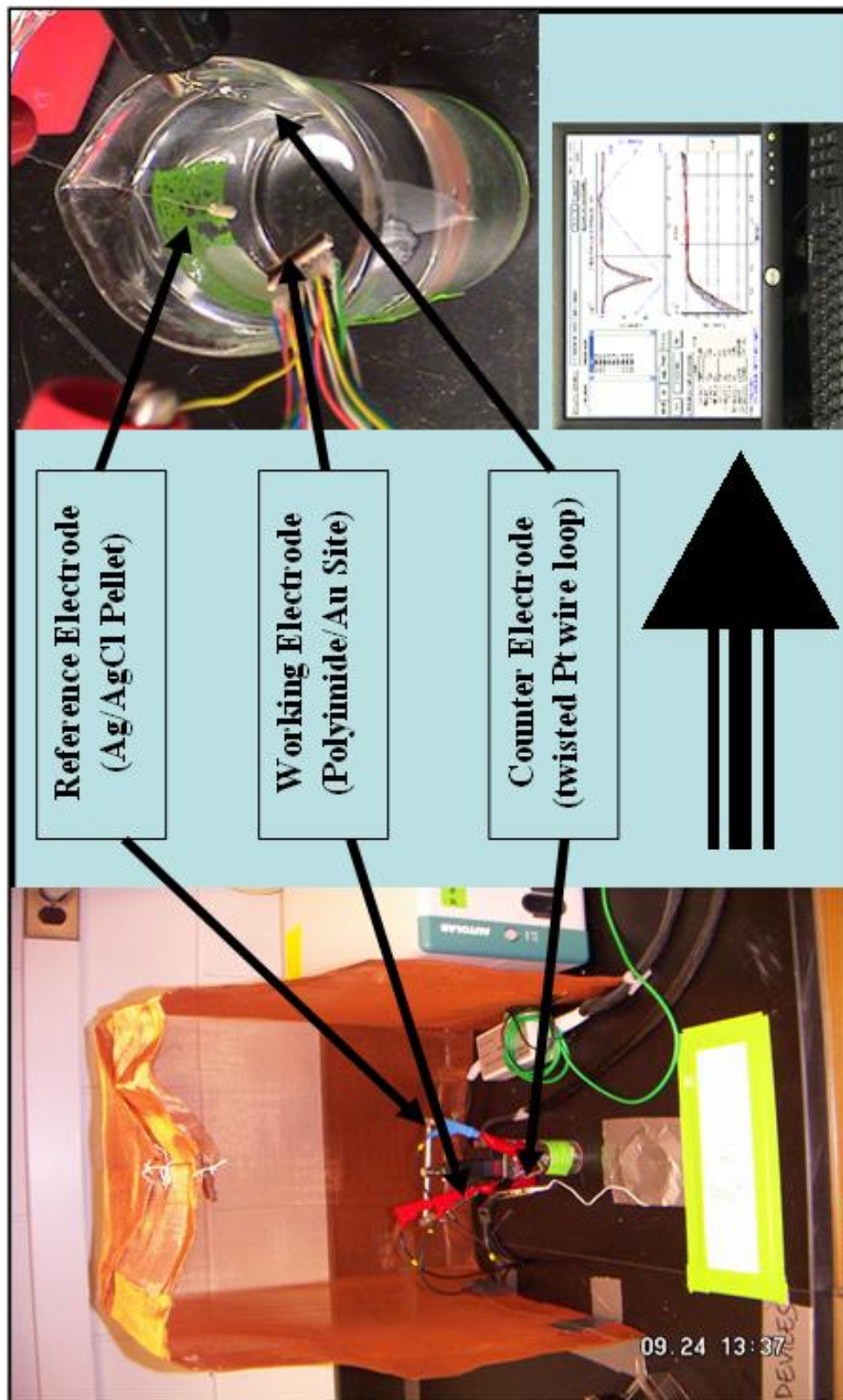


Figure 13: Three lead electrochemical test setup.

3.4 ANIMAL EXPERIMENT PROTOCOLS

3.4.1 GENERAL SURGICAL PROCEDURE AND RECORDING PROTOCOL

All animal experiments are conducted on adult 8 weeks old Sprague-Dawley rats. During surgical procedure animals are anaesthetized with an initial intramuscular injection of Ketamine (100 mg/kg), Xylazine (5 mg/kg) and Acepromazine (2.5 mg/kg). Supplemental doses of Ketamine (100 mg/kg) and Xylazine (5 mg/kg) is used as needed for maintenance of anesthesia (0.1 ml KX mix per 100 g body weight, concentration of 100 mg/ml Ketamine and 20 mg/ml Xylazine). The animals heart rate, oxygen saturation, corneal reflex withdraw and paw pinch withdraw (eyes and a hind limb were made accessible under the sterile drapes for reflex testing) were used to monitor the level of anesthesia and to ensure an areflexic state is maintained throughout the duration of the procedure. Appropriately anaesthetized animals should have a very slight corneal reflex and a very slight or non-existent paw pinch reflex. In addition, heart rate increase in excess of 20% of baseline was used to indicate the need for additional anesthesia.

Animals head is shaved after the animal is placed under anesthesia. Animals head is secured in stereotaxy frame using ear bars and jaw bit. A midline incision is made and fascia is cleared to expose animal skull. A craniotomy is performed over the appropriate auditory cortex area depending on the intended location (left or right) of implant. The specific auditory cortex area is identified using stereo tactic coordinates and/or blood vessel landmarks. The craniotomy is performed on the lateral surface of the cranium posterior to the lateral suture. The primary auditory cortex is located 3.3 mm to 6.3 mm anterior-posterior and 6 mm lateral relative to bregma.

Following the craniotomy procedure, several stainless steel bone screws are inserted at the craniotomy margins and on the opposite hemisphere. The dura over the implant site is excised using small scissors. Electrodes are inserted through the pia by hand to a depth appropriate to the target. After successful implant, relevant several hours of electrophysiology experiments are conducted. The surgical procedures last roughly 3 hours - 4 hours.

Complications during surgery include possible blood loss from the exposed vessels on the cortical surface and cerebral edema. Additional fluids are delivered subcutaneously as needed (5 cc dextrose, 5% in saline). Slight edema is typical in these procedures. If the cerebral swelling does not subside enough to allow for electrode insertion and Gelfoam packing, the animals were sacrificed. Figure 14, shows a typical craniotomy. A two shaft electrode rests on the cortical surface prior to insertion.

3.4.2 MODIFIED SURGICAL PROCEDURE FOR SURVIVAL SURGERIES

Implants are performed under aseptic conditions as follows. Animal's head is shaved and skin prepared for sterile surgery using iodine wash (3 repeated applications of alcohol and Betadine scrub followed by a single coating of Betadine skin paint). After which, same sequence as described in general surgical procedure is performed under sterile condition. Post implant, a protective layer of collagen-based gel-foam is placed to recover any exposed pia in case of survival surgeries. Dental acrylic is then be used to seal and protect the craniotomy and to hold a percutaneous electrode connector in place against the implanted bone screws. The skin is resutured around the now protruding connector/acrylic mound.

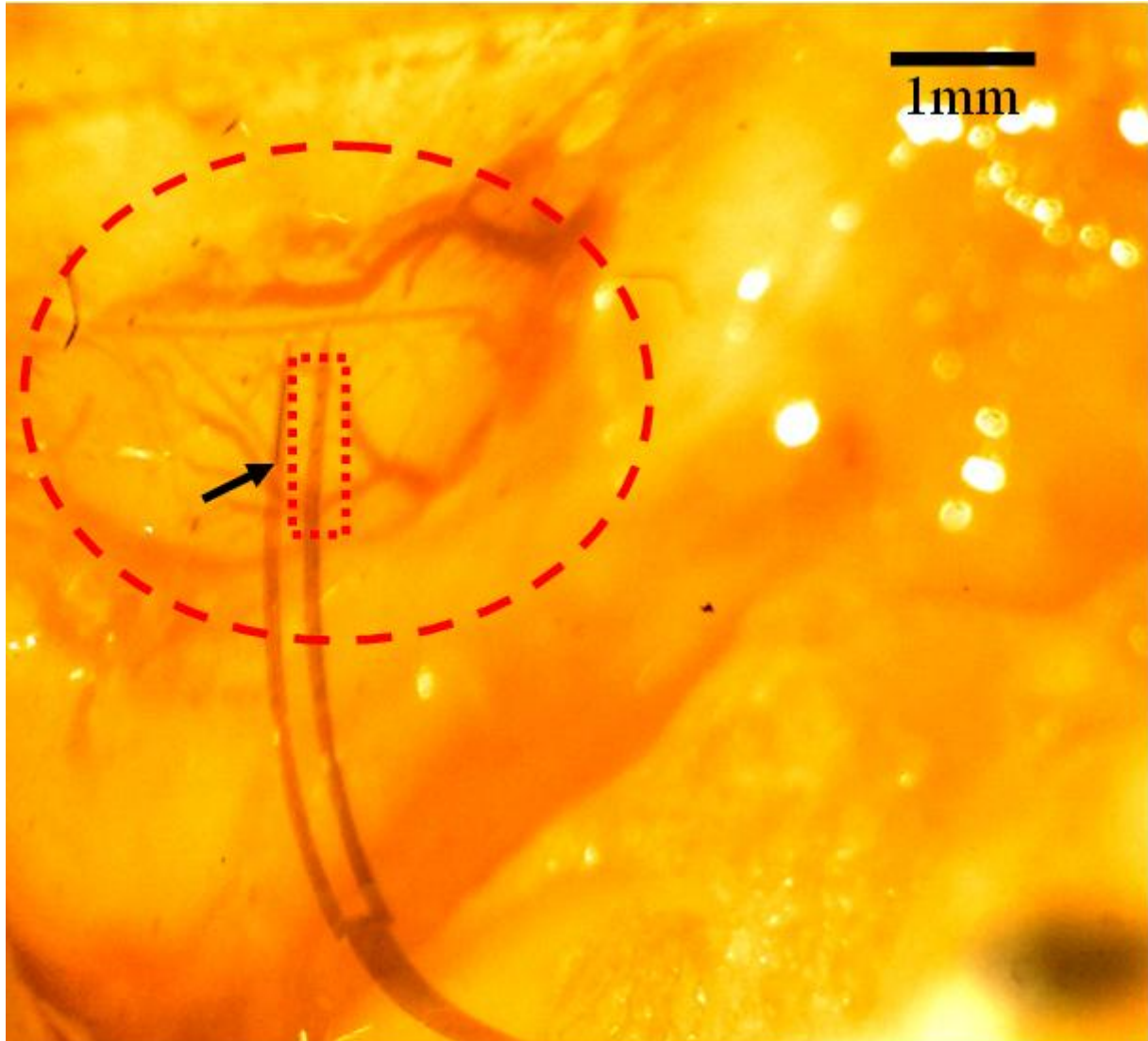


Figure 14: A craniotomy exposing left auditory cortex, indicated by a red circle. Two shafts electrode is resting on the surface before insertion, indicated by black arrow. Red box indicates the four working contact sites.

Topical antibiotic cream is applied to the wound, and 0.5 mg buprenorphine (**(subcutaneous administration)**) is given immediately post-operatively and then as needed based on visual or auditory observations of distress signs (Buprenorphine, dosage of 0.1 mg/kg - 1.0 mg/kg administered by a subcutaneous injection every 6 hours - 12 hours). Visual signs include seeing an animal compromising his motion or grooming due to obvious tenderness. Auditory signs could be excessive vocalizations when handled normally or even simply when sitting in the home cage, indicating pain or hypersensitivity. Animals are recovered in an incubator for several hours until initial signs of ambulatory motion are seen.

If excessive edema (the cortex swollen to 3 mm past its normal resting state) is observed during surgery, an anti-inflammatory agent is administered. In such a case, dexamethasone is administered post-surgery (200 micrograms/kg body weight pr day up to 7 days post surgery, subcutaneous injection).

Chronically implanted animals usually return to a normal state in 1-2 days, and at this point are considered recovered. Sutures are removed by hand 2 weeks post-surgery.

3.4.3 EUTHANASIA

Euthanasia is induced in the following cases;

1) Animals are sacrificed if they do not return to a normal state within 5 days following chronic, survival surgery (1-2 days of recovery time is considered normal).

2) Animals are also immediately sacrificed at any time following implant, if the connector mound becomes dislodged (rare event) or they show obvious physical stress

in response to the implant (for example: excessive blood or pus-lined discharge from the wound site, or excessive scratching and manipulation of the implant area)

3) Animals are sacrificed when they have fulfilled the electrophysiological testing or the implanted electrodes fail to produce satisfactory signals.

3.4.4 HISTOLOGY

For histological study, 8 animals were implanted as shown in Figure 15. Survival protocol was used for histological studies. Each animal had four individual craniectomies marked by injury control (I), polyimide control (PI), test device (X). The injury control was simulated by first inserting a polyimide device and then immediately removing it. Polyimide single shaft devices were implanted for polyimide controls and either polyimide devices (4 animals) or PGA coated devices (4 animals) were implanted as the test devices. Once the rats were implanted for a minimum of 15 days, histological procedures are performed to study the biocompatibility of the polyimide devices and the PGA coating under implanted conditions. This is started by first, anesthetizing the animals scheduled for histological examination of implanted brain tissue with administration of a large dose (doubled 0.2 ml/100 g body weight) of the normal 10:1 Ketamine (50 mg), Xylazine (5 mg) mixture. Next the animal is perfused with saline solution through the heart followed by formaldehyde fixation solution. Brain tissues are then extracted and stored in the above mentioned formalin solution. Each implanted brain area is separated by sectioning the brain tissue at the central sulcus and longitudinal fissure. Beyond formalin fixation, subsequent paraffin embedding technique is used to help harden the sectioned tissue to allow for obtaining very thin, 4-5 micron slices. This is

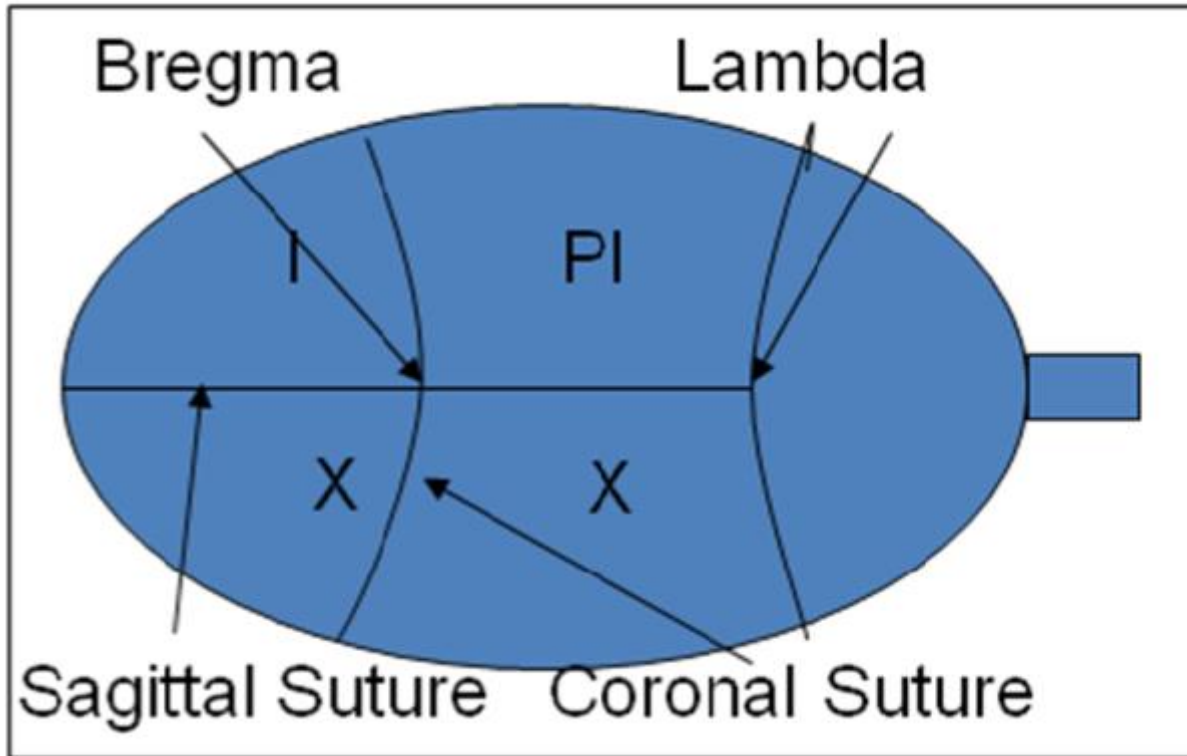
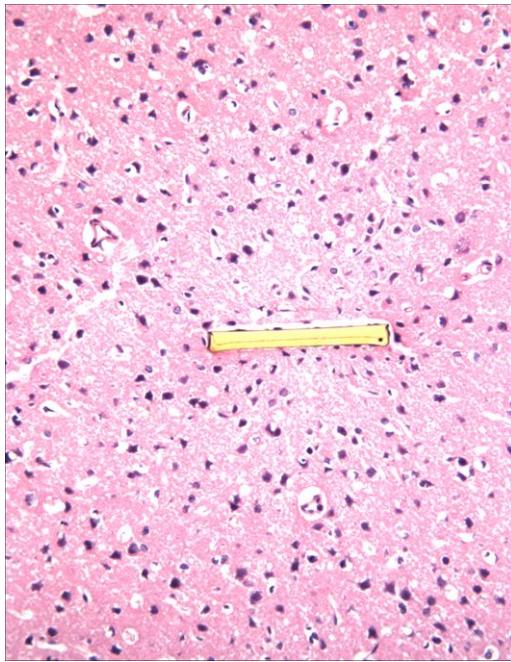


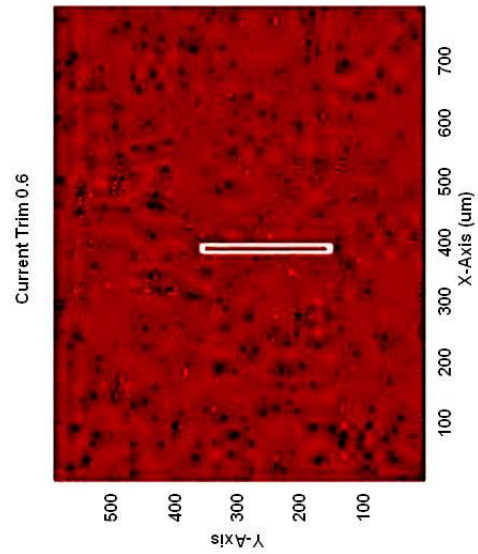
Figure 15: A Typical layout of implants done during histology studies. (I) marks the sites of injury where a device was implanted and then removed. (PI) marks the sites where polyimide devices were implanted. (X) marks the sites where test devices, polyimide or PGA coated devices, were implanted.

followed by mounting and staining of slides with H&E and GFAP histological stains. See appendix B for detailed staining protocol. Figure 16 shows one such H&E stained slice, cut perpendicular to the implant and illustrates the procedure to compute cell density. Figure 16a, is an original image showing a cross section of polyimide strip embedded in the cortical tissue. Figure 16b, shows a red filtered, increased contrast, contour plot of the original image. The figure is red filtered to reduce complexity of the image for analysis purpose. Also since the background tissue is rich in color red, red filtering provides highest contrast. The red filtered color values are normalized over the range of 0-1 (1-highest level of red, 0-complete absence of red). Then a trim value is selected to increase contrast. Any value of red above the trim value is assigned value of 1 and value of 0 is assigned otherwise. This increases the contrast and allows for cell detection. Furthermore, it also eliminates noise signal near the edges due to lower intensity of light. Figure 16c, shows the image after cell detection and counting is performed (513 cells were computed in this example). Lastly, a window size is selected to perform local cell count and compute cell density. The software allows choosing an overlap between two consecutive windows, but zero overlap was chosen of these dataset. Figure 16d shows a contour plot of cell density computed using $40\text{ }\mu\text{m} \times 40\text{ }\mu\text{m}$ windows.

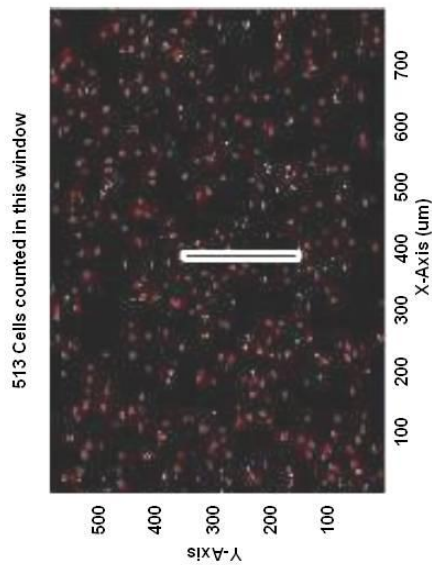
To characterize the GFAP stained gliosis, we obtain a gray scale intensity profile of the GFAP stained image. The darker gray regions in the image correspond to GFAP staining indicative of gliosis. The lighter regions are suggestive of the lack of glial fibers in the corresponding region. First we obtain a grey scale image of a GFAP stained



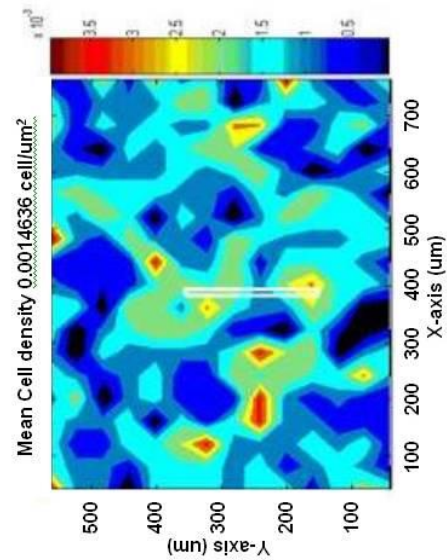
(a)



(b)



(c)



(d)

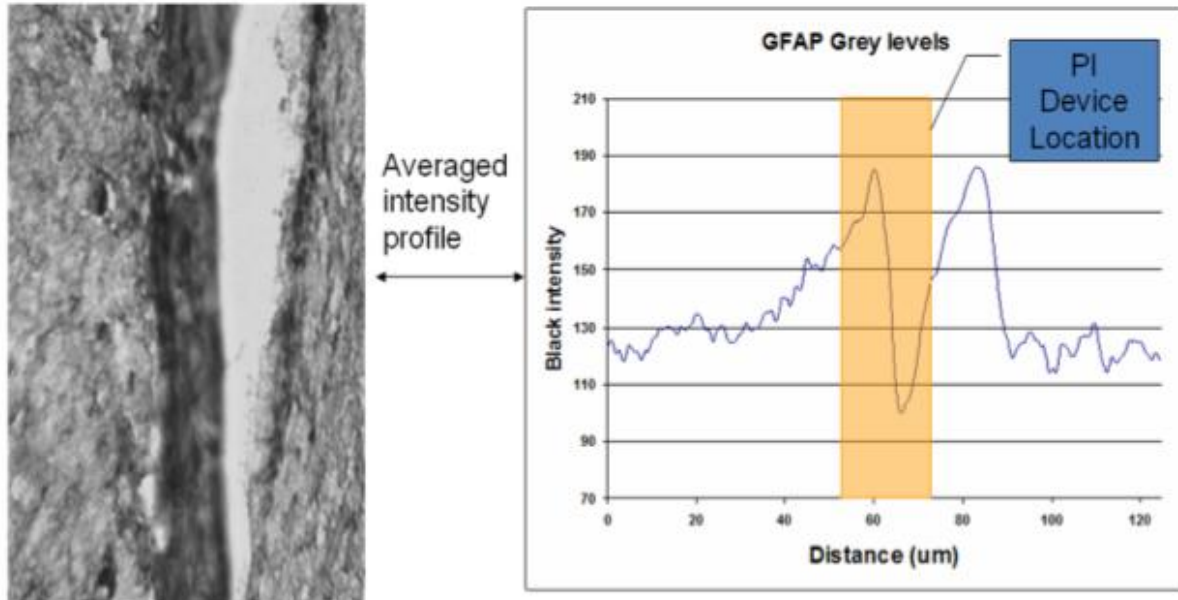
Figure 16: Outline of steps performed to compute cell densities. (a) Original picture capture under microscope. (b) Red filtered, high contrast image. (c) Image displaying detected cells, cell count displayed in the title. (d) Image displaying cell density, mean cell density displayed in the title.

tissue slide (Figure 17a). Then we align the sectioned device with y-axis along its length. The mean grey intensity profile is computed by summing the grey levels for all the pixels in a column and dividing it by number of rows. The mean intensity values are then plotted against the x-axis (Figure 17a). The region along the x-axis corresponding to device is visually ignored in computing the parameters, grey intensity peak and grey intensity width (Figure 17b).

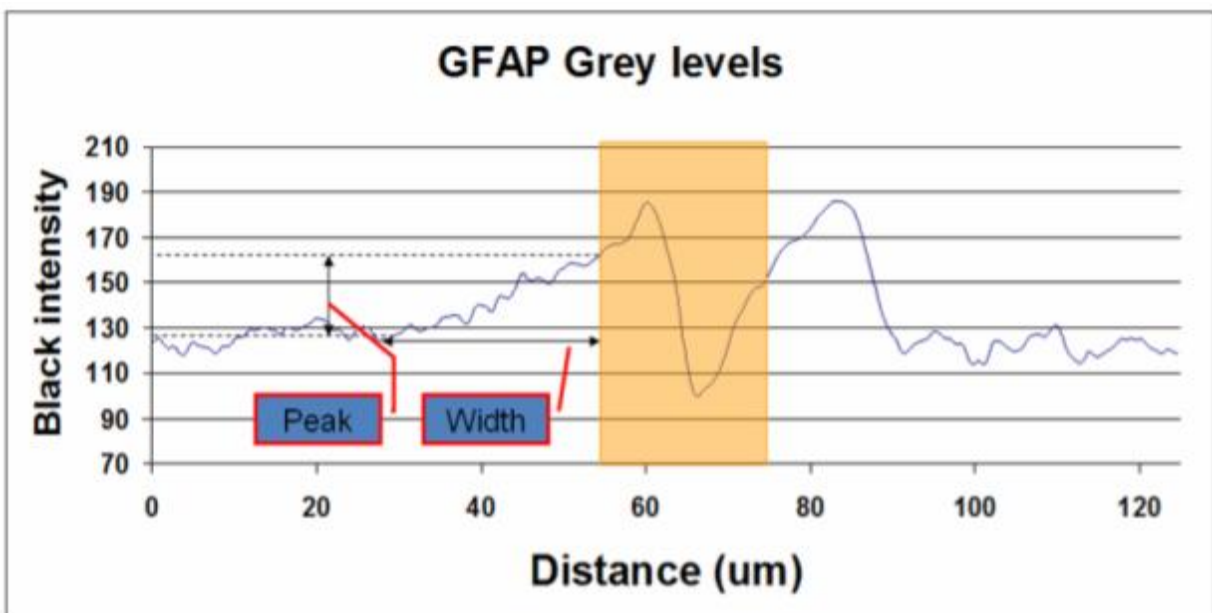
3.4.5 RECORDING PROTOCOL

Following craniotomy polyimide device is held over the exposed cortical tissue using stereotaxy frame. The device is then pressed onto the cortical surface and allowed to buckle. This allowed enough slack to develop between the anchor point on the frame and cortical surface. At this point the shafts of the device are grabbed simultaneously at approximately 2 mm to 3 mm from the tip using fine forceps and directed perpendicular to cortical surface. Insertion force applied across the short shaft distance allowed the electrodes tip to easily penetrate the cortical surface through pia and be inserted to appropriate depth of 700 μm to 1 mm. The device is anchored to the stereotaxy frame at the custom made interconnect already mounted onto the electrode prior to the surgery. Interconnect transforms the Hirose flip-lock connector to Omnetic 18 pin connector in order to interface with recording system.

A commercial multichannel recording system (Tucker-Davis Technologies Inc.) is used to collect simultaneous neural recordings from active polyimide probes. At the connector site, unity-gain head stage FET amplifiers provided high input impedance and current amplification to preserve signal-to-noise ratios along the cable to the bio-signal amplifier.



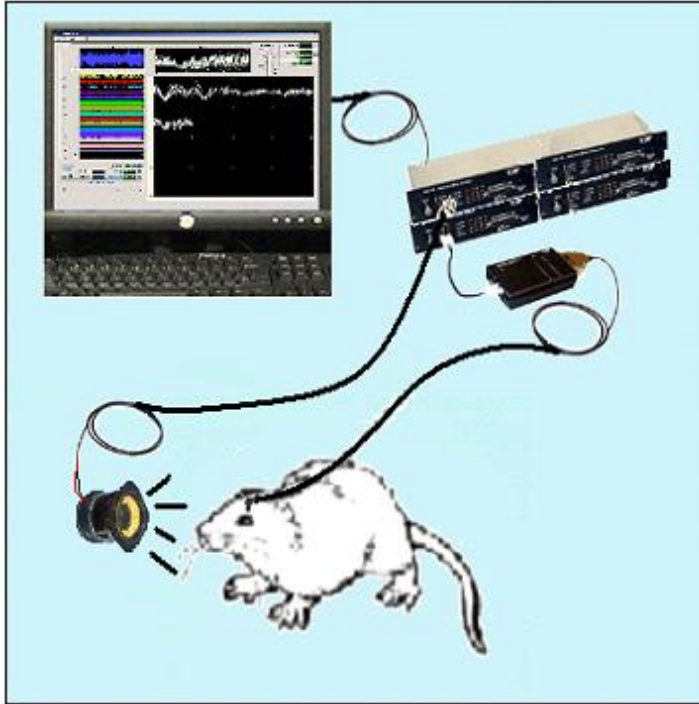
(a)



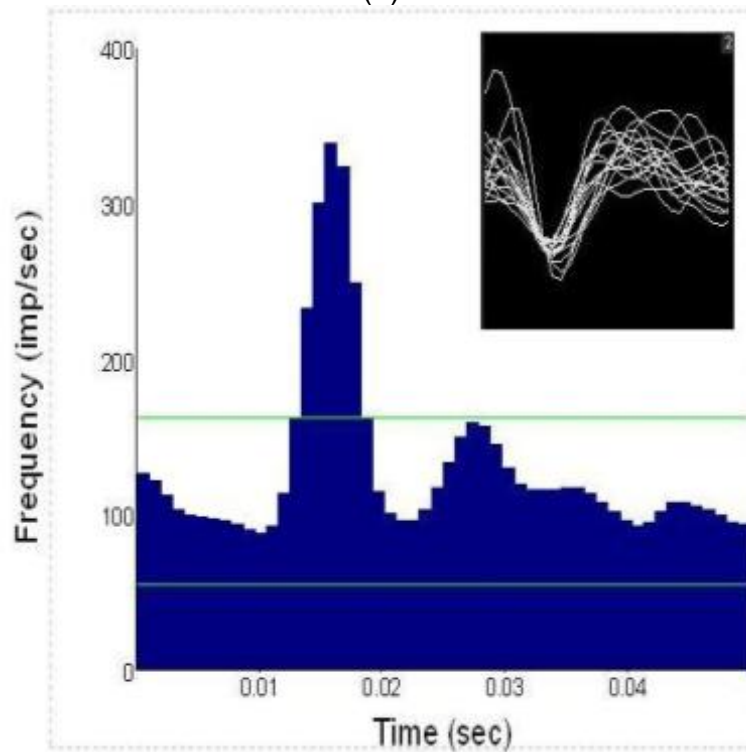
(b)

Figure 17: (a) Mean GFAP expressions (grey levels) are computed from the grey scale image of a GFAP stained tissue section and plotted along the x-axis. Darker regions in the image corresponds to higher GFAP staining and therefore higher glial fiber expression. The peaks in the grey scale profile correspond to the darker grey regions. (b) Peak GFAP expression is computed as peak deviation from the base line and GFAP expression width is computed as the distance from the onset of deviation from the baseline to the Peak GFAP expression. The orange boxes represent the device location.

The system digitizes the signals (25 kHz) with low-noise 16-bit A/D converters (± 7 mV operating range; $5 \mu\text{V}$ - $6 \mu\text{V}$ rms noise floor; $0.2 \mu\text{V}$ resolution) and then multiplexes the recorded signals on a 10 meter fiber-optic cable to the rack-mounted hardware. Signals are band-pass filtered from 300 Hz - 5000 Hz, and neural spikes are detected when signals crossed a threshold of 1.5 times the baseline RMS noise (1second calculation window). Click stimuli are used to characterize the neural responses on each electrode. Click stimuli were presented every 600 milliseconds for varying durations from 2 minutes to an hour. The recorded signals are then amplified 10000 fold and displayed by custom-written TDT open-ex software environment. Neuroexplorer (NEX) software (Plexon Inc.) or custom written Matlab software is used to create peri-stimulus time histograms (PSTHs). The majority of recordings were lower amplitude multiunit activity ($50 \mu\text{V}$ - $100 \mu\text{V}$); single units could not be readily isolated from the record. Figure 18 illustrates the recording setup (a) typical PSTHs are generated with (b) and a sample of unit activity (b-inset) recorded using the polyimide devices.



(a)



(b)

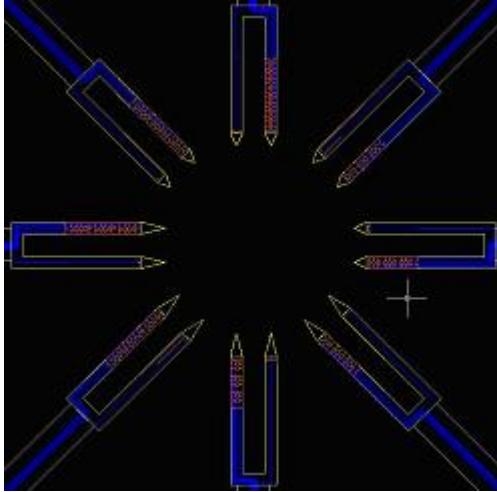
Figure 18: TDT recording setup used for electrophysiological recording (a). Typical PSTH generated using NEX software (b). Sample unit activity recorded and displayed by TDT (inset).

CHAPTER 4. RESULTS

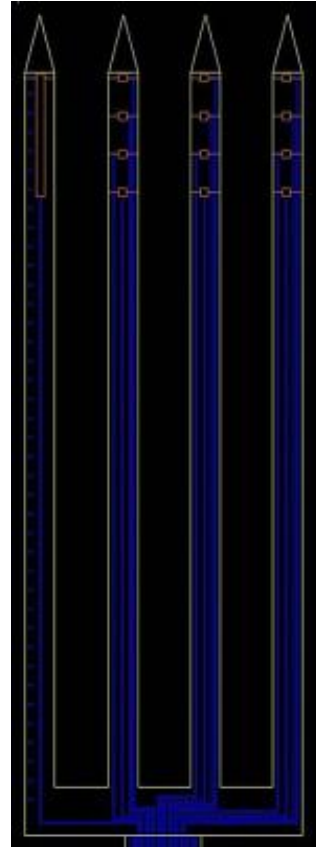
4.1 MANUFACTURING

4.1.1 AUTOCAD

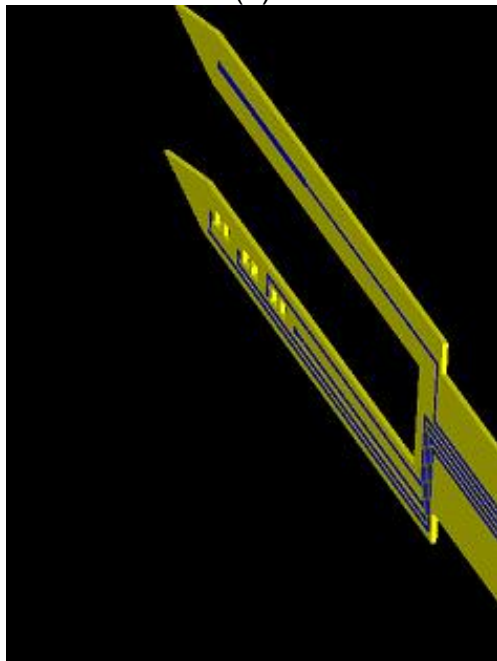
Layout and device design was done using AutoCAD software and is a significant step in device manufacturing. Determination of device shape and dimensions are done during this step. Connector selection, which was restricted by the recording system (TDT) discussed above, provided the first constrain on number of sites and therefore lower bound on the width of the devices. Two shafts device with four sites per shaft (Figure 19a) was chosen as standard device to allow for equal spatial sampling. Variations on the number of shafts were then considered. See Figure 19b for an example of a four shaft device. The taper tips were chosen to concentrate the force applied for insertion and allow for easier penetration into the cortical tissue. Also, Edell et al. in 1992, showed that tapered tipped devices induced smaller kill zone then dull tipped devices, due to reduced degree of trauma during insertion (7). Kill zone is a region of space in the brain near the inserted device exhibiting a significant decrease in viable cell density. Two different taper angles were arbitrarily chosen, as seen Figure 19a. The radial design was chosen to maximize device density and also to ensure uniformity in polyimide wafer coating. The design for connector end of the device was chosen to resolve connector mounting issues observed. Namely, during the soldering stage the heat of soldering iron would melt the polyimide, damaging the device and making soldering exceedingly difficult. Hence snap on connector was chosen with an



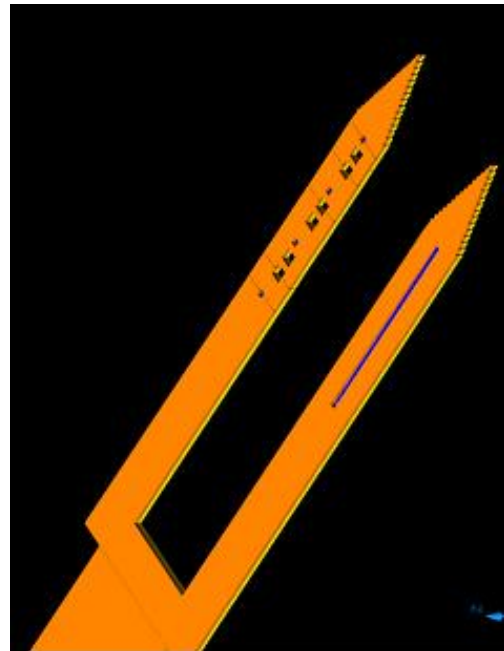
(a)



(b)



(c)



(d)

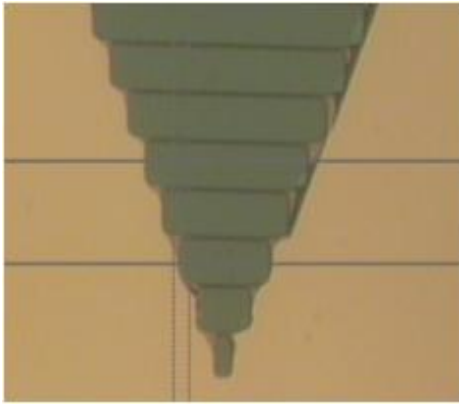
Figure 19: AutoCAD design of the masks manufactured in NCF facility. (a-b) Close up of shafts and connector modules. (c-d) AutoCAD models of a two shaft devices with and without top polyimide layer.

interconnect module to interface with TDT, recording system. Figure 19c shows a rendering of a two shaft structure; metal traces are shown in blue. Figure 19d shows an AutoCAD model of a completed two shaft structure. See Figure 23 for a sample of an actual device. The 3-D rendering was done using AutoCAD software. The connector module is standard for all the devices and is 9.55 mm wide. There are 18 connection pads corresponding to 18 connector sites accepted by TDT. The 10 mm long stem is also standard amongst all the devices and is 400 μm wide. Each stem holds eighteen 10 μm wide traces with 10 μm inter-trace distance, which connects the fork module with the connector module. This dimensionality for traces was chosen to maximize trace density, minimize line impedance and keeping in mind, allowed resolution for patterning on top of polymers (polyimide). The fork module consists of up to 3 shafts with 4 sites per shaft and an additional ground strip shaft. Local ground is chosen to study effects of local reference vs. bone screw reference located across the cortex with respect to the recording sites. 40 μm x 40 μm square sites to give 1600 μm^2 recording surface with 200 μm inter-site distance were chosen, which are deemed optimal as per literature. The local reference strip was chosen to be 40 μm x 640 μm spanning the same amount of space as taken by 4 sites along the shaft. Inter-shaft distance of 284 μm was arbitrarily chosen. Lastly, small 10 μm x 20 μm milestone markers were placed along the local reference shaft to approximate insertion depth, during implant procedure. Each of the three structures (namely, bottom polyimide in yellow, middle metal in blue and orange top polyimide) were designed onto their individual layers and then superimposed to give a continuous structure look, particularly illustrated in Figure 19c-d.

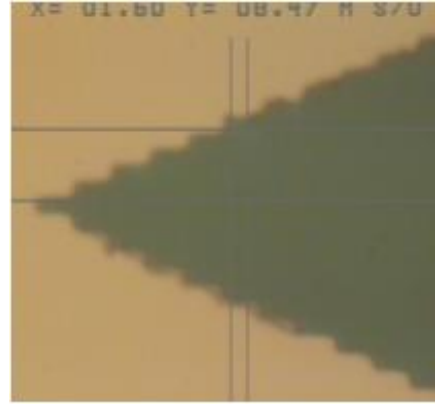
4.1.2 MASK PROCESSING

Next step in manufacturing was to produce masks corresponding to each of the layers discussed earlier. The masks are glass plates coated with chromium on one side.

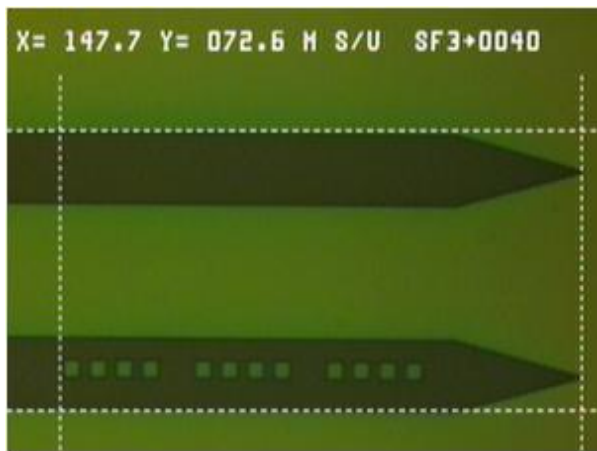
The chrome side is further coated with spun-on positive photoresist. The plates were purchased in the described state from NCF. Additionally, mask conversion software was used to convert AutoCAD layers into matrices of coordinates and given to NCF. NCF exposes the resist cover mask plates as per instructions. One exposed mask plate per layer was obtained from NCF. The exposed patterns on the plates were then developed and etched using same techniques as discussed previously for metal layer patterning of the devices. Figure 20 and Figure 21 samples images of different sections of the masks. A sample of incorrectly patterned mask of the bottom polyimide layer is shown in Figure 20a. Using this mask would produce a discontinuous strip of polyimide. Figure 20b, is a good tip image of the bottom polyimide layer mask of a shaft. Figure 20c-d, shows bottom and top polyimide layer masks, respectively, of a two shaft device. The measurement of $40\text{ }\mu\text{m} \times 40\text{ }\mu\text{m}$ contact sites openings in the top layer is shown in Figure 20e. The actual site opening was measured to be $38.3\text{ }\mu\text{m} \times 37\text{ }\mu\text{m}$. Finally, a four shaft device mask is shown in Figure 20f. Metal layer mask is shown in Figure 21. Figure 21a-b shows $20\text{ }\mu\text{m} \times 20\text{ }\mu\text{m}$ and $40\text{ }\mu\text{m} \times 40\text{ }\mu\text{m}$ contact sites respectively. Figure 21c-e samples the traces leading from contact sites to the connector modules. Lastly, sample of alignment marker used on each layer to aid in aligning with previous layers is shown in Figure 21f.



(a)



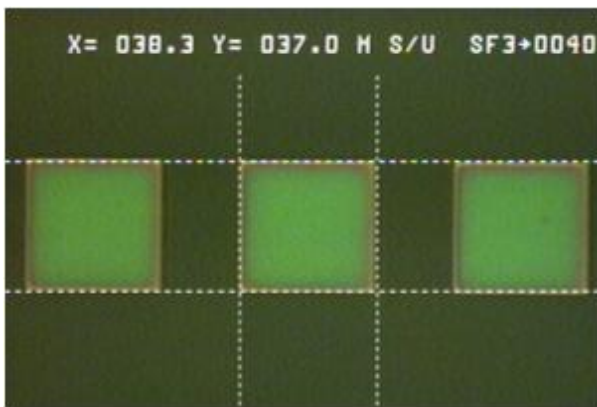
(b)



(c)



(d)



(e)



(f)

Figure 20: Processed polyimide layers masks. (a) Electrode tip patterned incorrectly. (b) Electrode tip, angular tip design was chosen to induce maximum pressure at the point of insertion. (c) Polyimide layer 1 for two shaft devices. (d) Polyimide layer 2 for two shaft devices. (e) Measurement of 40 μm x 40 μm via and contact site openings. (f) Multishaft device, polyimide layer 2

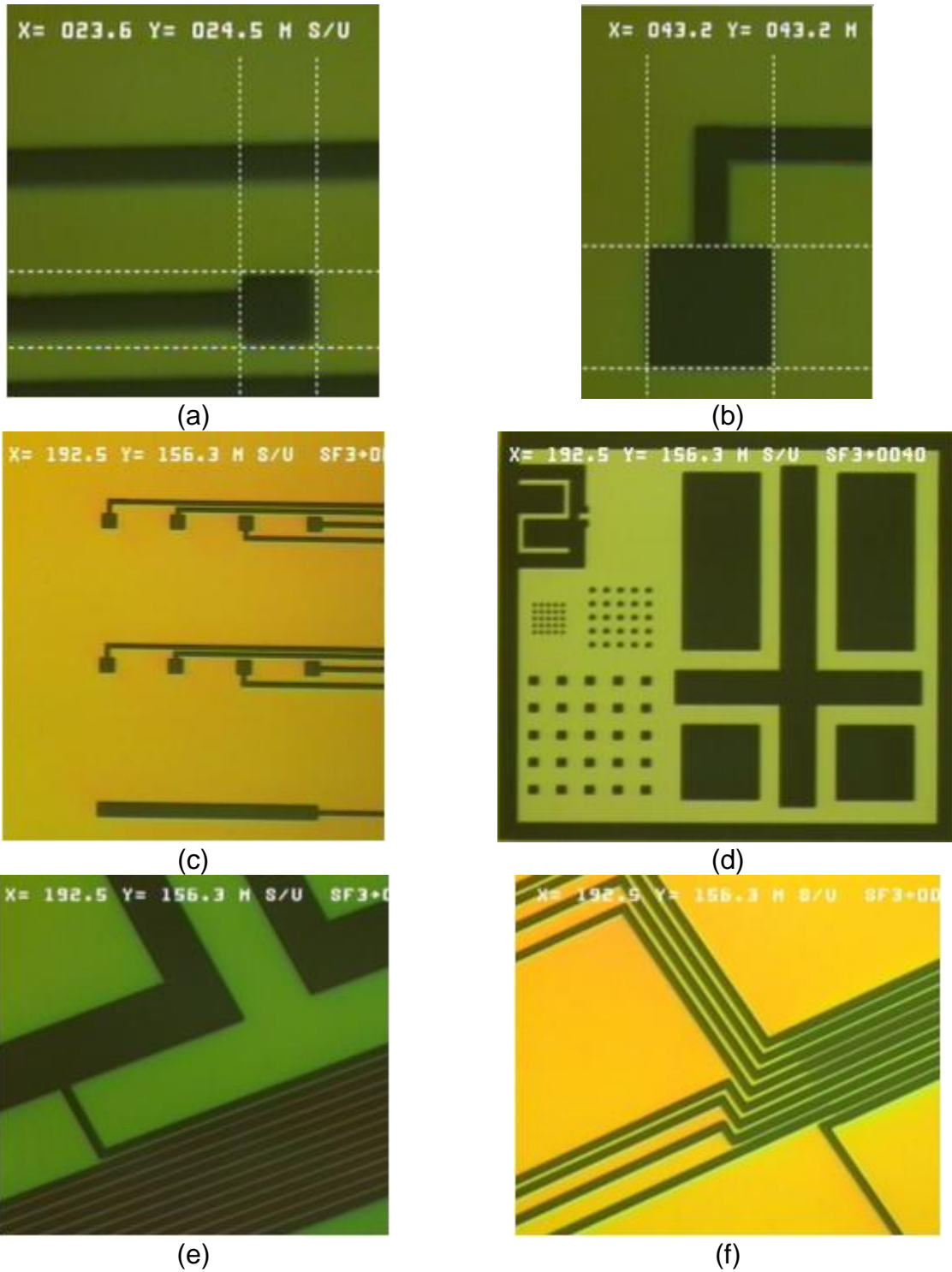
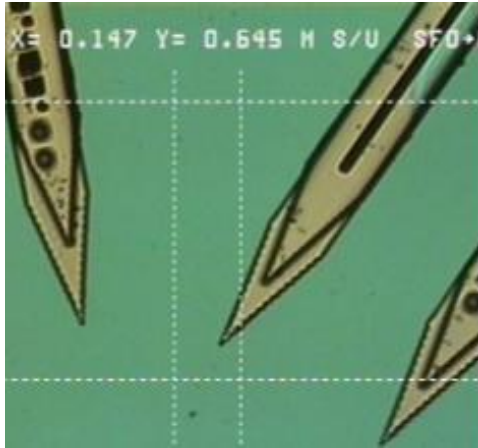


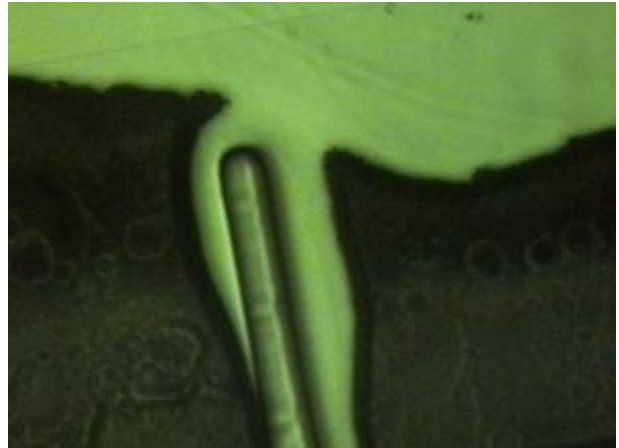
Figure 21: Processed metal layer masks. (a) 20 μm x 20 μm contact site. (b) 40 μm x 40 μm contact site. (c) Three shafts contact array with local reference in the bottom shaft. (d) Typical mask alignment markers. (e) Traces near connector pads. (f) Traces connecting contact sites to stem traces.

4.1.3 LITHOGRAPHY

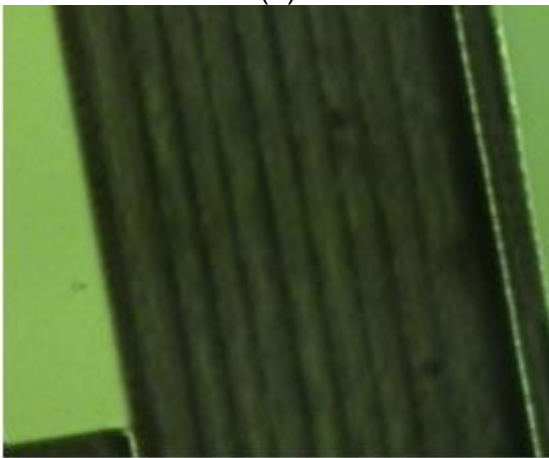
Lithography process had its own set of problems that were resolved as the process parameters were fine tuned. The next set of images outlines problems seen during lithography stage of the manufacturing process. Miss-aligned layers of polyimide, which was attributed to the lack of appropriate alignment markers are illustrated in Figure 22a. This lead to improper visibility of the substrate situated underneath the mask during exposure. Polyimide is a negative photoresist and therefore, polymerize upon exposure to UV light. This nature of polyimide forces one to use a dark field masks. In a dark field mask chrome is etched only within the device boundary, resulting in chrome coating majority of the masks field. This shortcoming was overcome by placing large open windows distributed over the field of the mask. The remaining set of images pertains to problems encountered during the processing of metal traces. **Error! Reference source not found.**b and c are examples of photoresist adhering to the metal surface too strongly and therefore not appropriately dissolving during development process. By shortening the bake time of the photo resist and removing reactive ion etch (RIE) cleaning step after metal deposition eliminated this problem. After implementing these two modifications to the protocol, traces were observed to lift off from the surface as seen in **Error! Reference source not found.**d-f. This was discovered to partly result from inappropriate development of underlying polyimide layer. The process protocol for polyimide was discovered to inadequately remove non-polymerized polyimide leaving a thin film on top of the surface. This film would later dissolve during metal processing as the wafer was submerged into water for cleaning of solvents. Increasing the develop time of polyimide



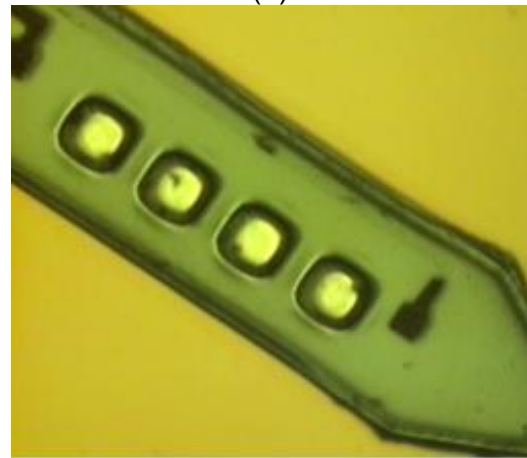
(a)



(b)



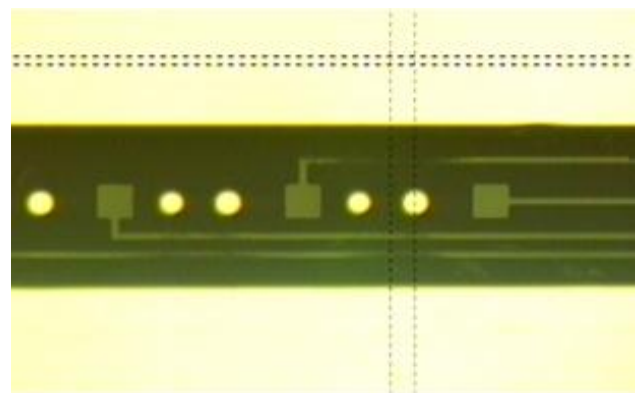
(c)



(d)



(e)



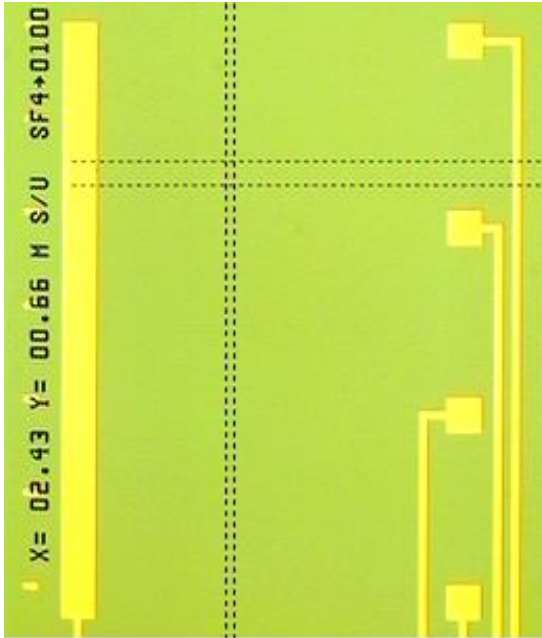
(f)

Figure 22: Issues encountered during device processing (a) Miss aligned polyimide layers due to improper alignment markers (b) Metal fails to etch uniformly, especially between traces as seen in (c). (d) Traces fail to adhere to polyimide surface. (e) Traces peel off near corners. (f) Traces disappear near via due to shadowing effect.

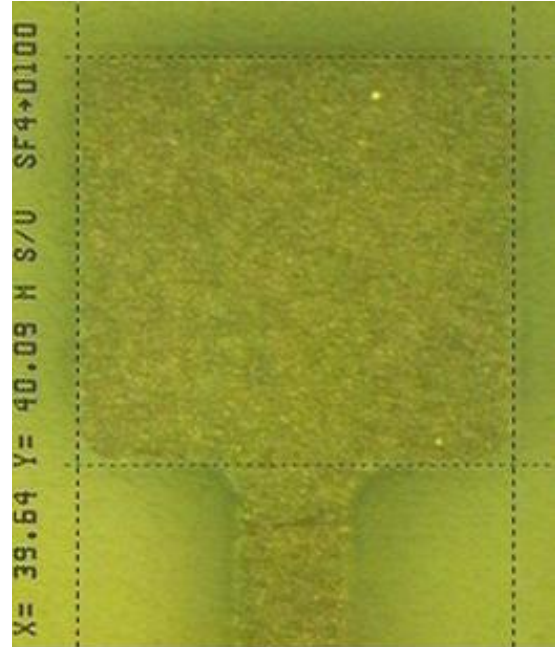
from manufacture recommended 1 minutes to 5 minutes eliminated the peeling of the metal layer from random locations.

The peeling of metal, especially, closer to the edges and corners still remained. The metal processing protocol was verified by successfully patterning metal directly onto the silicon surface and onto a uniform sheet of polyimide spanning the entire wafer. The results from this process are shown in Figure 23a-d. Contact and Optical profilometer images, shown in Figure 24a, c and Figure 24b, d respectively, revealed that the surface of the polyimide curved with depths of 0.2 μm to 0.5 μm . This curvature is comparable to the average thickness of 1 μm obtained from the spinning the photoresist. The curvature in the device caused the photoresist to pool towards the center resulting in an inadequate coating of the photoresist towards the edges of the device.

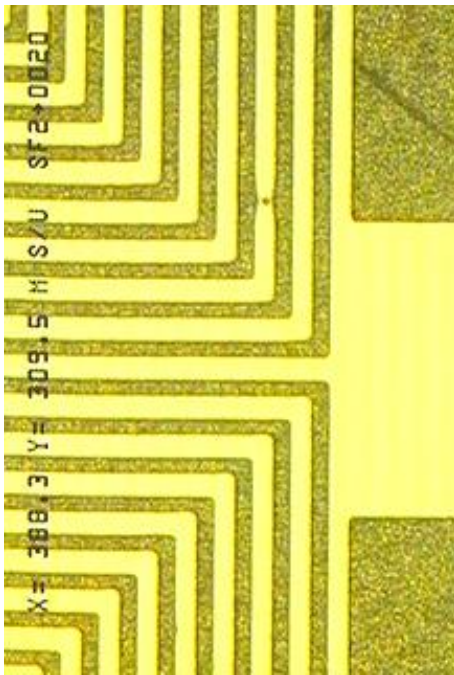
The surface curvature of the polyimide can be attributed to either the interfacial stress or an uneven heating profile during the bake step promoting uneven mass transfer. The case of interfacial stress could occur during the curing phase when, the substrate is heat to 85 $^{\circ}\text{C}$ followed by 95 $^{\circ}\text{C}$ and then cooled to room temperature. During the cooling phase, silicon substrate would cool faster than polyimide, warping the overlaying polyimide. The consistency of the surface profile curvature suggests that the interfacial stress might not be the actual culprit. On the other hand, the proprietary nature of the HD-4000 polyimide solution's chemical composition does not allow us to quantitatively study the exact nature of the heat and mass transfer. Nevertheless, an order of magnitude approximation, model for the heat transfer was studied using Ansys. The transient temperature profiles at two stages of the baking phase, shown in



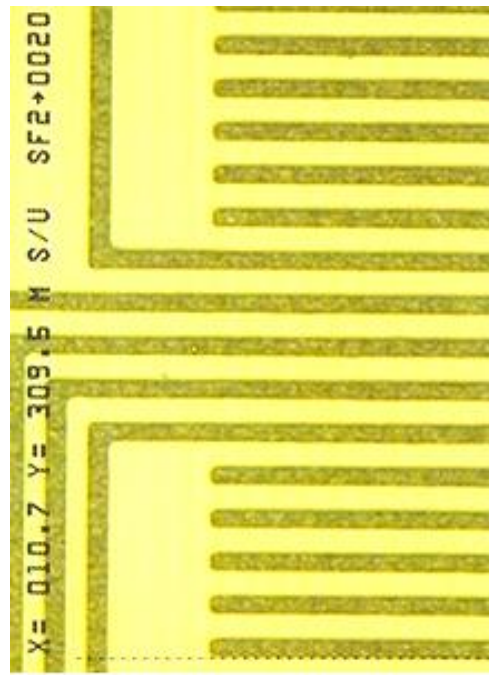
(a)



(b)

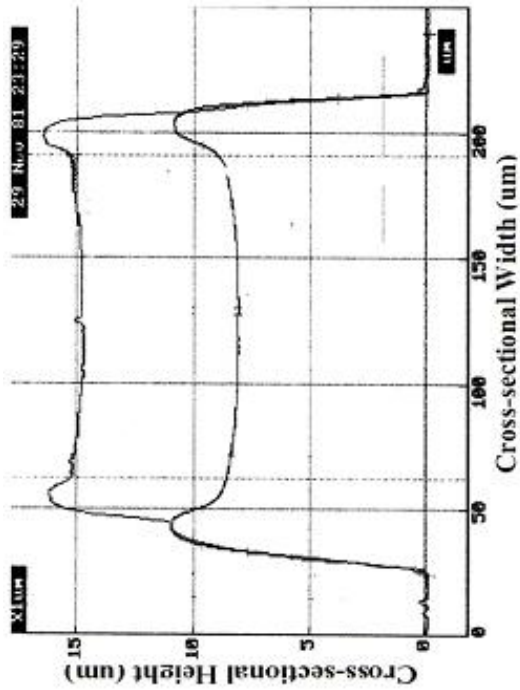


(c)

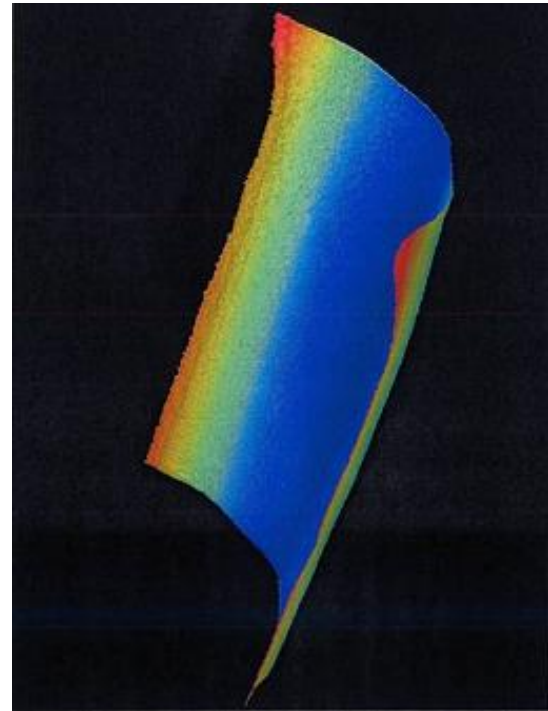


(d)

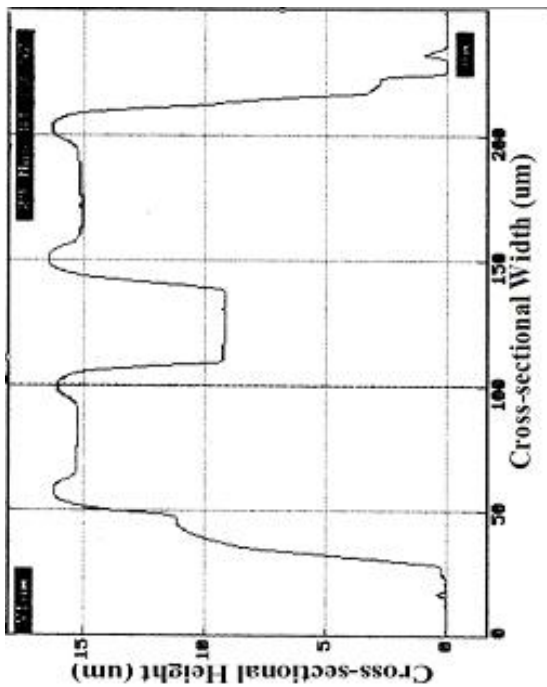
Figure 23: Metal traces reproduced on wafer and sheet of PI surfaces. (a) Traces reproduced on wafer itself. (b-d) Metal traces reproduced on polyimide sheets after pre-curing, polyimide.



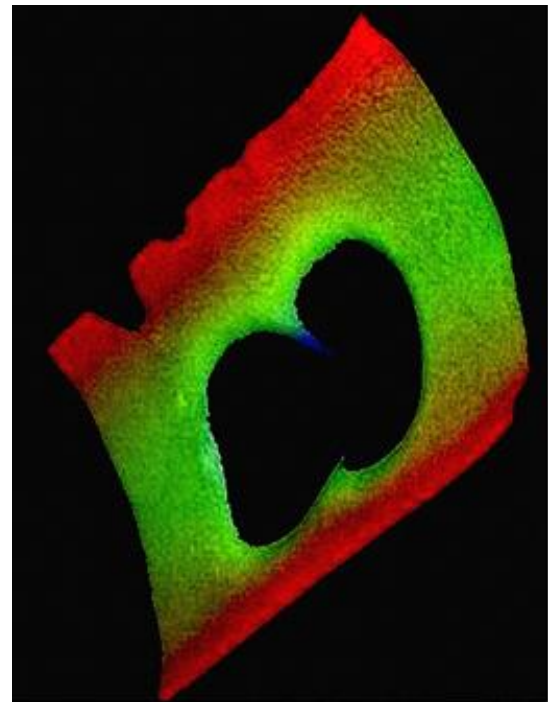
(a)



(b)



(c)

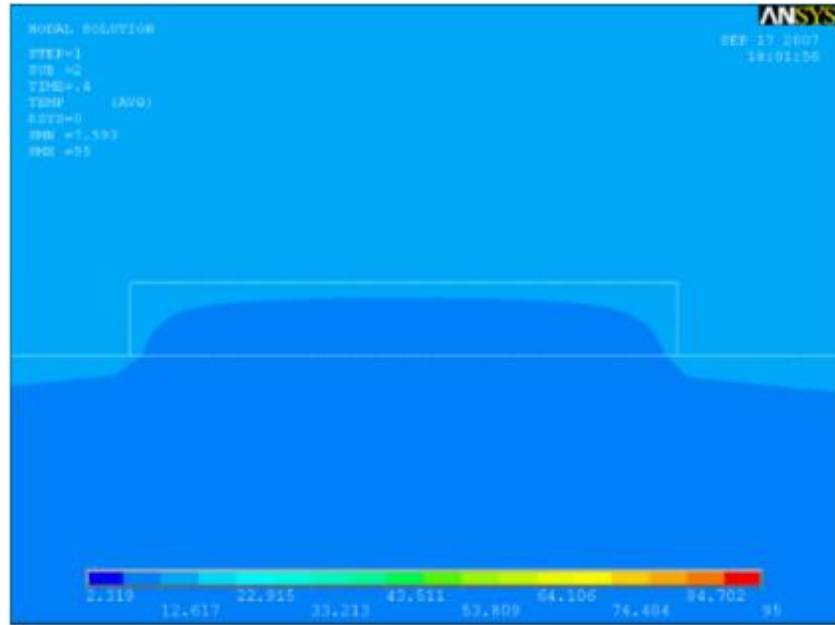


(d)

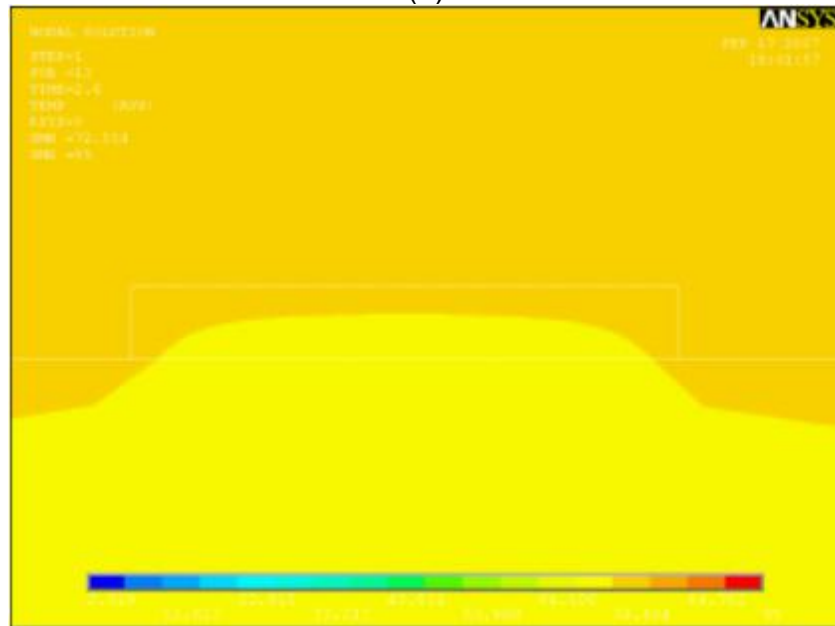
Figure 24: a) Typical profile of layers 1 and 2 (super imposed graphically) of the patterned polyimide shaft. b) Optical profile of a shaft surface shows the curvature of the first layer of a device. c) Surface profile through a contact site. d) Optical profile around via.

Figure 25a and b, revealed non-uniform profile suggesting non uniform mass transfer. Table 2 lists the material properties used in Ansys to create the model.

Ideally, a variable heat source to compensate for the non-uniform heating profile would be a solution to the surface warping, but such source was not available. Therefore, as a last resort to overcome poor coating quality of the photoresist on the warped polyimide surface, it was necessary to increase the thickness of the photoresist layer such that the warping was negligible. Lowering the spin speed of photoresist to 2000 rpm allowed for sufficient surface coating while still being able to use manufacturer recommended processing parameter. Lastly, **Error! Reference source not found.** illustrates a final hurdle that was encountered in metal processing. Holes in the bottom polyimide layer presented a shadowing effect, pooling the photoresist into the holes and depriving the nearby traces of photoresist coating. This was resolved by further lower the spin speed to 1500 rpm, 500 rpm below the manufacturer recommended lower spin speed. At this speed, manufacturer claims that, the surface of the photoresist, even though is thicker, and does not have a uniform surface. All the same, non-uniformity of the photoresist surface did not present any measurable impact on the patterned traces. A manufactured device is shown in Figure 26a in comparison to a penny. Figure 26b shows a dummy device similar to the once using in histology studies. Figure 26c-f shows a tip and 40 μm x 40 μm via measuring 35.7 μm x 35.6 μm of a device's first layer, and bottom layers of four and two shaft devices with the top shaft in Figure 26f measuring the width to be 145 μm . Figure 27a shows a sample of completed two shaft device used in animal studies. Figure 27b shows different contact sites measuring 35.6



(a)

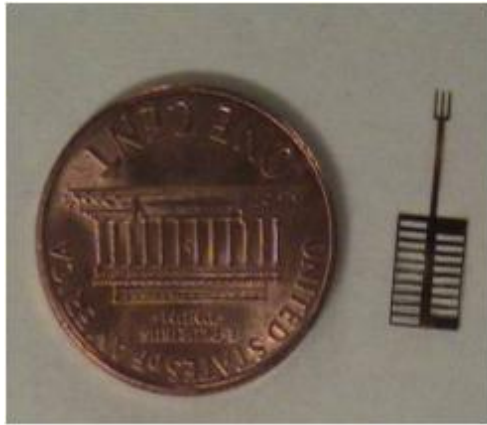


(b)

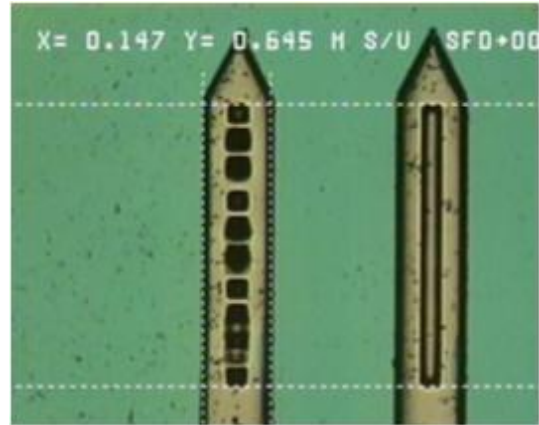
Figure 25: Temperature profile across the cross sectional view of first layer of a polyimide device (polyimide layer is outlined with white rectangular box in the center of the image) resting on 1 mm thick silicon wafer. The 95 °C heat temperature source was applied to the base of the silicon wafer. The temperature across the cross section shows similar but inverted profile in comparison to the measured surface profiles. Scale-bar range is from 0 °C to 95 °C. (a) Heat profile at 0.4sec after the onset of the heat source. Temperature displayed in the image is between 5 °C and 15 °C. (b) Heat profile at 2.6sec after the onset of the heat source. Temperature displayed in the image is between 65 °C and 75 °C.

Properties Material	Density (kg/m³)	Thermal Conductivity (Kxx – W/mK)	Specific Heat (C – J/kgK)
Air	1.2	0.025	1012
Polyimide	1430	0.225	1150
Silicon	2330	4.745	710

Table 2: Material properties used to construct the model in Ansys.



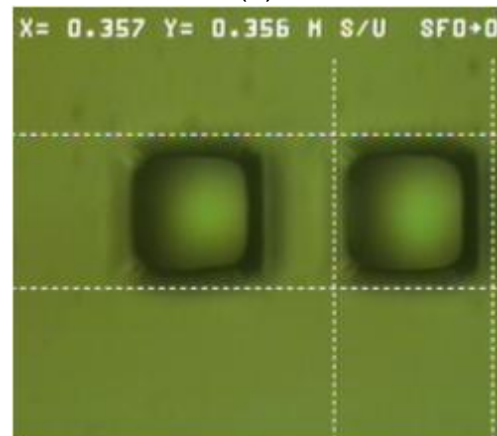
(a)



(b)



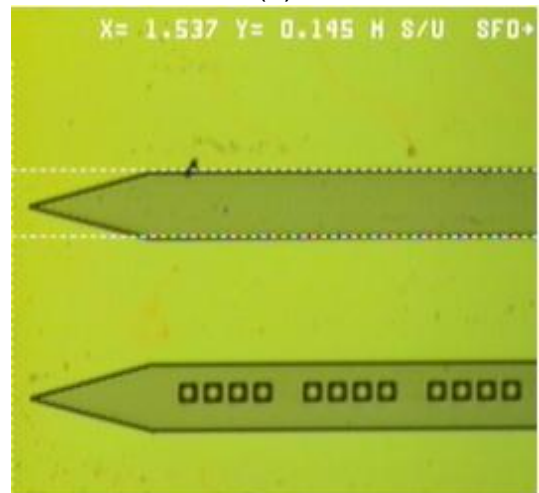
(c)



(d)



(e)



(f)

Figure 26: (a) A device in comparison to a penny. (b) Two shaft polyimide device, similar to the ones used in histology studies. (c) Tip of a shaft, the first layer of a device. (d) Via (holes) in the first layer of the polyimide device. (e) First layer of a four shaft device. (f) A shaft of two shaft device measuring 145 μm wide.

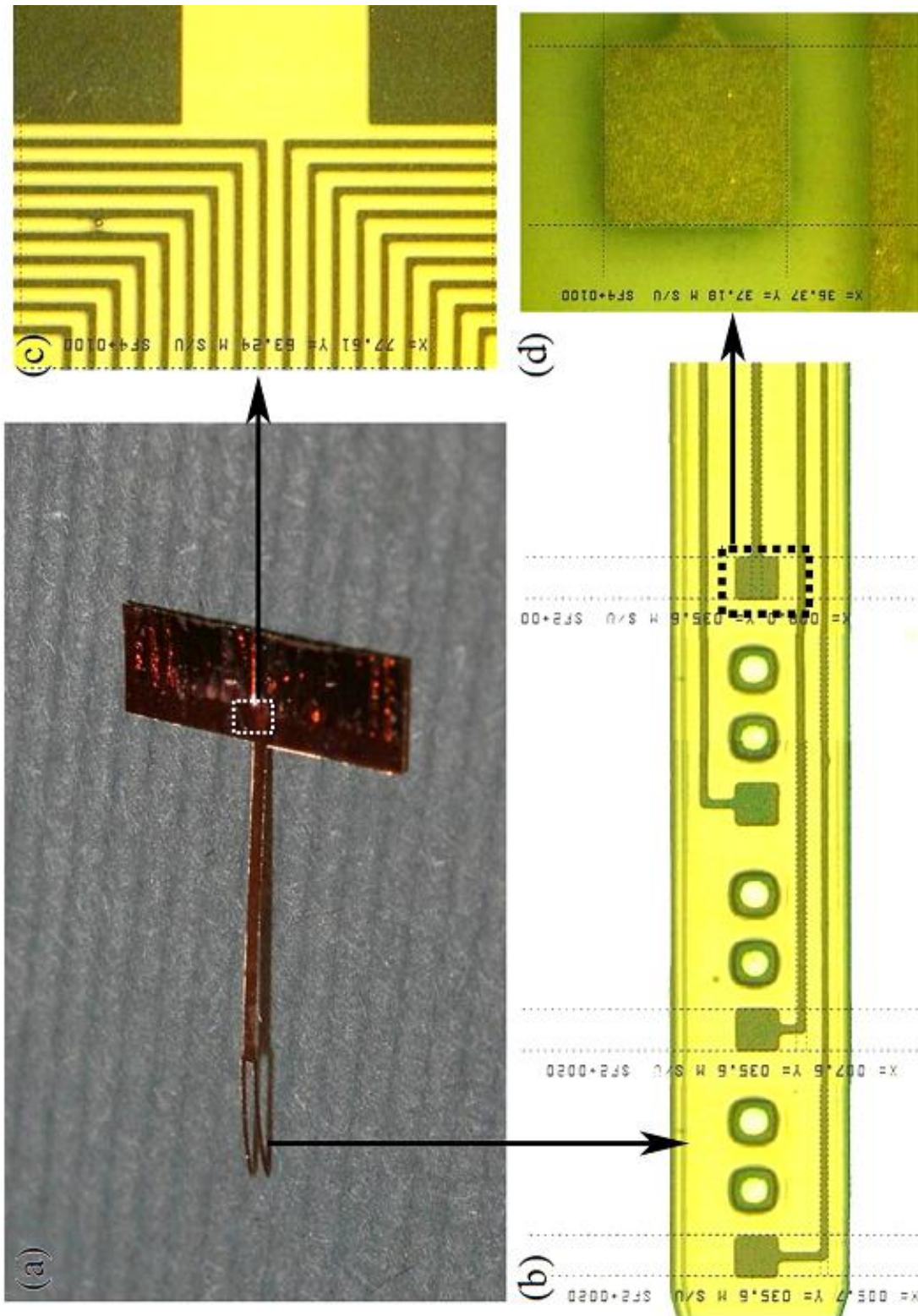
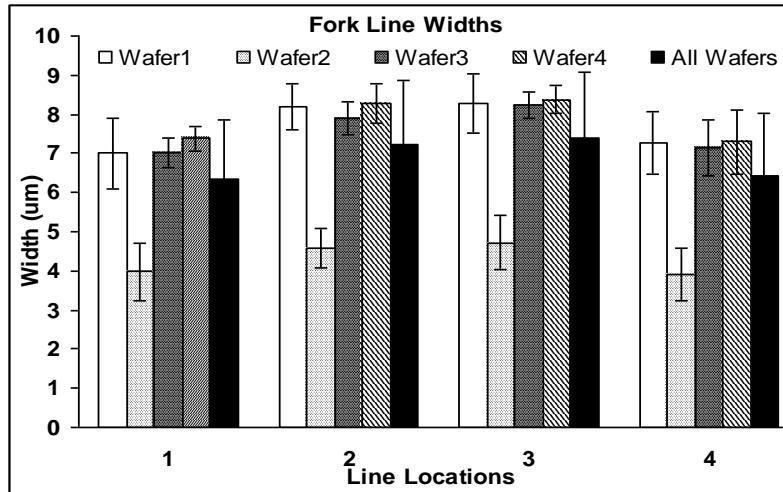


Figure 27: a) A complete two shafts device. b) Four contact sites interspaced with via (image digitally stitched). c) Metal traces leading to the connector pad. d) A close up of a 40 μm x 40 μm contact site.

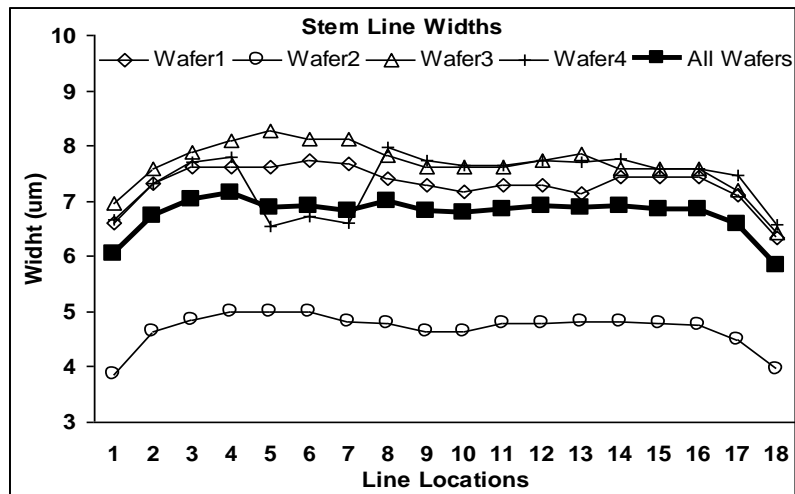
μm in width and neighboring traces with their widths measuring from $5.7\ \mu\text{m}$ to $8.0\ \mu\text{m}$ (note: this image is digitally stitched using three different images). Figure 27d shows a close up of one such contact site. Figure 27c shows traces and inter-trace spacing along the stem and near connector pads. Inter-trace distance measures approximately $12.2\ \mu\text{m}$. Figure 28 summarizes the averages of the measurements of several features of the device. The lines along a shaft of the fork of the device on and average are $6.9\ \mu\text{m} \pm 1.7\ \mu\text{m}$ wide (Figure 28a). The lines along the stem on average measures $6.8\ \mu\text{m} \pm 1.5\ \mu\text{m}$ wide, with wider lines towards the center of the stem width (Figure 28b). The contact sites measures $1369\ \mu\text{m} \pm 677\ \mu\text{m}$ or $37\ \mu\text{m} \times 37\ \mu\text{m}$ (Figure 28c). The width of the contact pads measured $347\ \mu\text{m} \pm 10\ \mu\text{m}$ with no particular trend in size variation in respect to its position on the device. Lastly the thickness of first and second layers of polyimide measured $8.4\ \mu\text{m} \pm 0.3\ \mu\text{m}$ and $14.8\ \mu\text{m} \pm 0.7\ \mu\text{m}$ respectively (Figure 28d).

4.2 IMPLANTATION TECHNIQUE: PGA SURFACE COATING

A 4 GPa young's modulus of polyimide gives the device an excellent mechanical flexibility once implanted, but this also creates a problem while implanting it through a tougher pia membrane blanketing the surface of the brain. Even though implantation can be achieved by carefully dissecting the pia membrane, it results in a greater damage to the underlying brain tissue. Furthermore, removal of the pia membrane also removes some of the smaller blood pathways embedded in the pia tissue. As an alternative, PGA coating is applied to the device that temporarily enhances the mechanical stiffness of device and allows insertion of the device right through the pia membrane minimizing the damage to the brain. Figure 29a shows a set of sample

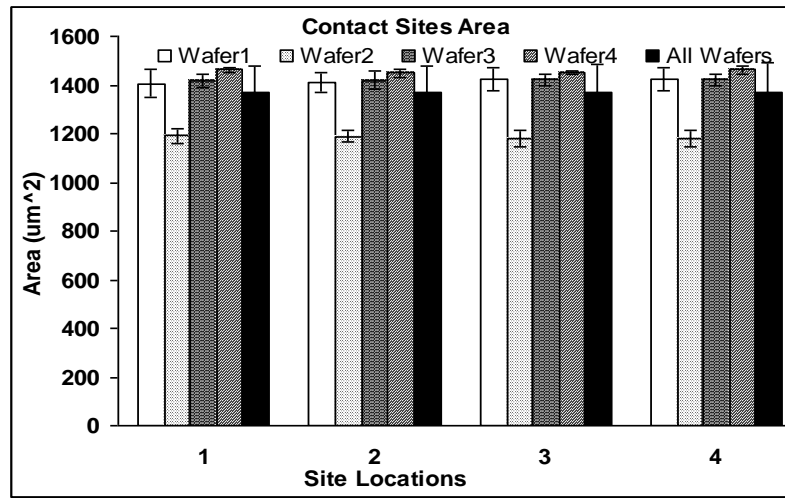


(a)

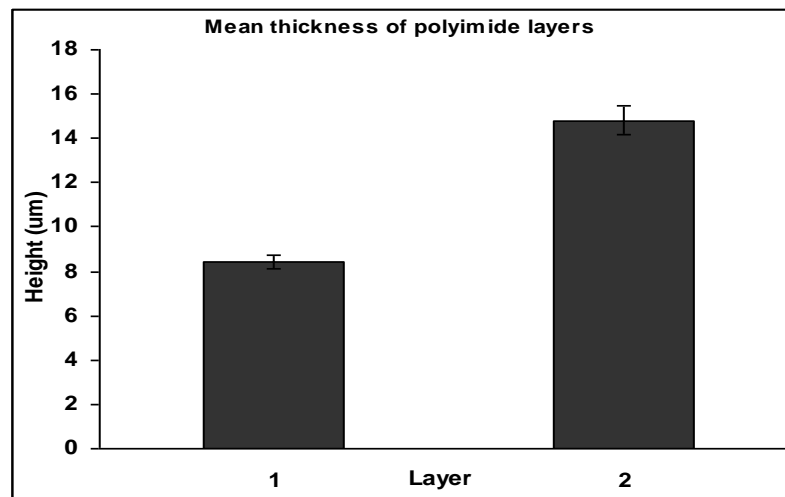


(b)

Figure 28 (a-b): a) Mean line widths along the shaft of devices respective of their location (n=16). b) Mean line width across the stem connecting the electrodes to the connector respective of their location (n=16).

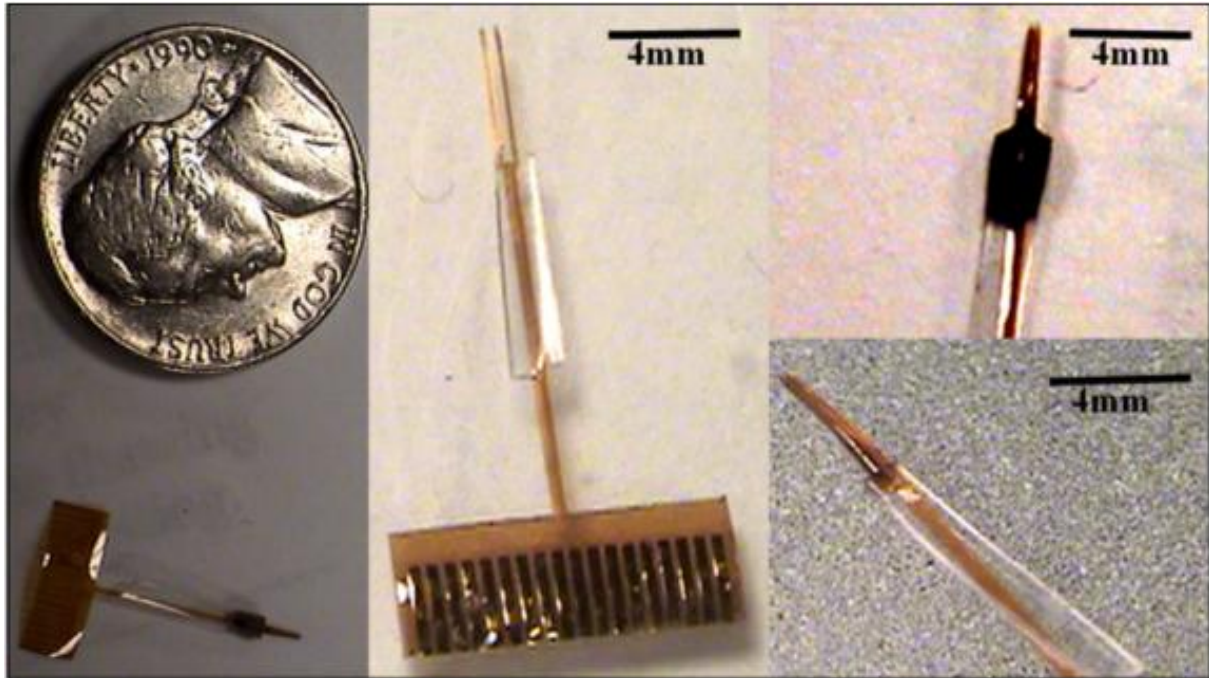


(c)

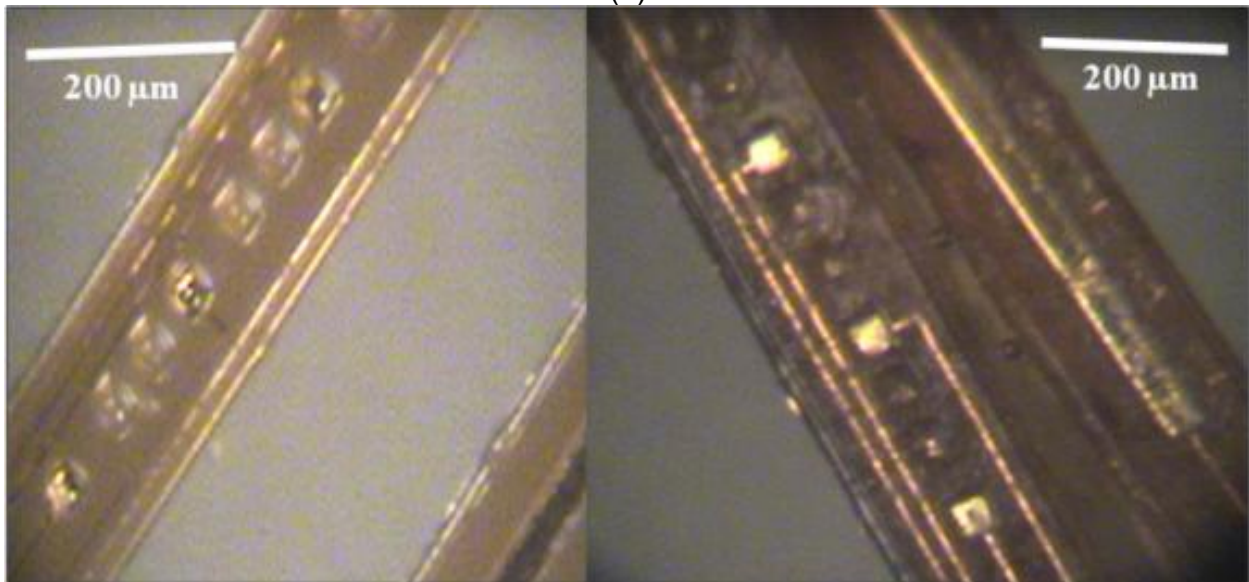


(d)

Figure 28 (c-d): c) Mean contact sites area ($n=16$). d) Mean thickness of polyimide layers ($n=12$).



(a)



(b)

Figure 29: (a) PGA coated final device compared with US nickel (left), uncoated device (center) and close ups of a coated fork (right). (b) Uncoated device showing exposed contact sites (left). PGA Coated device showing exposed contact sites. You can also see air bubbles within the PGA coating.

devices with PGA coating. The second frame in Figure 29a shows the device before PGA coating is applied. Figure 29b shows a close up of a device before (left) and after (right) PGA coating is applied. As can be seen in the images the contact sites remains uncovered and darker PGA coating can be seen behind the two shafts. The PGA coating also bends the two shafts of the devices closer together changing the horizontal geometry of the contact sites placements. Even though dimpling of the surface is observed during the insertion, the surface and the underlying brain recoils back to the initial level once the surface pia is pierced. Figure 30 shows scanning electron microscopy images of the PGA coated devices showing backside coating of the device with exposed (uncoated) contact sites.

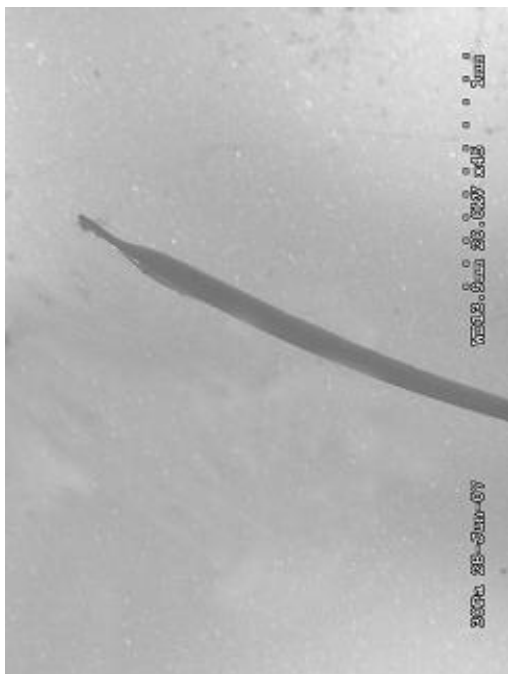
The increase in mechanical strength of the device due to PGA coating is measured in vitro. Figure 31a shows a typical force displacement curves obtained from displacing the tip of the device by 1 mm into the face of the load cell. The peak of the curve occurs when the PGA coating snaps and the device buckles. Each curve represents the forces generated by the same displacement process repeated on the same device. Because the PGA coating was broken after the first displacement procedure, the subsequent force-displacement curves (M2-M5) have weaker peak force. Figure 31b shows mean peak forces generated by uncoated devices (n=28), coated devices (n=15) and recoated devices (n=25). PGA coating enhances the mechanical strength of the device by 20 fold from an average peak force of 0.33mN in uncoated devices to 7.08mN in the PGA coated devices. The recoating of the device, after the initial coating is broken, regains 50% of the strength of the device with initial PGA coating. Once implanted it is important that the PGA coating degrades rapidly,

without producing excessive changes in the pH of the local environment. From the first set of experiments discussed in methods section it can be deduced that nearly 100% of a 1 mm³ cube of PGA is degraded over the period of 7 days (Figure 32). Ignoring perfusion the same degradation process produces nearly 1.5 point pH drop in the fluid surrounding the implant (Figure 33a). But the coated amount of PGA being greatly smaller in volume, and perfusion of the fluid surround the PGA must also be considered. Results from the second experiment suggests that their maybe half a point drop in pH within 10 minutes after the coated amount of PGA comes in contact with water, but that it quickly recovers above pH of 7 within half hour of the experiment, if perfusion of the surrounding fluid is to clear away the degrading PGA (Figure 33b).

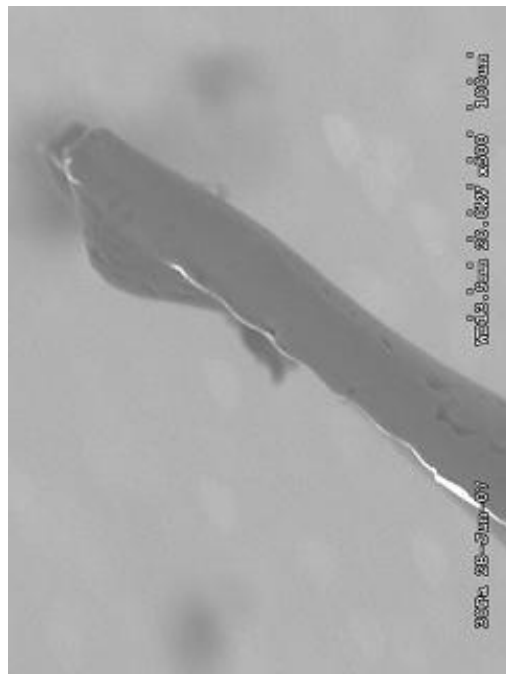
4.3 ELECTROCHEMICAL ANALYSIS

4.3.1 CYCLIC VOLTAMMETRY

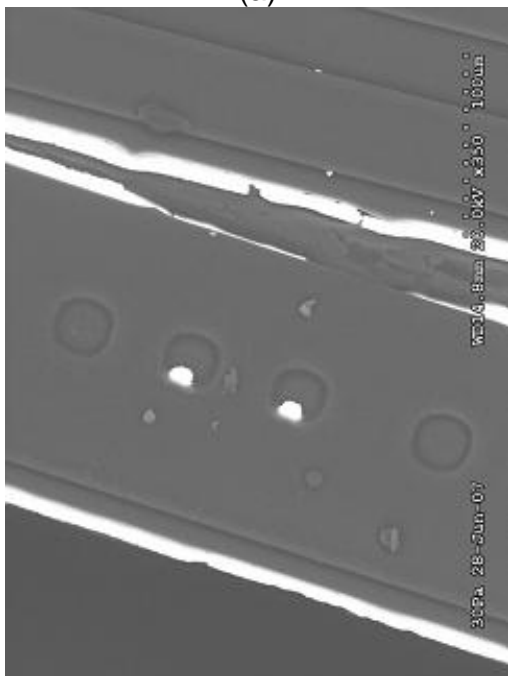
After manufacturing of the device, electrochemical analysis is the next logical step to verify the functionality of the device and to provide a tool for characterizing them. Cyclic Voltammetry (CV) was used to measure devices ability to conduct current at the interface. Figure 34 is collection of 10 scans run on individual sites from 1 through 4; ground strip and a contact pad not connect to a contact site. In each of the CV figures, the top plot shows current vs. time (solid lines) and potential vs. time (dotted lines). On an average the positive peak current was $0.064 \mu\text{A} \pm 0.01 \mu\text{A}$ and negative peak current was $0.066 \mu\text{A} \pm 0.005 \mu\text{A}$. The peaks were only observed near water window, and are attribute to hydrolysis of water. This is very typical of gold, as it does not under go any oxidative or reductive reactions. The current transfer is primarily through capacitive



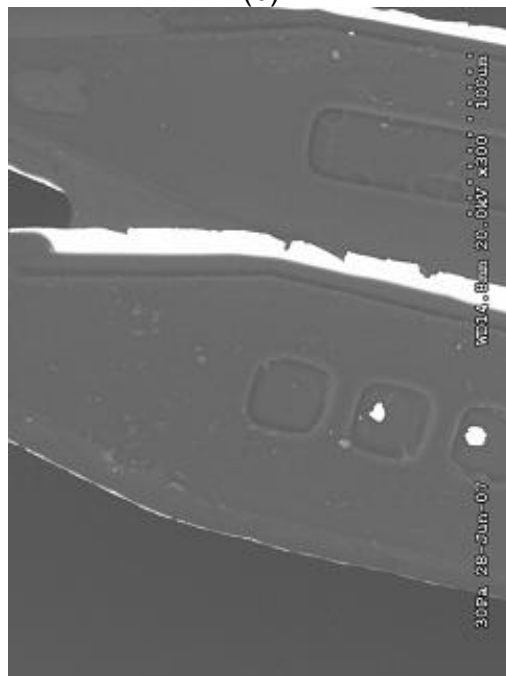
(a)



(b)

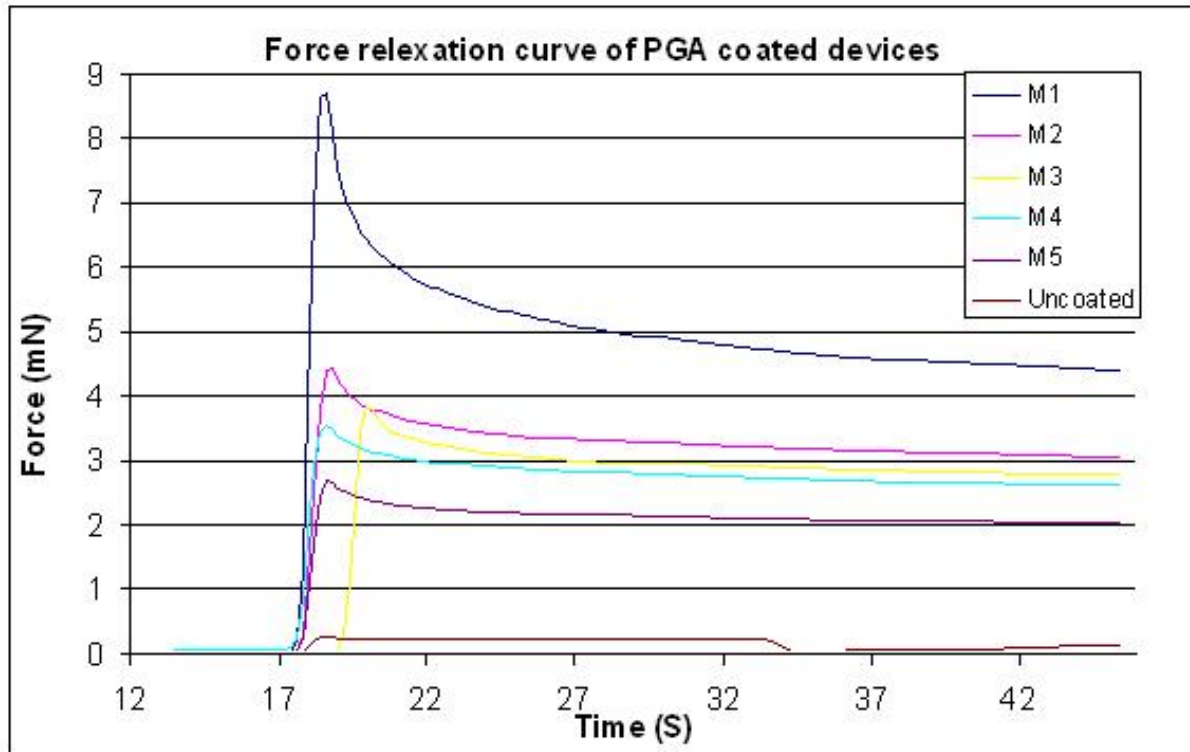


(c)

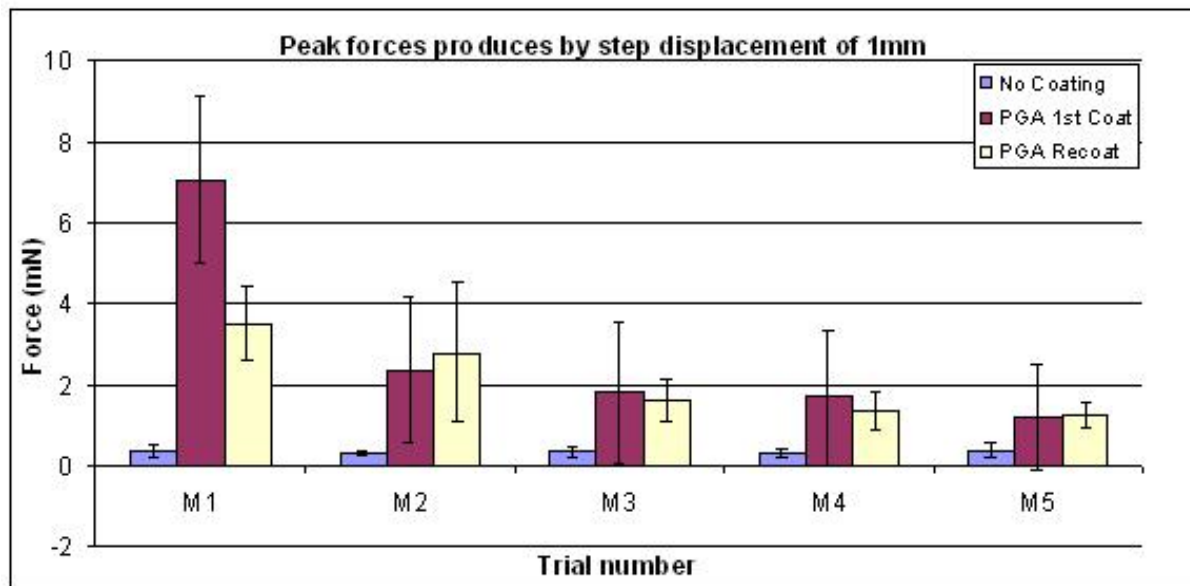


(d)

Figure 30: (a) A SEM image of a typical single sided coat of the device along the fork length. (b) Close up view of the tip of the device showing backsplash coat of the tip. (c) Close up view of the shaft showing exposed contact sites and via with back coated PGA seen in between two fork shafts. (d) Another sample of the exposed contact sites and via.



(a)



(b)

Figure 31: (a) Typical force relaxation curves obtain by displacing the device 1 mm perpendicular to weighing surface. (b) Peak forces generated for the coated and uncoated polyimide devices PGA coated devices produce 10 times larger peak forces then uncoated devices. Re-coating PGA restores the mechanical strength by 50% of the original. (n=28, no coating; n=15, 1st coat; n=25, recoat)

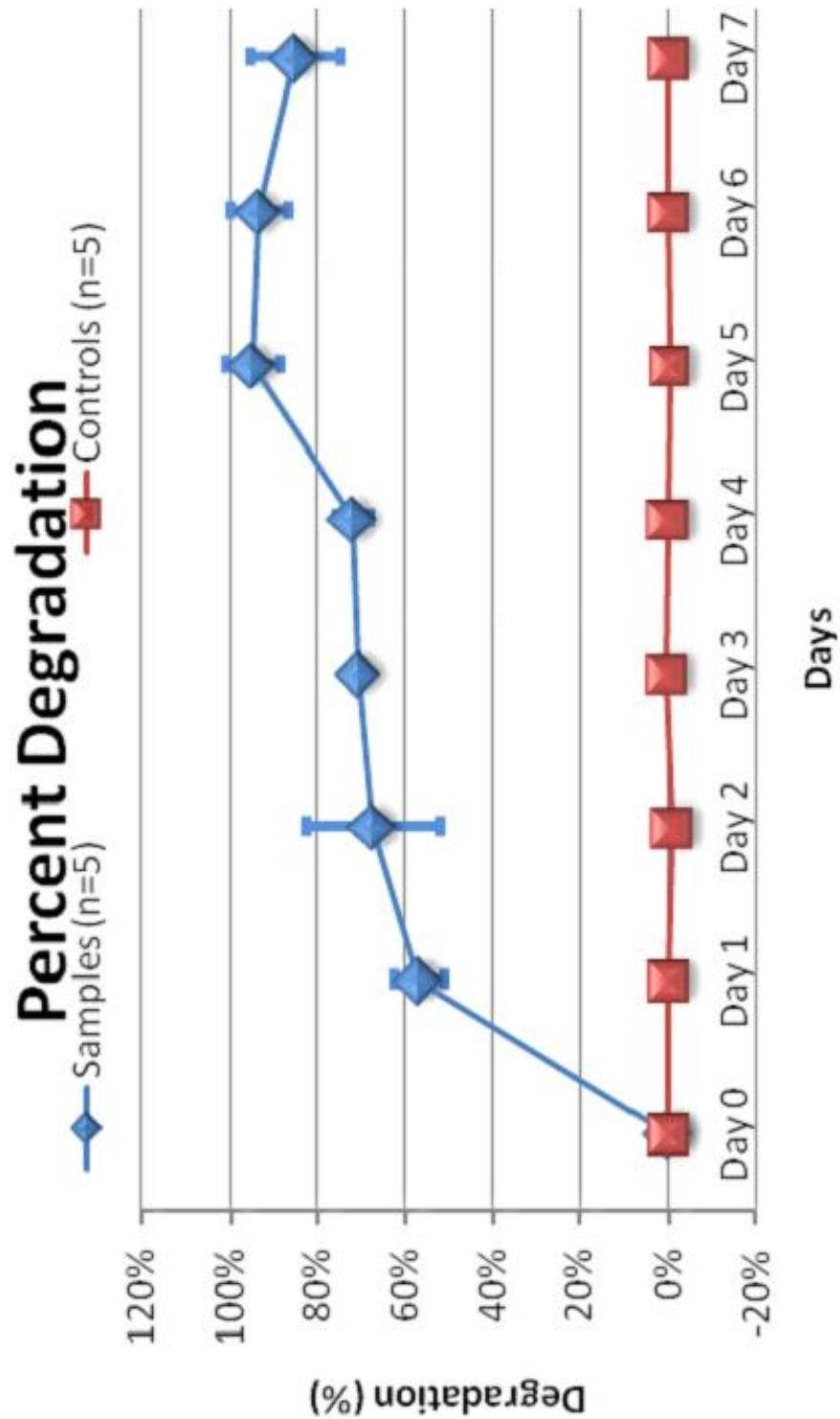
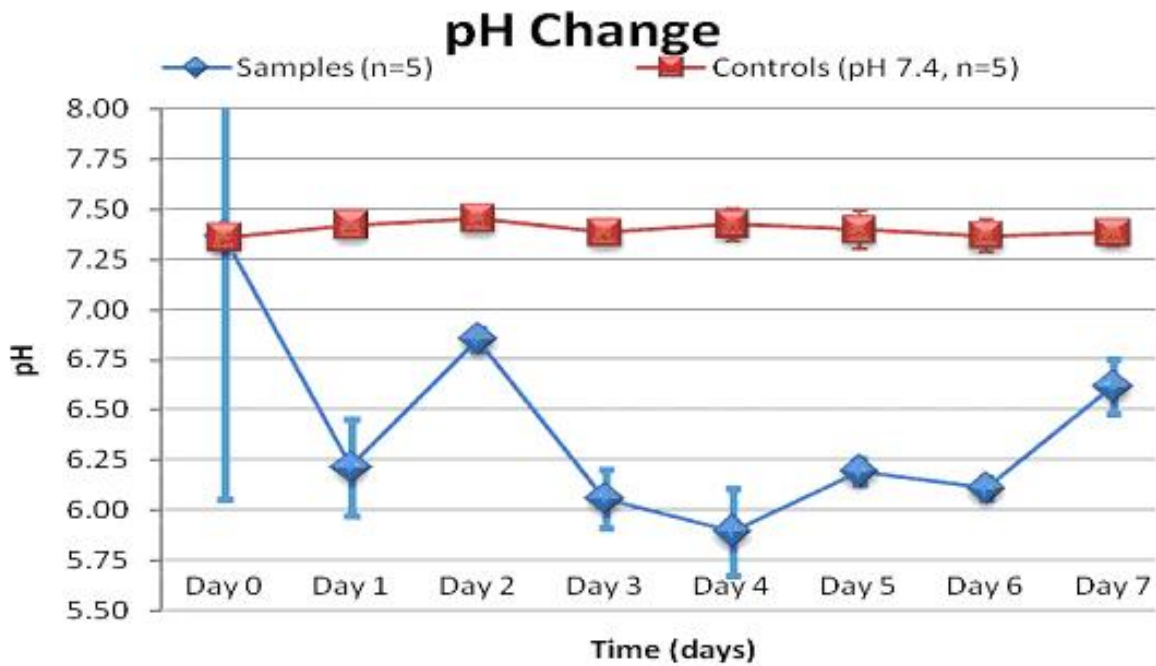
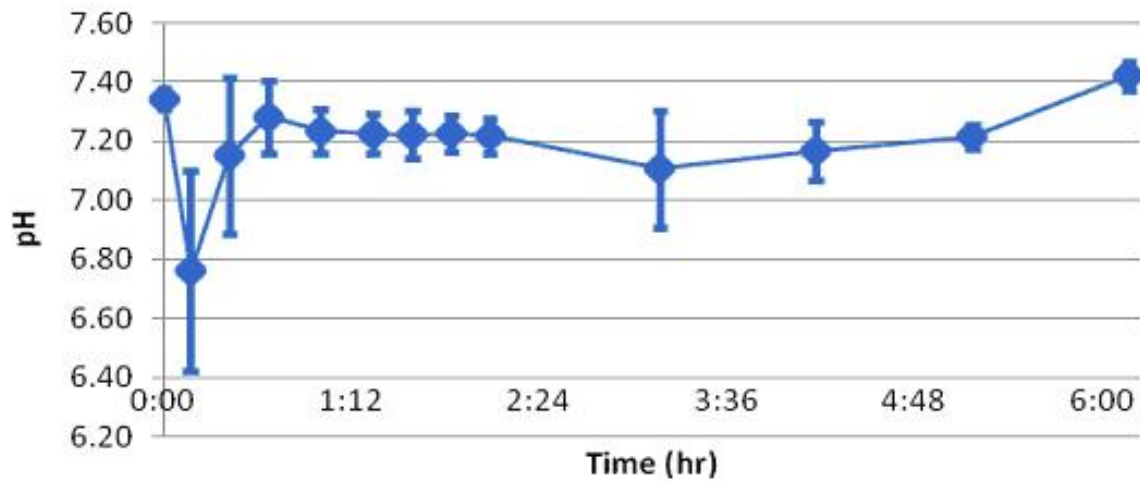


Figure 32: Percent Degradation of 1 mm x 1 mm x 1 mm cubes of PGA over the period of 7 days



(a)

pH changes of PGA coated devices (with saline change, n=12)



(b)

Figure 33: (a) pH change of a 1 mm x 1 mm x 1 mm PGA in PBS solution over the period of 7 days, measured once daily. (b) pH changes of PGA coated devices in PBS over the period of 6 hours. The PBS saline was changed after each measurement to simulate perfusion.

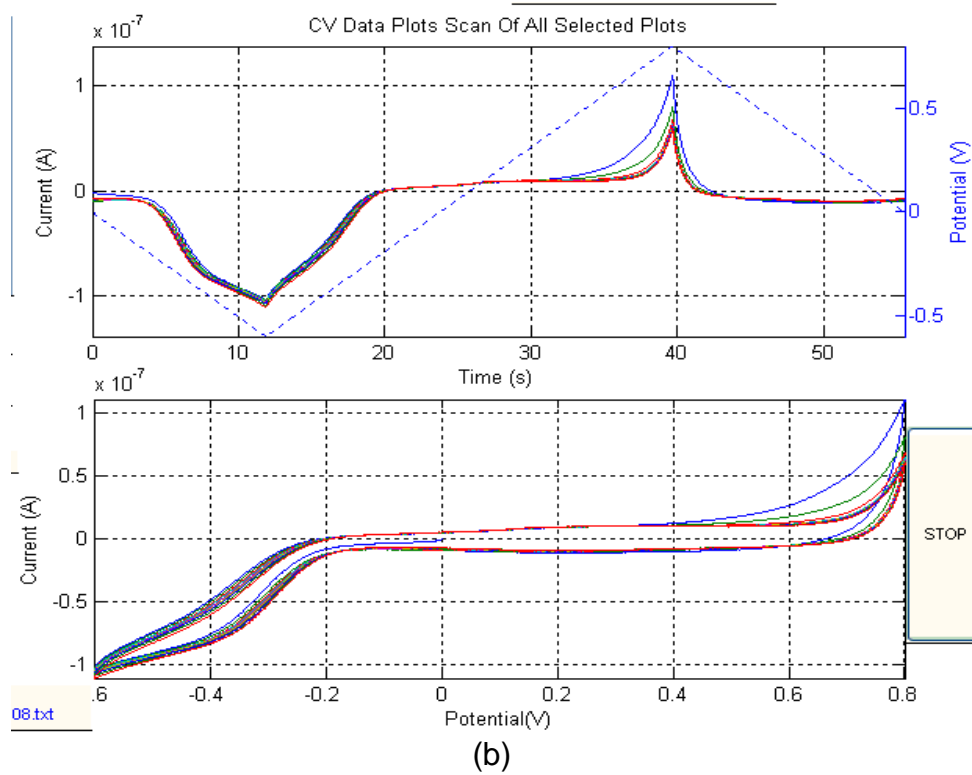
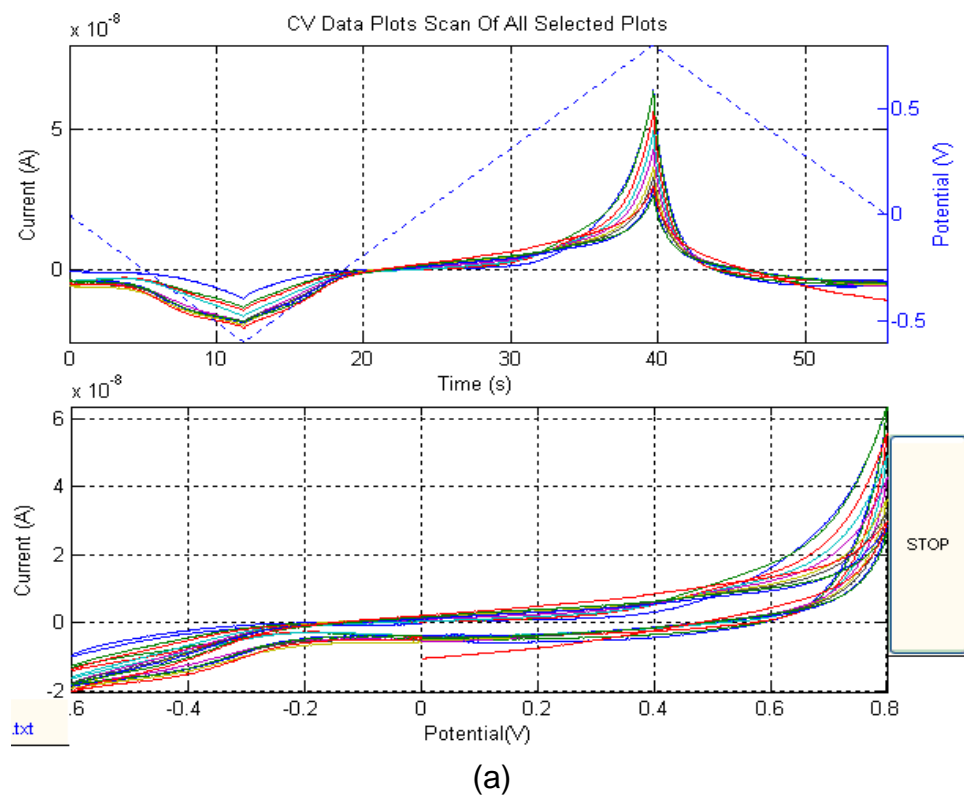


Figure 34: 10 scans of cyclic voltammetry performed on (a) Site 01 (b) Ground Strip.

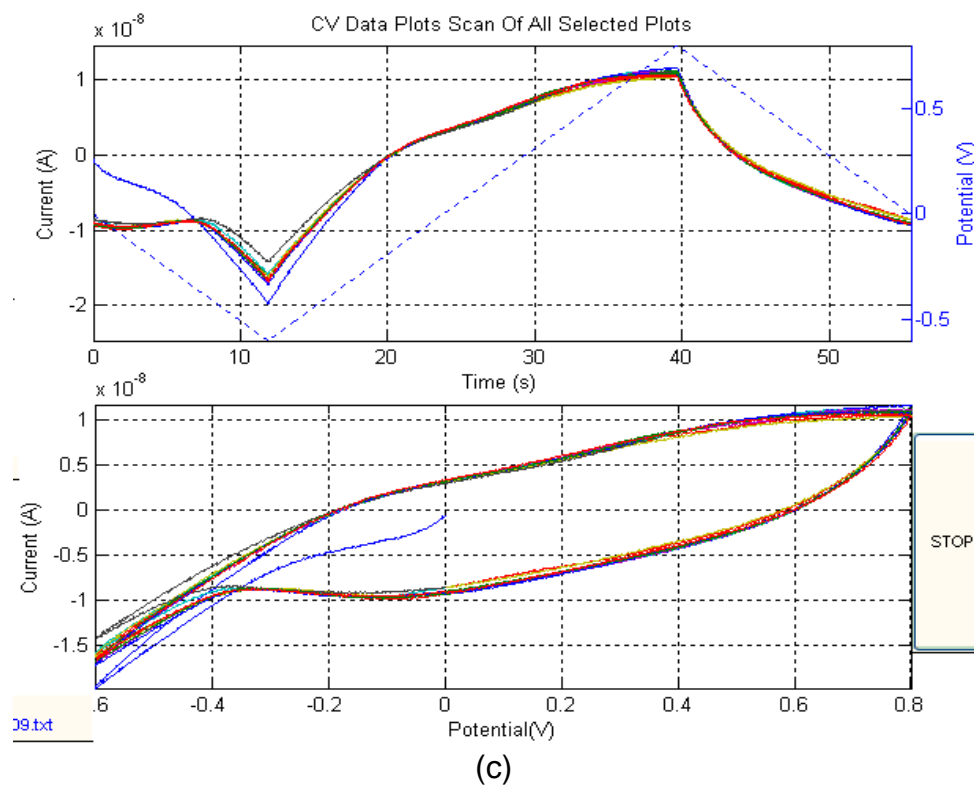


Figure 35: 10 scans of cyclic voltammetry performed on (c) Dummy Site of a polyimide device

currents. Oxidative and reductive reactions typically provide larger charge transfers and can be recognized by large peaks along the CV cycle. Therefore, gold devices make excellent recording electrodes, but rather poor stimulating electrodes. The positive region of the anodic phase measured to have charge capacity $0.45 \mu\text{C} \pm 0.06 \mu\text{C}$ and negative region $0.29 \mu\text{C} \pm 0.02 \mu\text{C}$. The charge capacities of positive and negative regions of the cathodic phase were $0.32 \mu\text{C} \pm 0.06 \mu\text{C}$ and $0.37 \mu\text{C} \pm 0.03 \mu\text{C}$ respectively. Figure 34f measured CV signal similar to that of gold device but of an order of magnitude lower. This is an indicative of cross talk between traces. I failed to obtain its impedance spectroscopy, due to very large inter-trace impedance, rendering the signals below noise level. Therefore, it is safe to assume that the cross talk will be negligible if any. Figure 34f is reproduced again in Figure 36a to show comparison between a dummy contact pad and a polyimide device with no metal traces. Figure 37, shows comparison between one of the contact site and gold wire. It is observed that the water window in the case of the device is left shifted compared to the gold wire.

4.3.2 ELECTRODE IMPEDENCE SPECTROSCOPY

Electrical Impedance Spectroscopy (EIS) was used to measure impedance observed at the interface of the device. With the exception of a single site which showed impedance an order of magnitude lower, all the sites showed similar impedance spectroscopy curve. On an average the magnitude of the device's impedance was around $300\text{k}\Omega$ with phase of 74 degrees. The first mentioned exception device had magnitude of $31 \text{ K}\Omega \pm 7 \text{ K}\Omega$ and phase of $-51 \text{ degrees} \pm 4 \text{ degrees}$. The top plot in Figure 38 shows nyquist plot for the impedance and bottom plot of Figure 38 shows bode plot for the same devices.

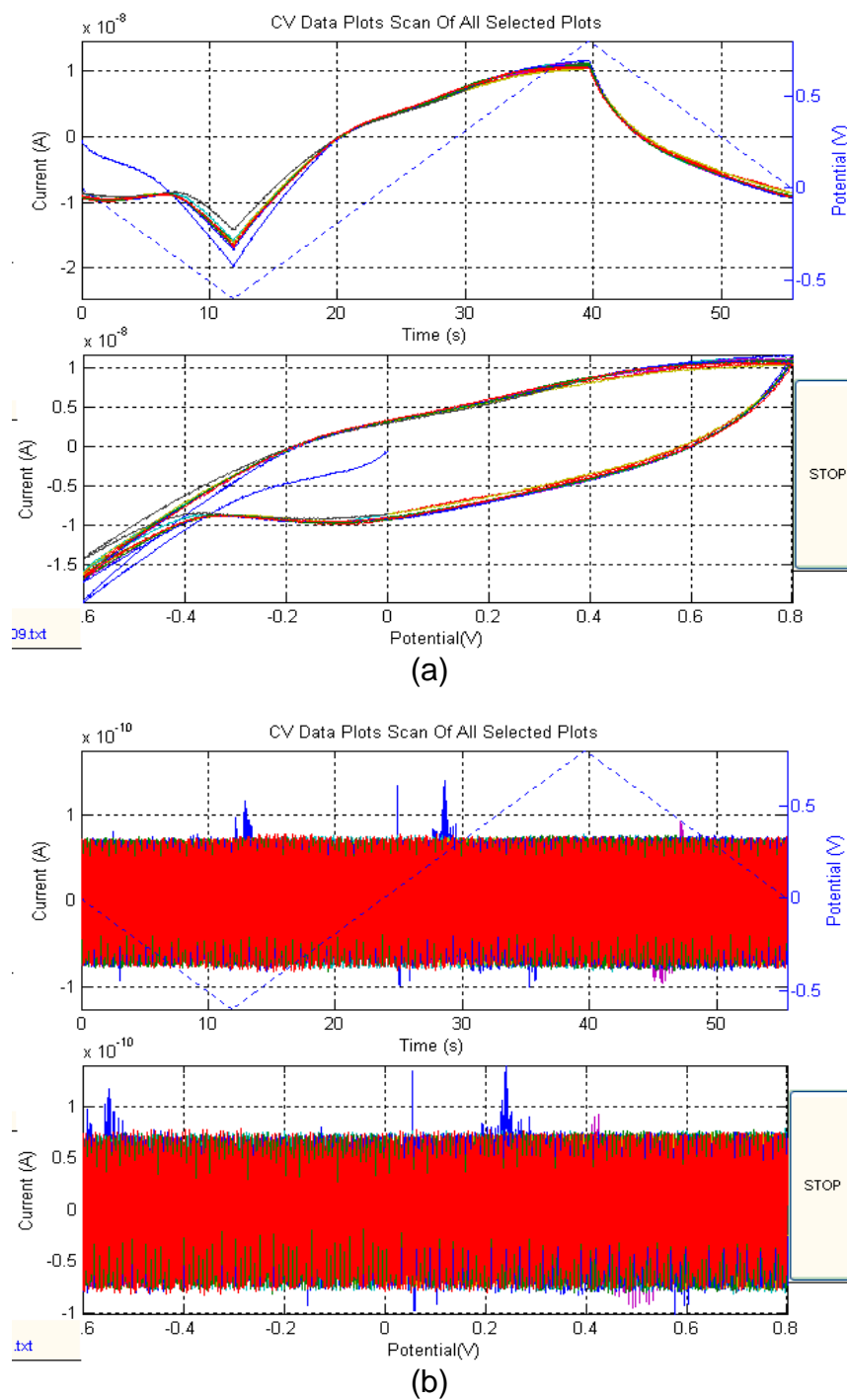


Figure 36: Comparison of CV performed on a dummy site of a device from previous figure (a) and a device without metal traces (b)

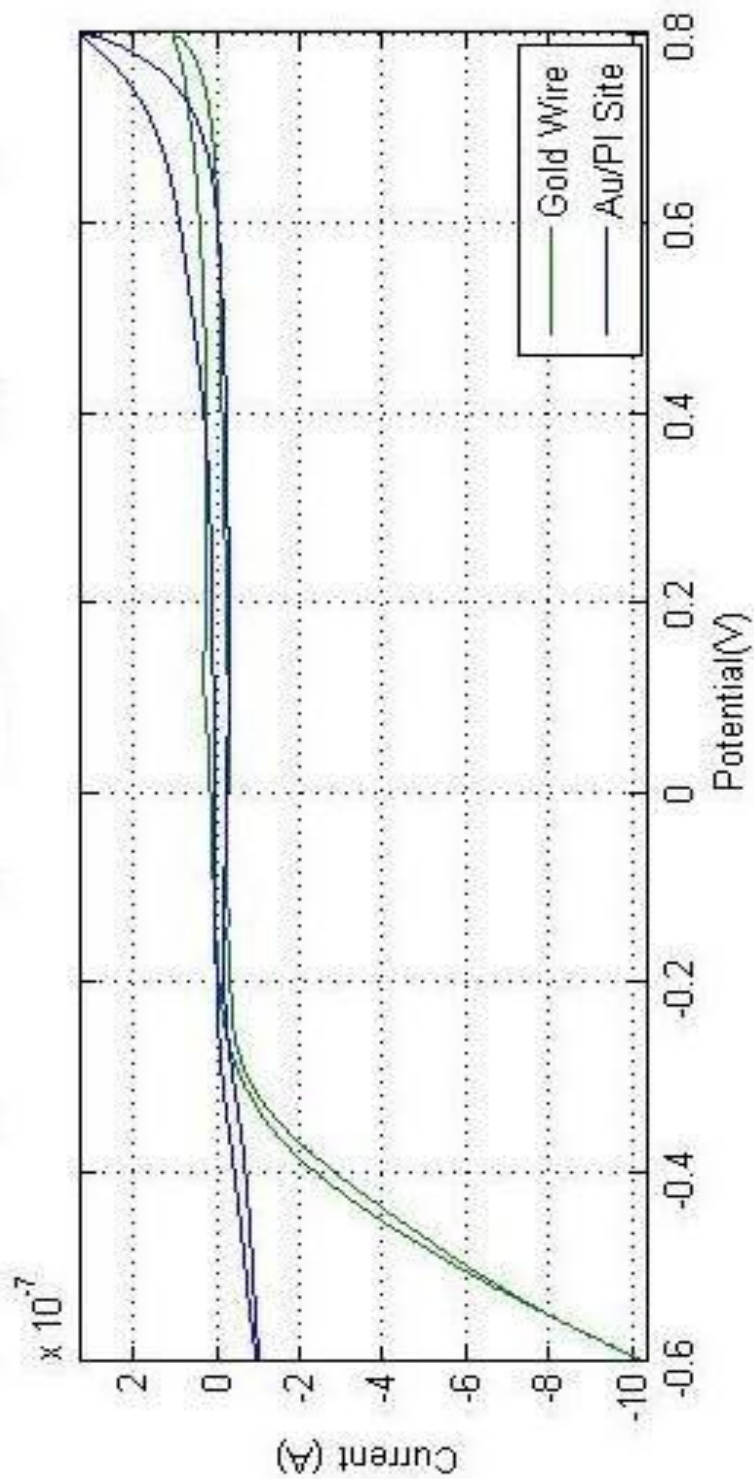


Figure 37: Comparative mean (10 scans each) CV plots of Gold wire (green) and a PI device site (blue). The CV curve for the device is left shifted as compared to the gold

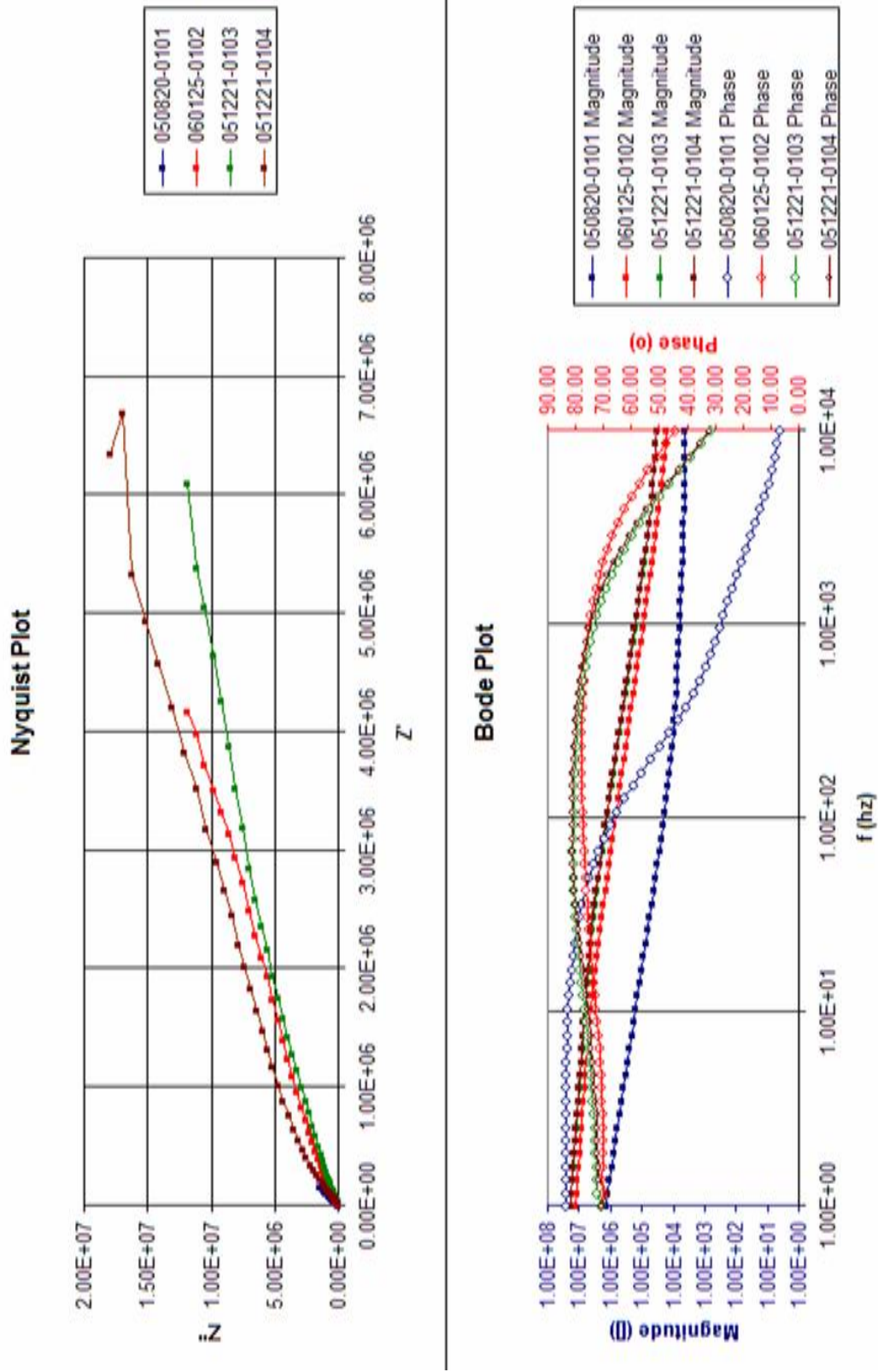


Figure 38: Nyquist and Bode plots of four different sites on four individual devices.

For bode plots, magnitudes is indicated with (•) and phase with (o). Figure 39 shows comparison between gold wire EIS and EIS for a contact site of a PI device.

4.3.3 IN-VIVO ELECTROCHEMICAL ANALYSIS

In-vivo electrochemical analysis was performed using bone screw as auxiliary as well as reference lead. Where as in-vitro measurements was done using standard setup as discussed earlier. The increase in impedance is observed for in-vivo EIS measurements are shown in Figure 40 for all three channels. The phase of the impedance also increase at lower frequencies below 100Hz and decreased near higher frequencies above 1 KHz. Also a decrease in CV peak currents was observed possible related to the increase in impedance, for in-vivo scans (Figure 41). Furthermore, EIS curves for post implant scan done using standard three leads setup described earlier, maintained the change in impedance trend observed during in-vivo scans.

Additionally, site 02 completely failed to record during in-vivo recording, suggesting extremely high impedance at the interface. But, during scan 3 of post implant CV measurement site 02 returned to its original functioning state (

Figure 42). EIS done post implant and post recovery on site 02 also showed a similar trend as other channels.

4.4 ACUTE ANIMAL STUDIES

4.4.1 ACUTE ANIMAL RECORDINGS

Following the electrochemical analysis of the devices, they were implanted in six different animals. Figure 43, shows a typical recording obtained in response to a click stimulus. The top figure shows a typical neuronal firing, with line activity interspaced

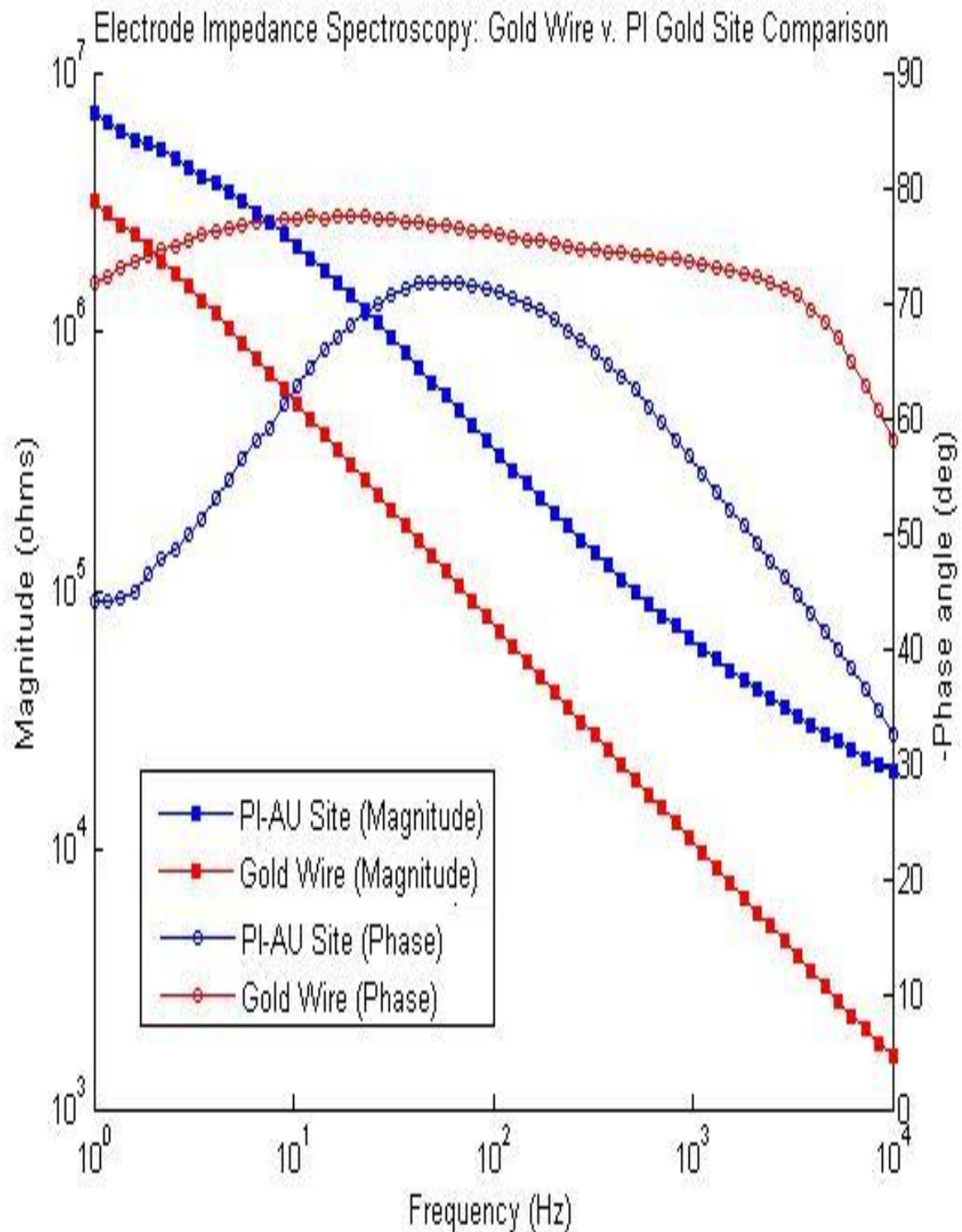
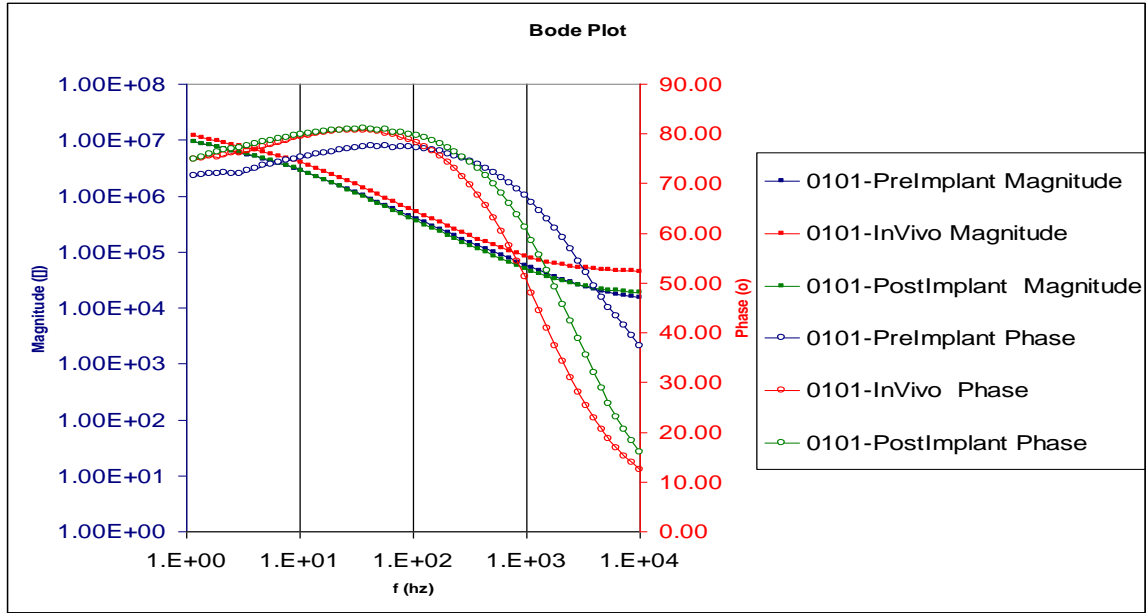
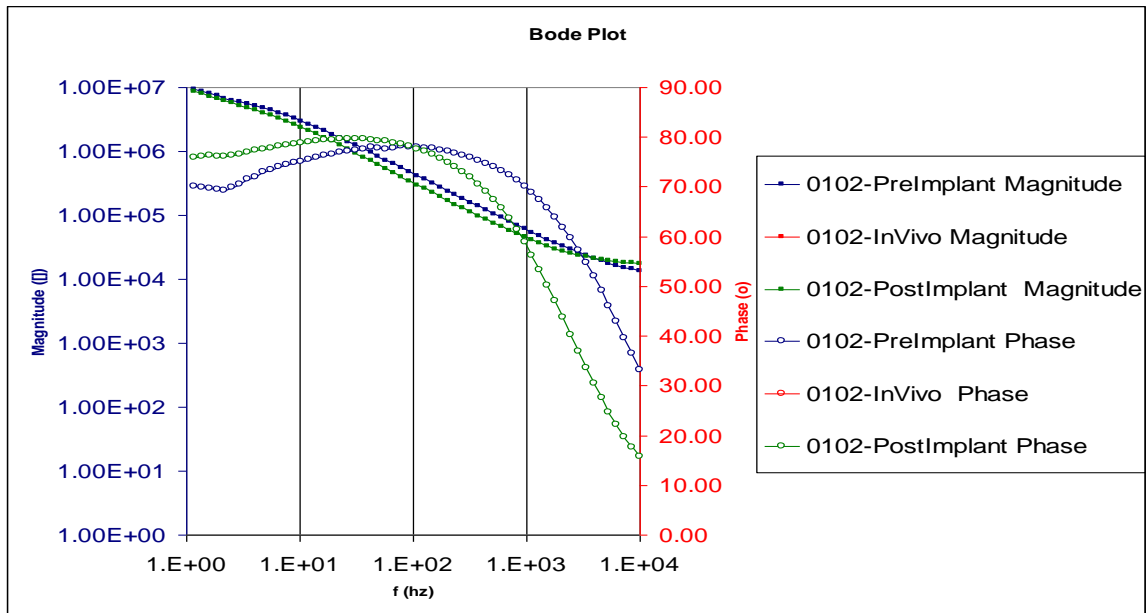


Figure 39: Bode plots showing comparison between gold wire and a site on a PI device. The wires lower impedance was due to its larger surface area.

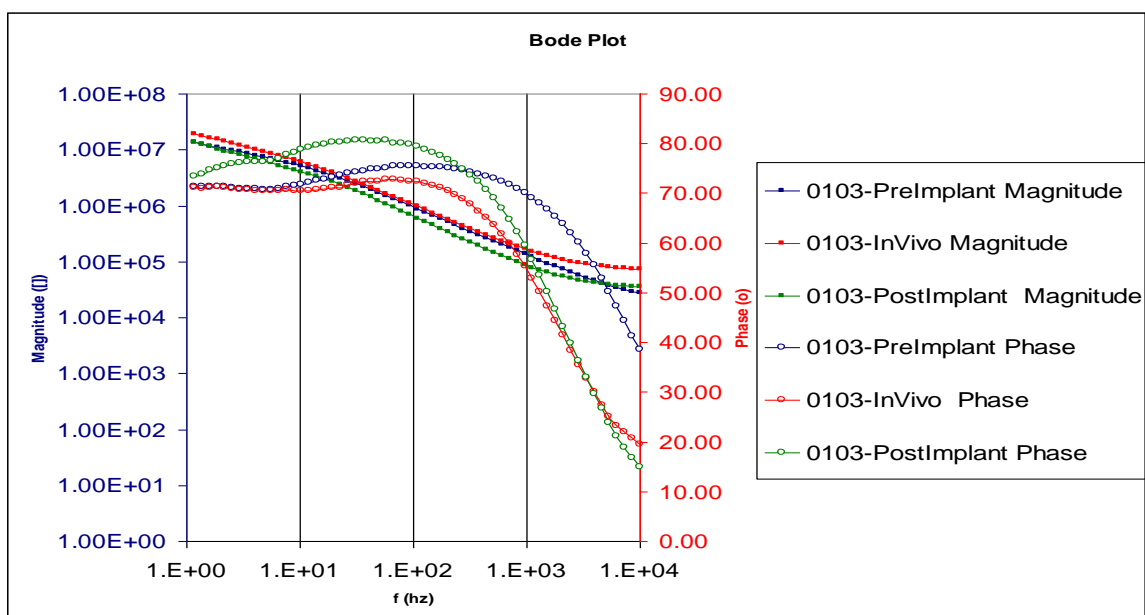


(a)

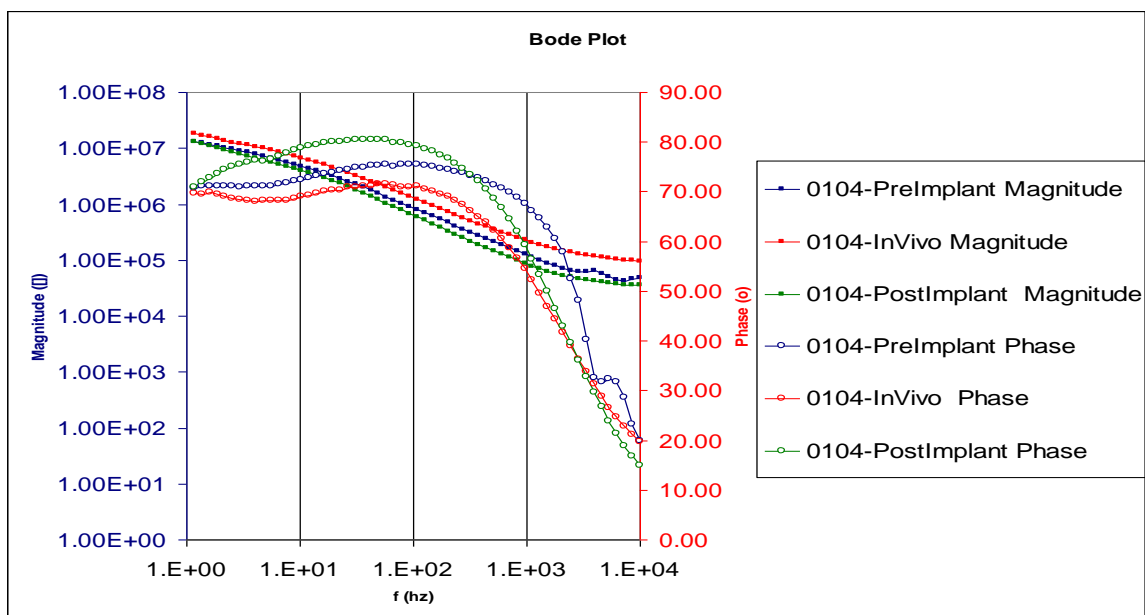


(b)

Figure 40 (a-b): Slight increase in impedance was observed for all the channels for In-Vivo measurements. Also, an increase in phase angle near DC and decrease in phase angle near as was observed for all the channels. (a) Site 01 (b) Site 02: no in-vivo signal was recorded



(c)



(d)

Figure 39 (c-d): Slight increase in impedance was observed for all the channels for In-Vivo measurements. Also, an increase in phase angle near DC and decrease in phase angle near as was observed for all the channels. (c) Site 03 (d) Site 04

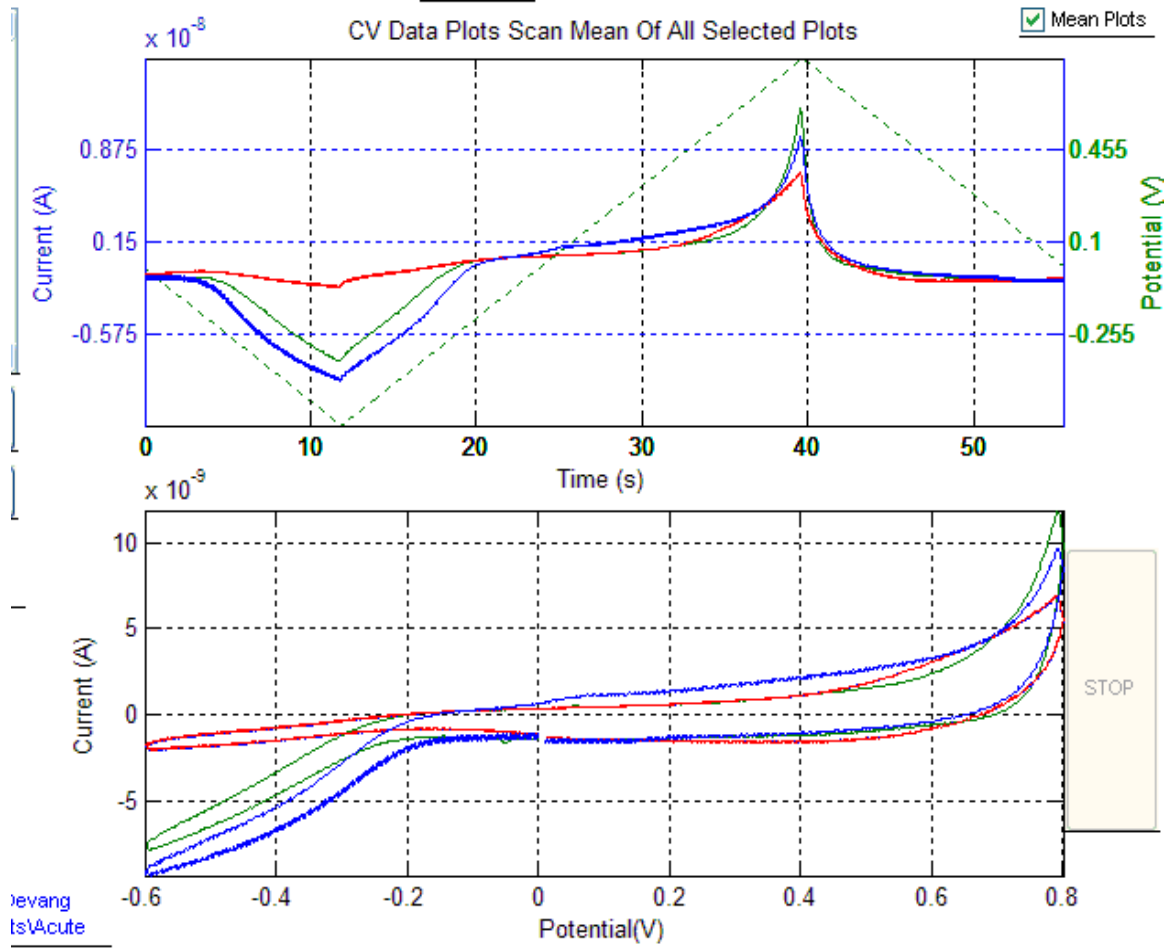


Figure 41: Mean CV curves for Site 01 prior to implant (Green), during implant (Red) and post implant (Blue)

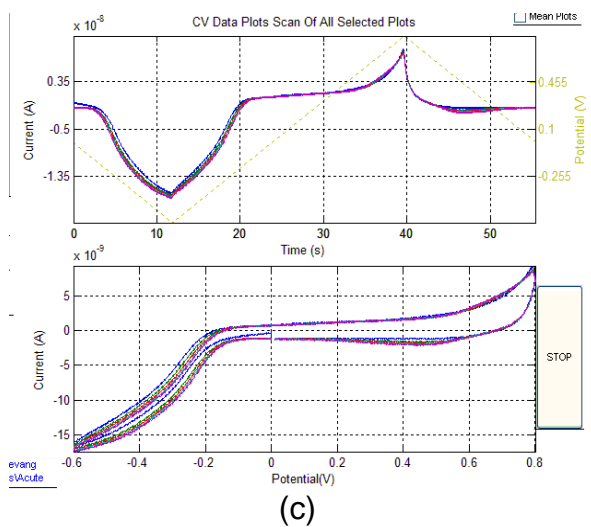
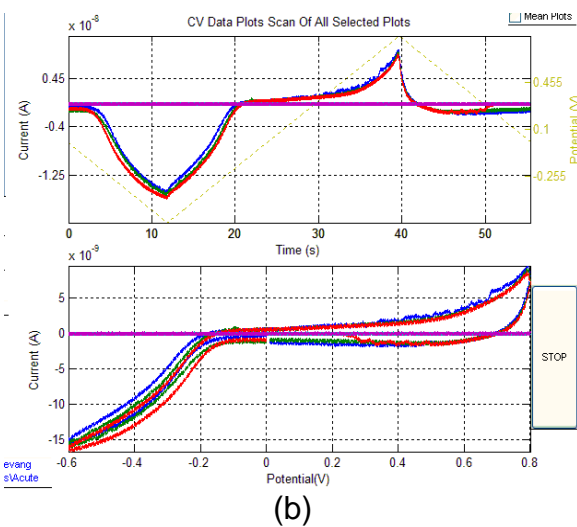
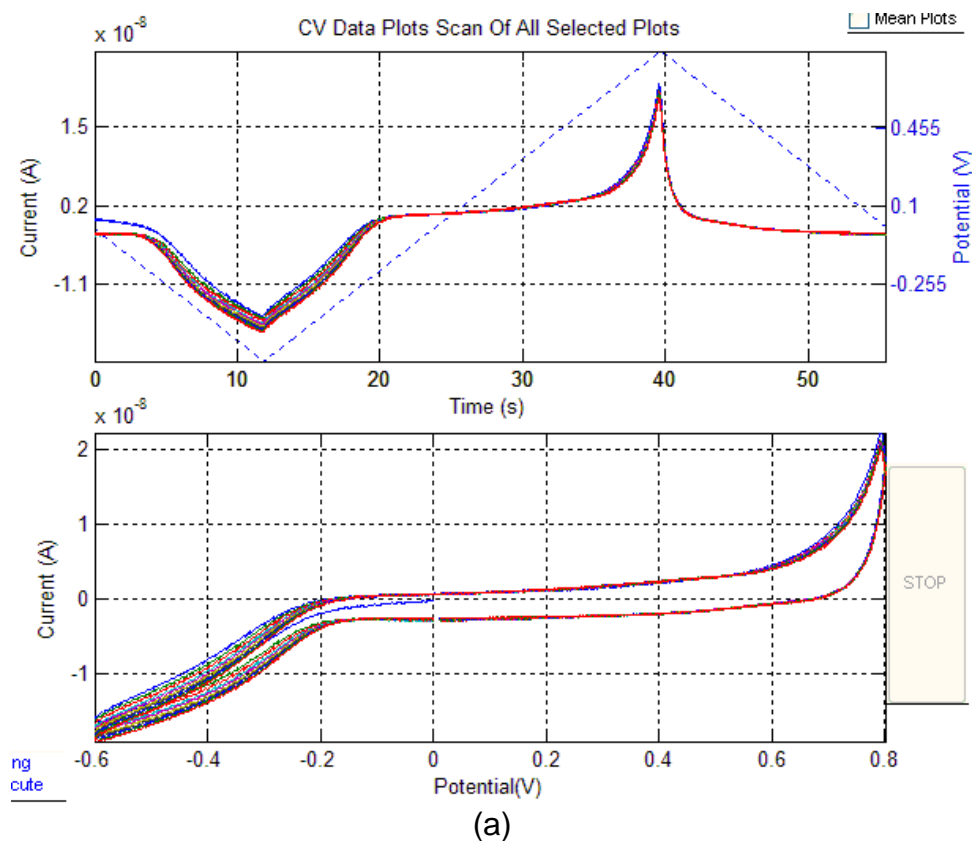


Figure 42: (a) For site 02 five CV scans were performed prior to implant, site 02 provided no signal during implant. (b) During 3rd scan of the first five scans post implant site 02 started to measure signal again. (c) Five additional CV scans were performed post implant.

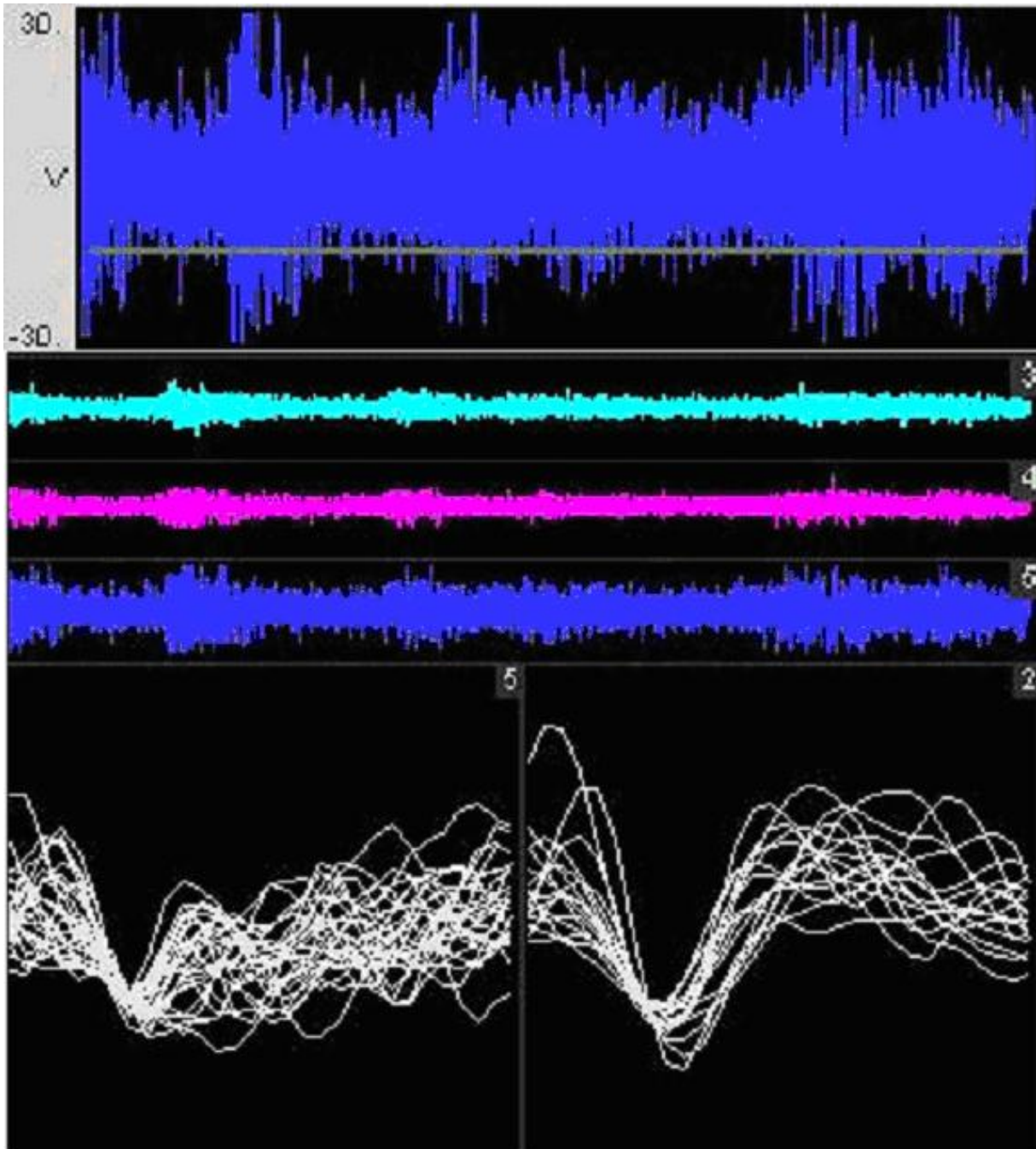
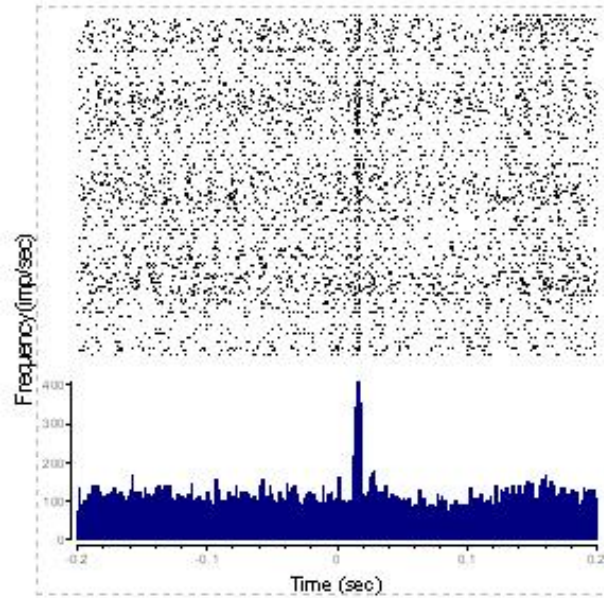


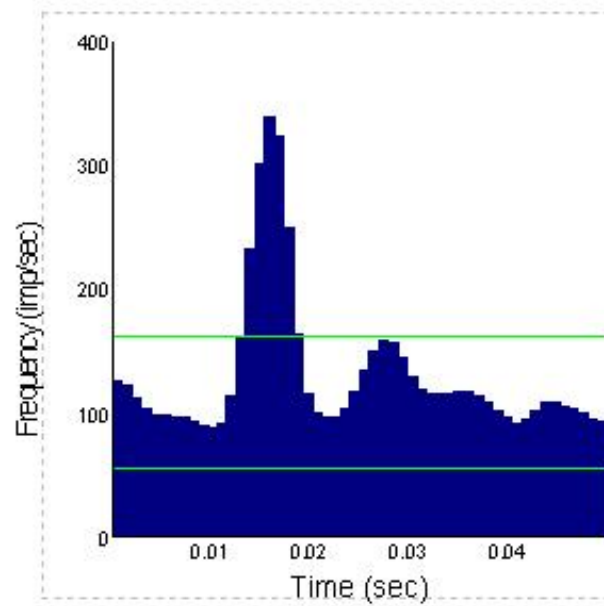
Figure 43: Typical signals recorded from the cortex using the PI devices. Traces from three of the channels recorded simultaneously is shown in the middle frame, the third channel is enlarged in the top frame. The bottom two frames show typical capture action potentials.

between bursting of action potential. A thin line set at 1.2 standard deviation below mean ($SNR=1.2$) thresholds the signal. The middle figure shows three such traces recorded from three different channels simultaneously. The bottom two figures shows typical action potentials captured, after they are detected to cross the threshold. They are expanded along the time axis, and appear as a single line or cluster of lines bunched together during the burst of activity. For every action potential detected a dot is placed along the time axis to generate raster plots. These raster plots are re-aligned in column by resetting the stimulus occurrence time at $t=0$. Figure 44a shows a raster plot of one of the channels below. The dots are further binned together and count along each bin to compute a time base histogram or peri-stimulus time histogram (PSTH). PSTH of the same channel is shown in Figure 44b along with $\pm 99\%$ confidence intervals indicated by green lines. Figure 45 shows baseline firing on four different channels recorded simultaneously. Figure 46 shows the PSTHs for recorded signal over duration of 40 minutes with click stimulus presented at 1.8Hz. PSTH as a function of time are shown in Figure 47 and Figure 48 for two different devices. These plots give indication of the stability of the interface. Consistent width, onset and offset of the PSTHs indicated by the orange strip are suggestive of a stable interface as seen in Figure 47. On contrary Figure 48 shows the device whose interface is failing to record action potential. In this study animal had suffer severe blood loss and was not able to respond very well to the presented stimuli.

Figure 49 shows PSTHs as function amplitude obtain from each of the channels. Here the individual PSTHs for each amplitude level are placed along the PSTH Time axis



(a)



(b)

Figure 44: (a) Raster plots of a channel shown in figure 29. (b) PSTH of the same channel, with 99% confidence interval indicated by green lines.

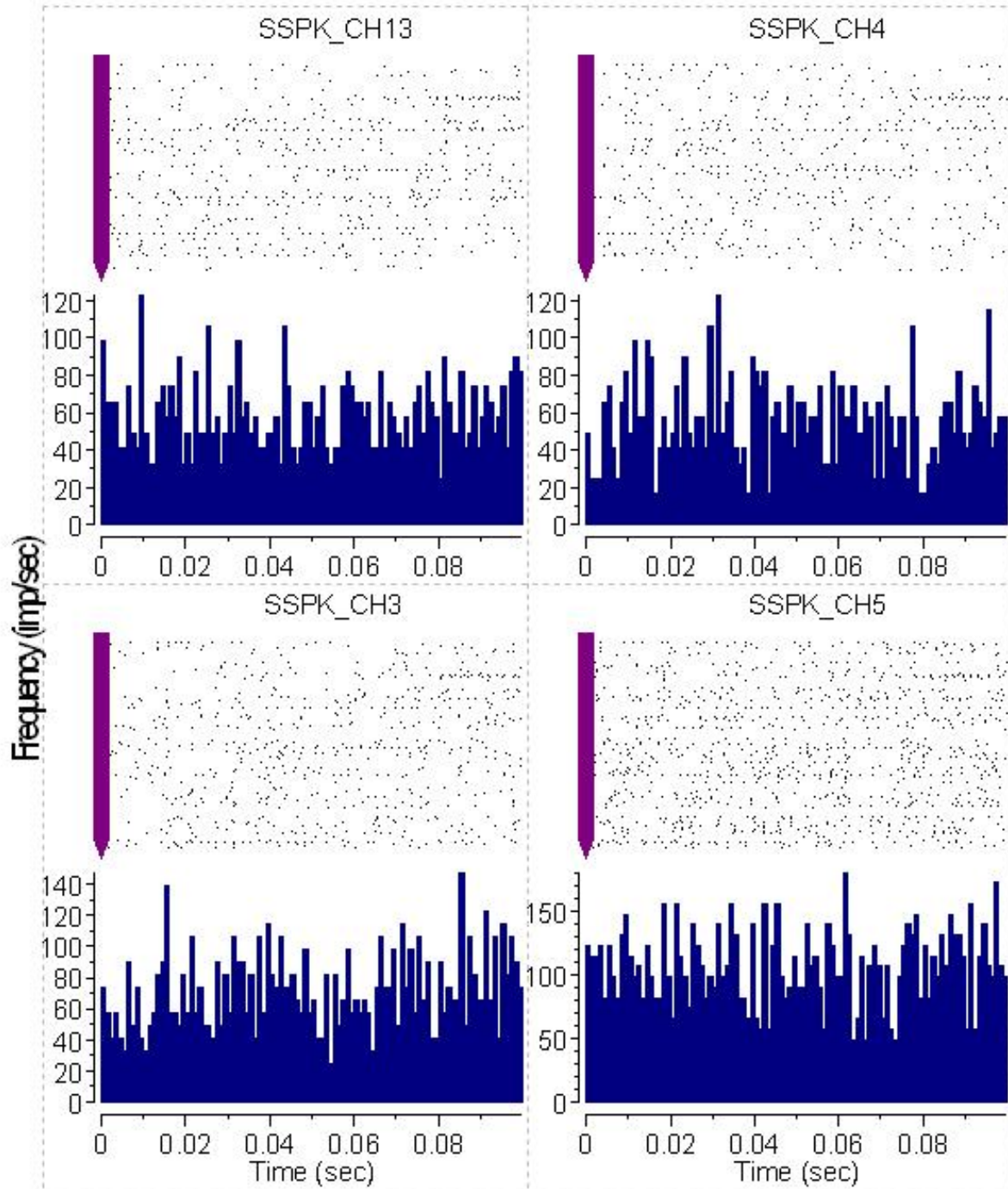


Figure 45: Baseline recording performed simultaneously on four individual channels of a two shaft device.

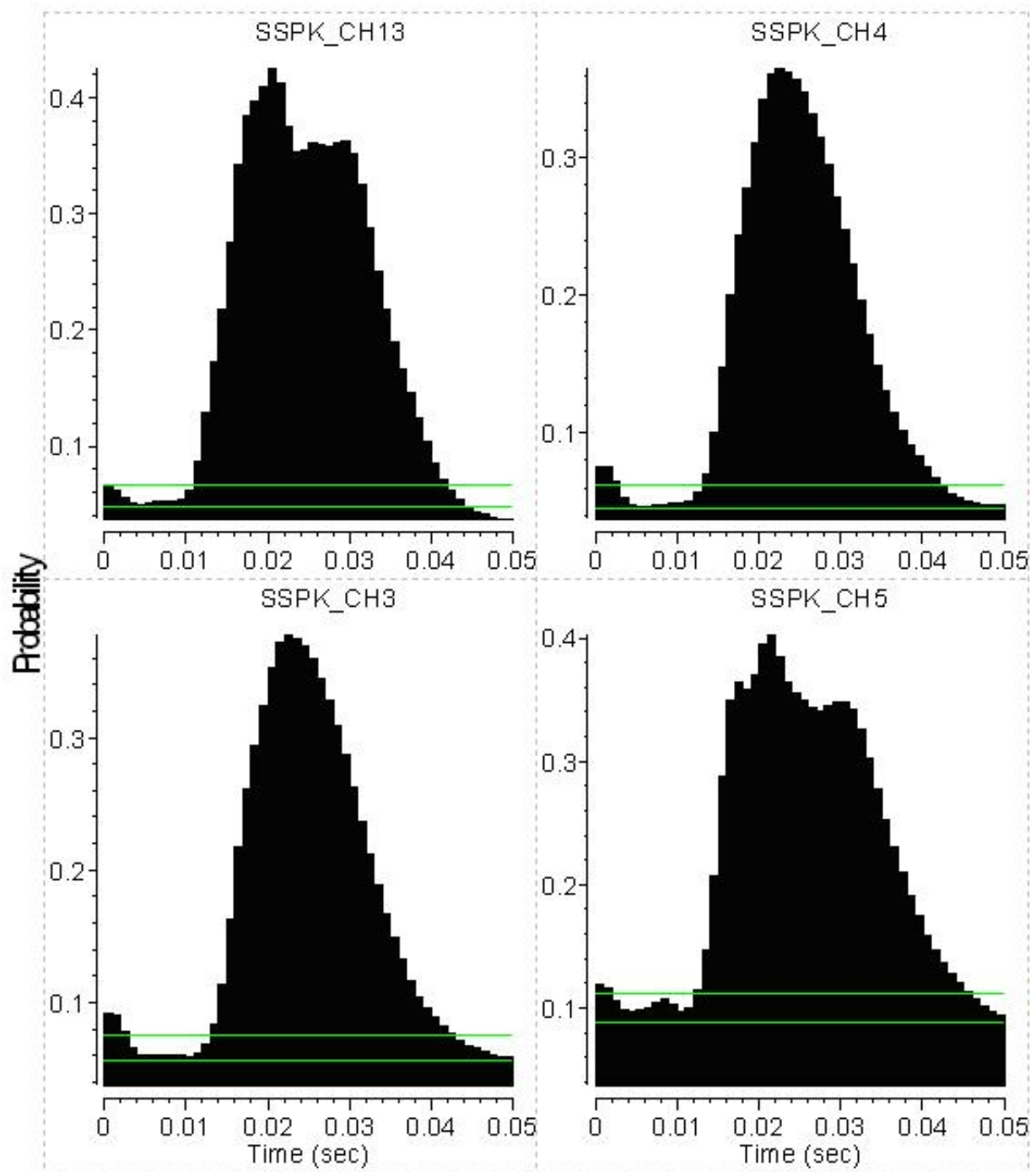


Figure 46: PSTHs generated using click stimuli present over a period of 40 minutes.

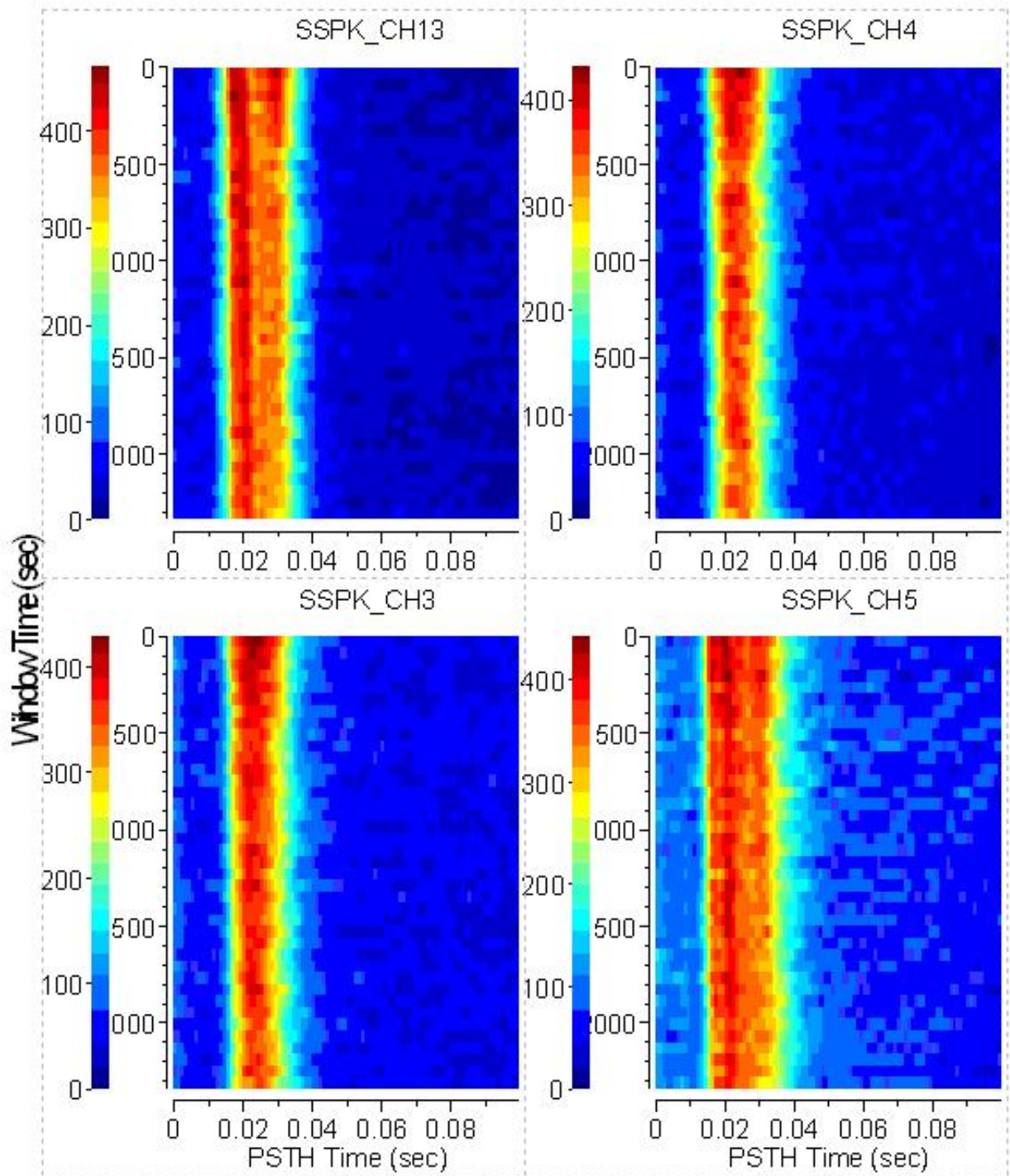


Figure 47: PSTHs vs. time of the same signal as in figure 32, indicates a stable interface.

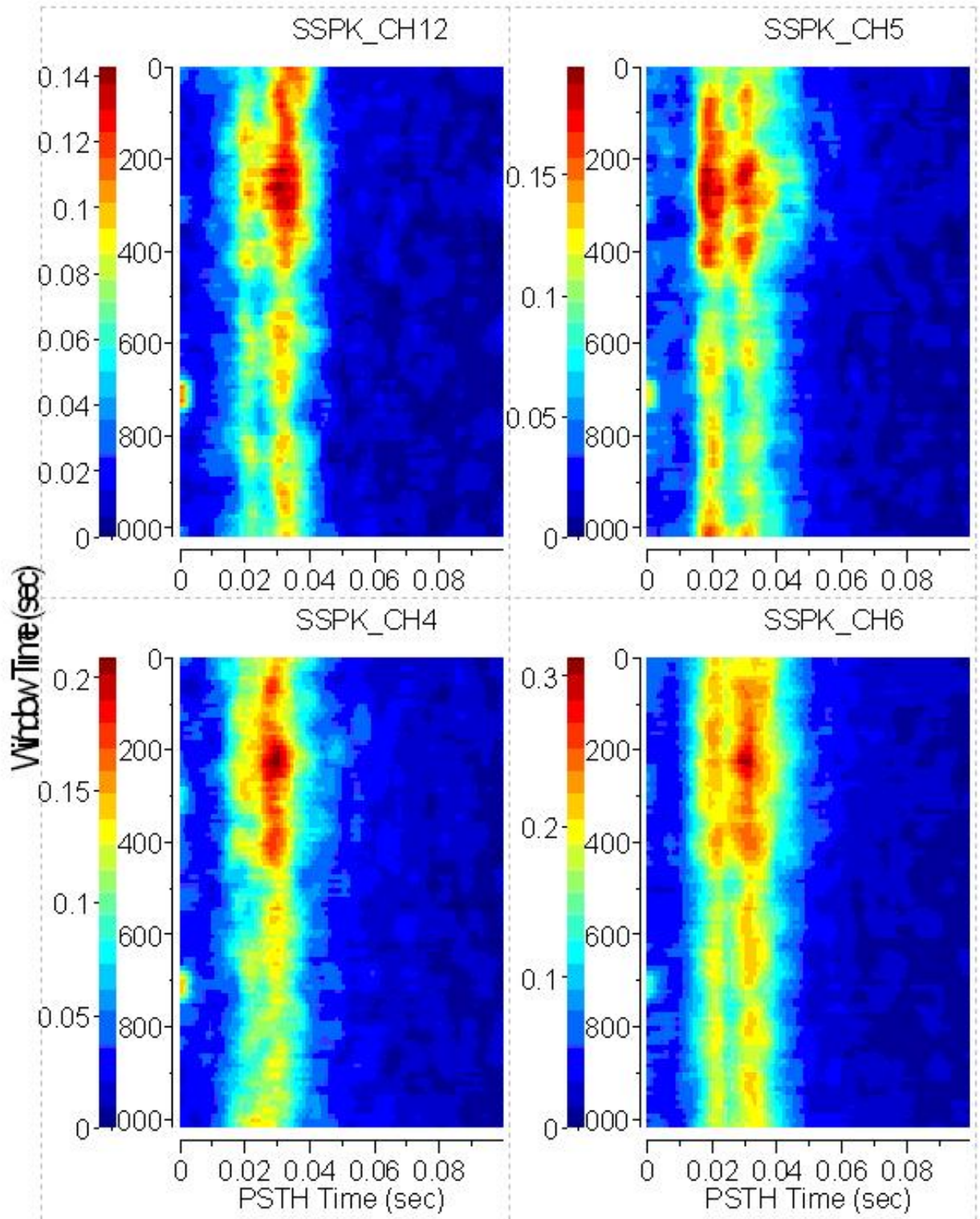


Figure 48: Another study performed on another animal to establish short term interface stability; here the animal had suffered severe blood loss during surgery.

and stacked next to each other along the amplitude axis. Probability axis indicates the probability of spike occurring at a particular location, and it is computed by dividing spike counts in individual bins with total number spikes in the considered graph. Here, 2 KHz tonal bleep stimuli were presented at 1.8Hz.

Lastly, Figure 50 shows PSTHs as a function of tonal frequencies, where the individual frequency stimuli were presented with amplitude of 100db.

4.4.2 HISTOLOGY

Although, biocompatibility of polyimide has been shown, by Kanno et al. (15), studying polyimide devices under implanted condition has not been done before. Polyimide technology enables us to section the paraffin embedded tissue while the polyimide devices are still in their original location. Even though it would be ideal to perform this study using a functional device, it is a challenge to extract the intact brain-device interface while the device is anchored to the skull. Nevertheless, we studied the material response under implant condition by implanting the device into the rats' cortex without anchoring it to the skull. This technique renders the device electrophysiologically nonfunctional but enables us to section and study the intact brain-device interface by slicing through the polyimide device.

We implanted four polyimide devices per rat, in 8 different rat's cortex and then performed histological procedure, discussed in methods section, 15 days post implant. To observe any changes in cell expression near implant sites, cell density was observed in H&E stained slides and glial fiber expression intensity was measured in GFAP

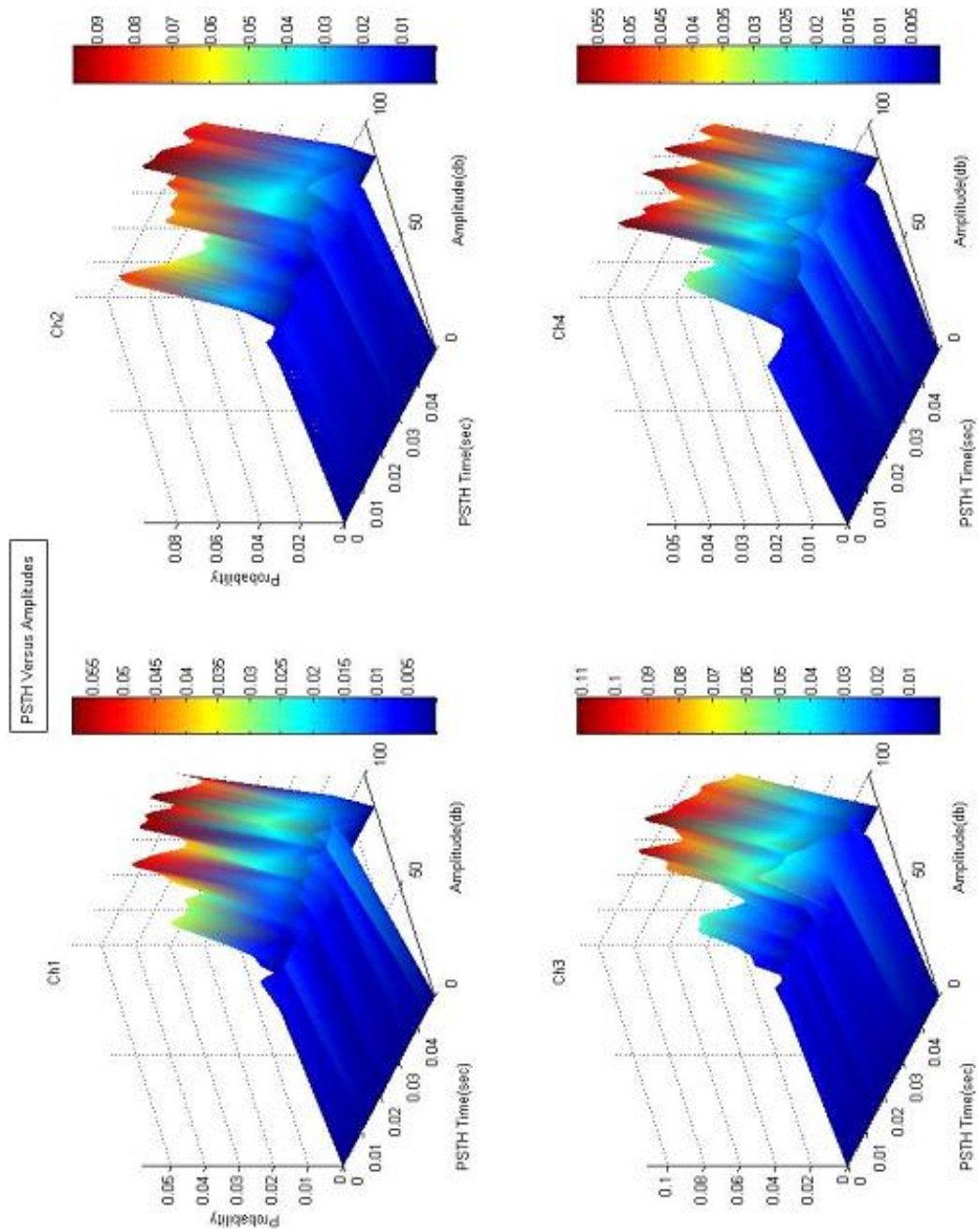


Figure 49: PSTHs vs. amplitude plot, showing increase in response with increase in stimulus amplitude. Frequency was fixed at 2 kHz.

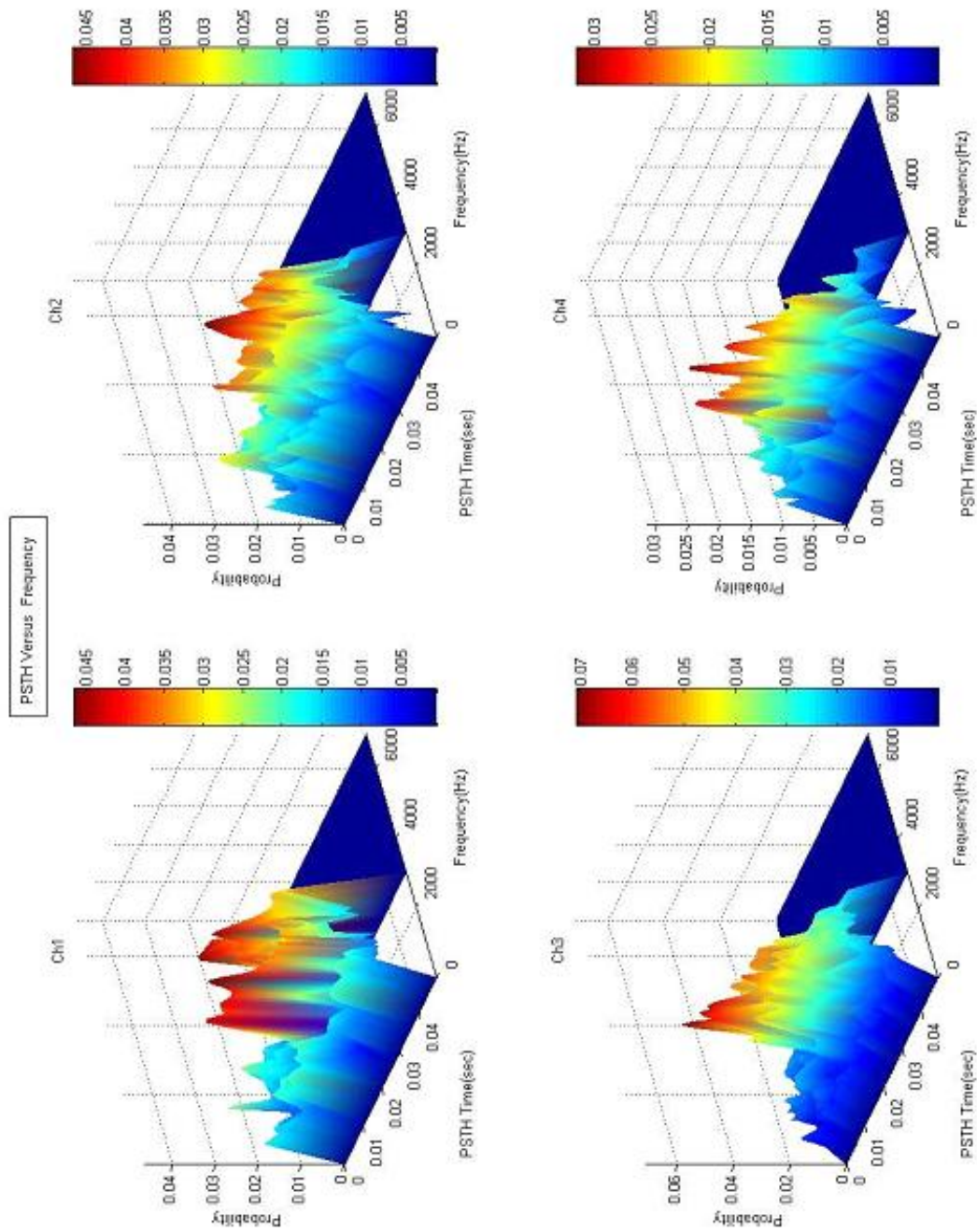
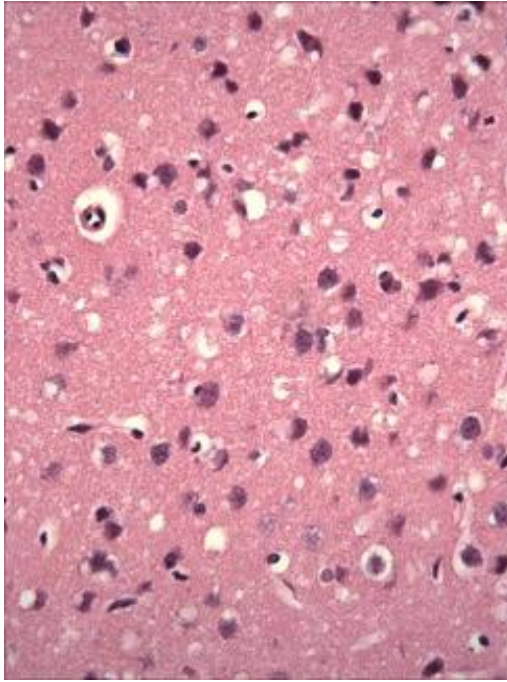
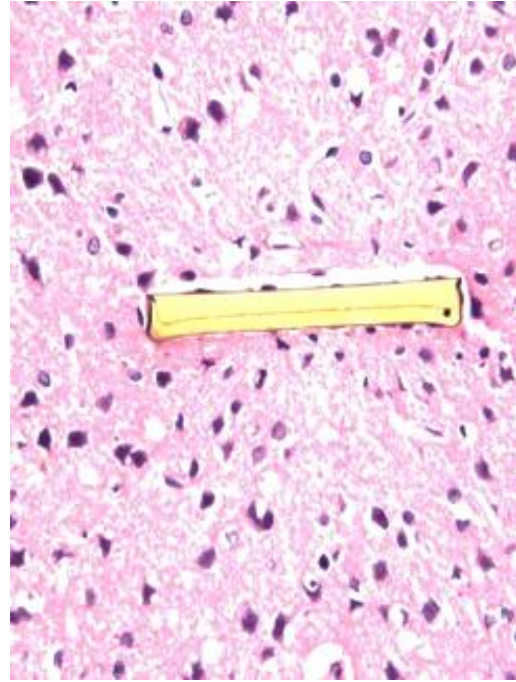


Figure 50: PSTHs vs. frequencies shows that strongest responses were recorded for stimuli with frequencies between 1 kHz to 3 kHz. Amplitude was fixed at 100 db

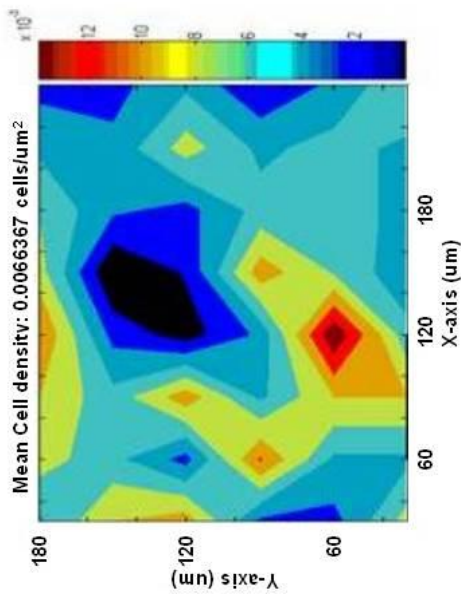
stained slides. Figure 51 shows comparison in cell density between normal tissue and tissue around the implant site. Visual and computational inspection of the two slices in Figure 51 does not indicate any changes in cell density. Very limited encapsulations were observed in either PI or PGA coating cases with no significant change in cell density. Figure 52 shows several examples of H&E stained uncoated polyimide devices (a-d) and PGA coated polyimide devices (e-h) sectioned at various depths. Being able to slice through the implanted devices, allowed the tissue-device interface to remain intact. Figure 53 shows several examples of GFAP stained uncoated polyimide devices and PGA coated devices (e-h). The single sided response can easily be seen in GFAP stained PGA coated slices. GFAP stain intensity is proportional to the density of the glial fibers, which in turn is a response to the foreign body (implanted electrode). This intensity was quantified as described in the methods sections. The measured mean Peak Intensity and mean GFAP expression width is displayed in Figure 54. The mean peak intensity for PGA coated side of the devices was 61.79 ± 14.79 on the scale of 256 being the highest intensity (Black) and 0 being the lowest (white). The uncoated side of the same devices and the uncoated polyimide devices had mean peak intensity of 31.42 ± 15.80 and 21.98 ± 12.89 respectively. The range of GFAP expression measured in distance from the device edge for the coated side, uncoated side and uncoated devices are $80.4 \mu\text{m} \pm 35.5 \mu\text{m}$, $16.4 \mu\text{m} \pm 8.8 \mu\text{m}$ and $36 \mu\text{m} \pm 29 \mu\text{m}$ respectively.



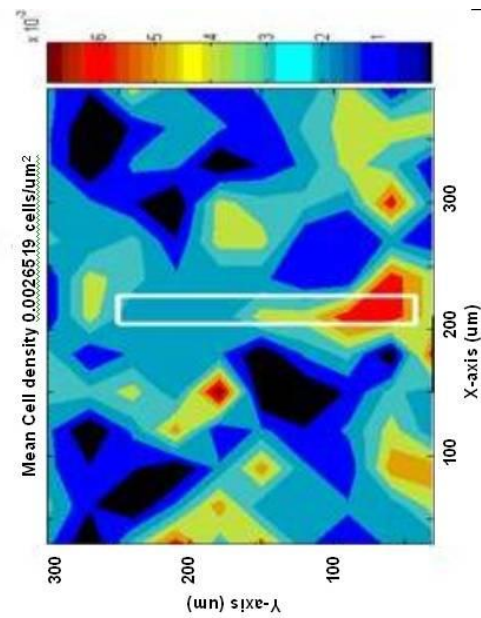
(a)



(b)

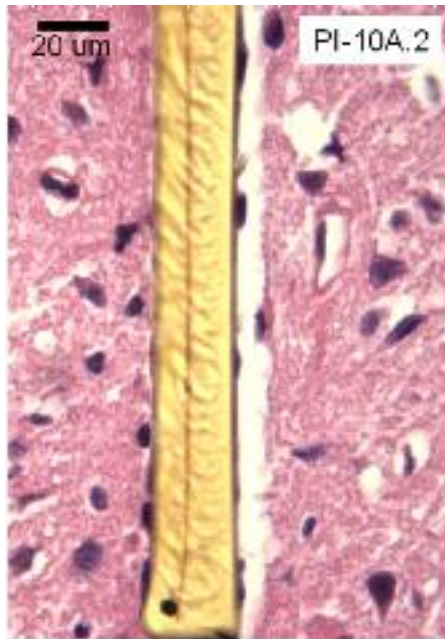


(c)

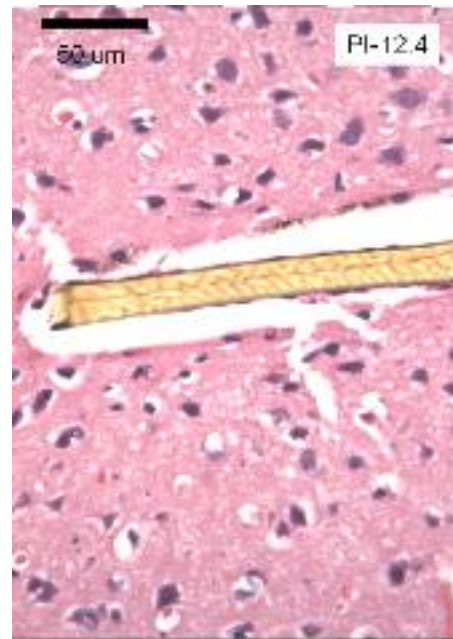


(d)

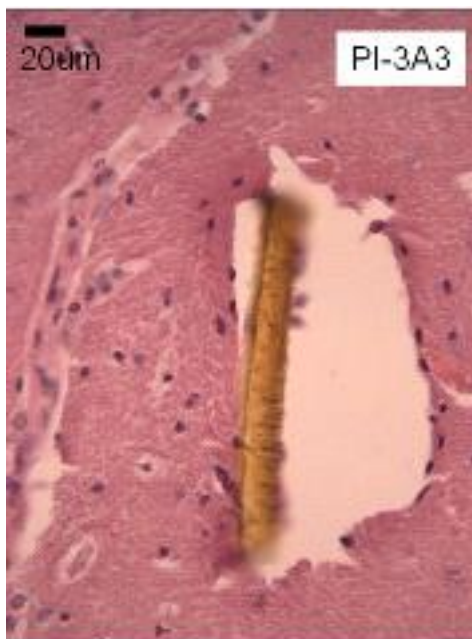
Figure 51: Comparative results of healthy tissue with implanted tissue. 248 cells were computed in healthy tissue and 217 cells were computed in the implanted tissue. (a and b) Original images capture under microscope. (c and d) Cell densities with mean cell densities displayed in respective titles.



(a)



(b)



(c)



(d)

Figure 52 (a-d): H&E stained images of the tissue and the implant sectioned at various depths keeping the implanted device (orange) in place and preserving the device-tissue interface. Uncoated polyimide devices show minimal encapsulation and cell density variation. The spacing between the electrode (orange) and tissue (pink) is due to tissue tearing and pulling away during the slicing process for preparing the histology slides.

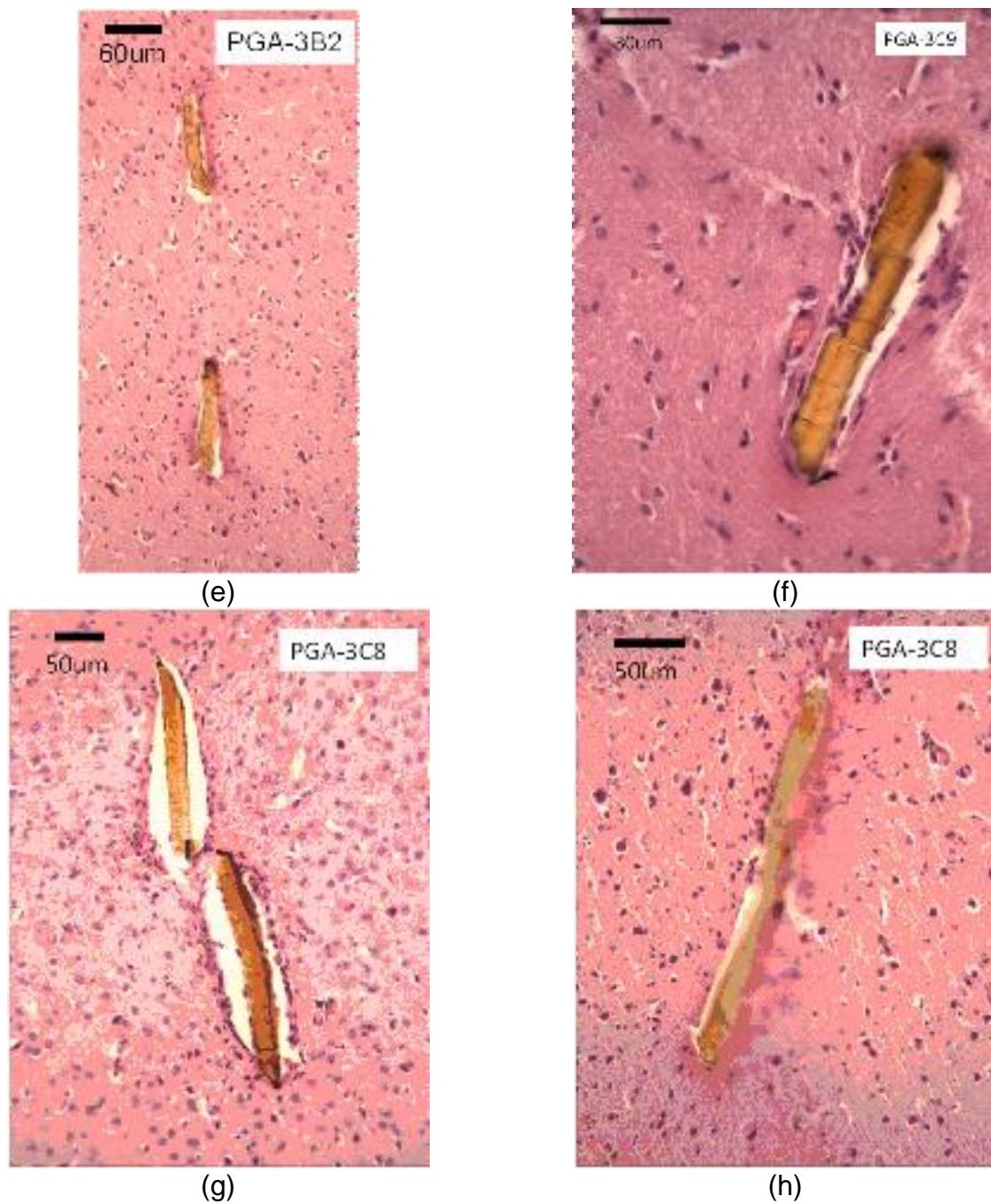


Figure 51 (e-h): H&E stained images of the tissue and the implant sectioned at various depths keeping the implanted device (orange) in place and preserving the device-tissue interface. PGA coated devices show a slightly greater immune gliosis response on the coated side.

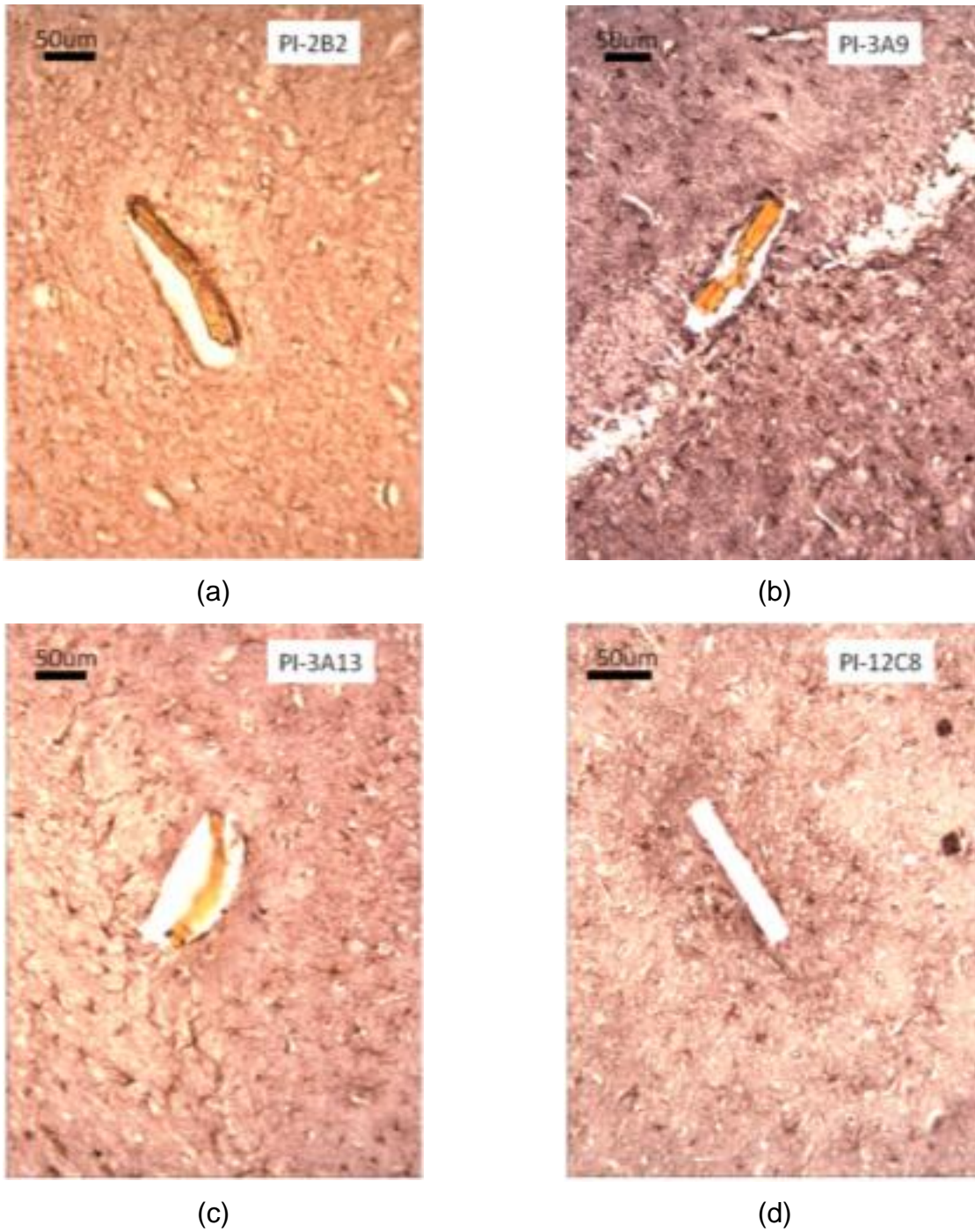


Figure 53 (a-d): GFAP stained images of the tissue and the implant sectioned at various depths keeping the implanted device (orange) in place preserving the device-tissue interface. Uncoated polyimide devices show minimal encapsulation and cell density variation.

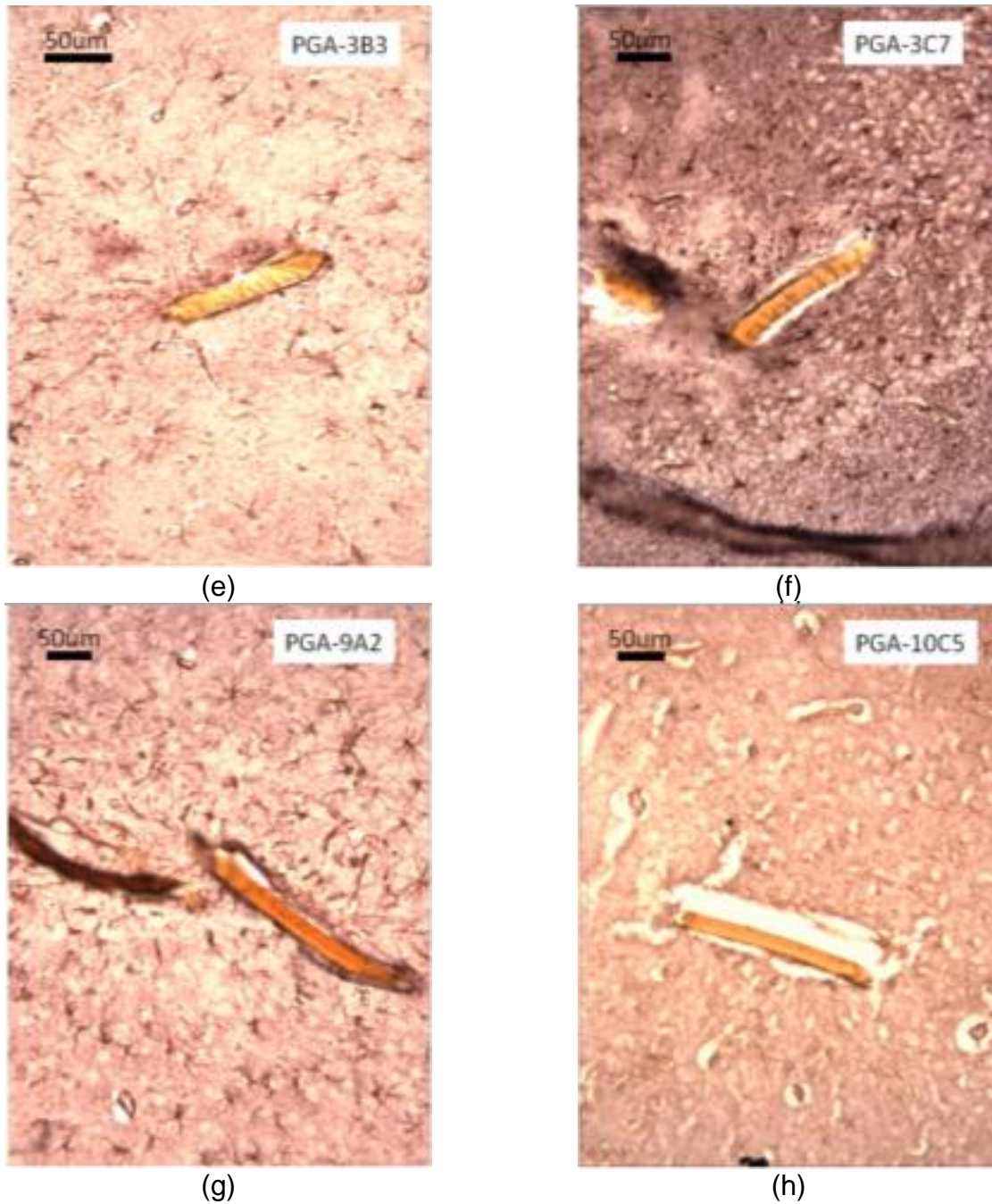


Figure 52 (e-h): GFAP stained images of the tissue and the implant sectioned at various depths keeping the implanted device (orange) in place preserving the device-tissue interface. PGA coated devices show a slightly greater response on the coated side.

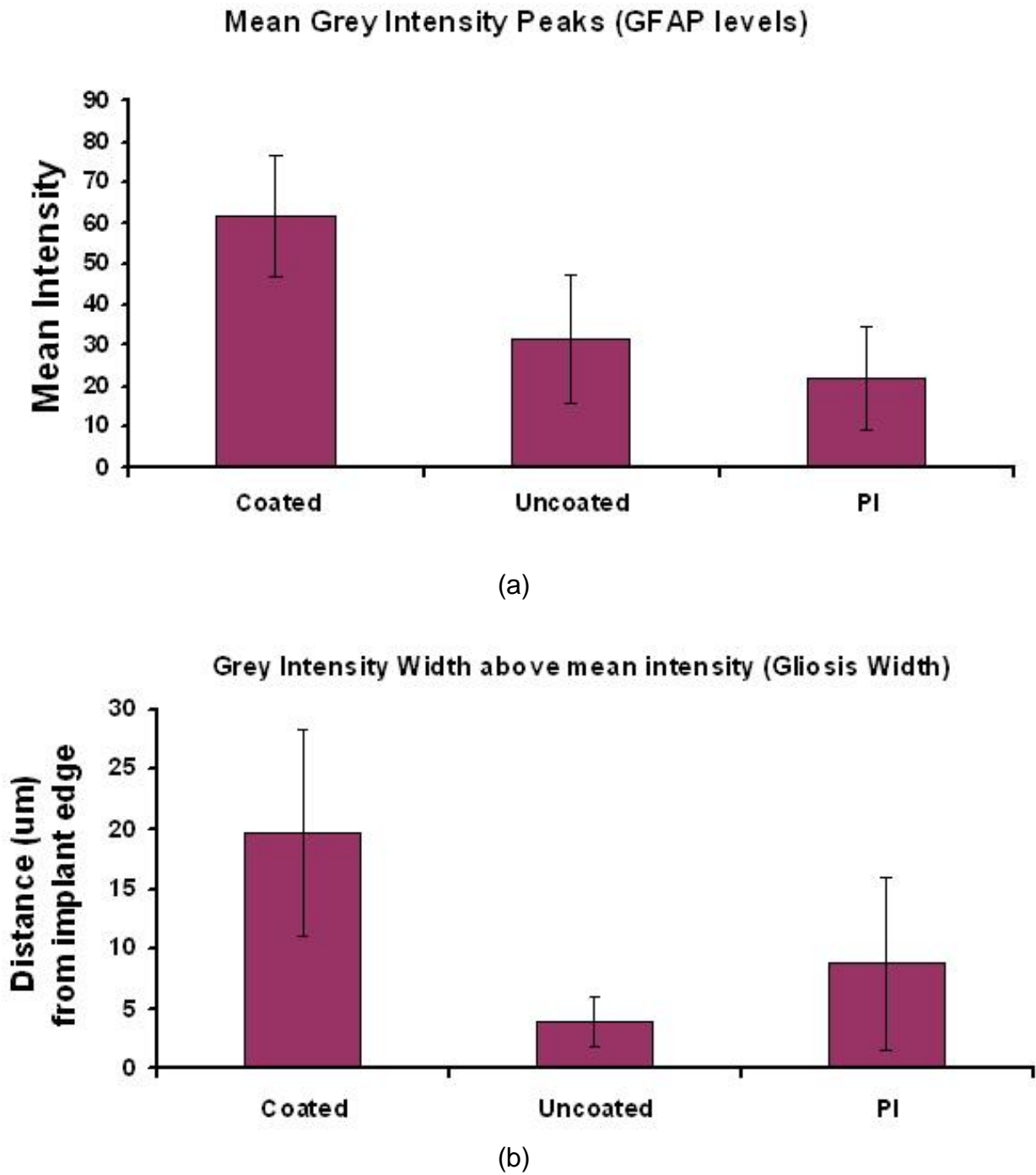


Figure 54: GFAP stains appear as darker gray levels in the black and white images. Peak gray intensity near the implant edge is taken and the intensity and width is computed across the samples (n=5). (a) Peak GFAP levels. (b) Distance from the implant edge to the approximated smallest increase from the mean GFAP expression.

CHAPTER 5. DISCUSSION

Intracortical recording microstructures give promising direction for neural prosthesis, as they provide higher spatial resolution compared to surface recording techniques. Yet, there are many milestones the technology must overcome before it can be used successfully for that application. As many hurdles are overcome, longevity and therefore in turn physical and chemical biocompatibility are the target goals to accomplish. In order to attain these goals, surface chemistry as well as mechanical properties of the implant material must be closely considered. Approximately 10 research groups are trying to address these issues. Even though it is commonly accepted, very few pay much attention to the mechanical impedance matching of the implanted devices with its cortical tissue counterpart. To address the issue of impedance mismatch, we are using polyimide as the flexible backbone material for gold recording devices. As discussed in the introduction section, the Young's modulus value of polyimide being closer to that of cortical tissue, should aid in reducing tissue damage over the lifetime of the implant. We used photodefinable polyimide to simplify the manufacturing processes and have successfully developed two shafts recording devices. The design considerations were done based on the literature review to determine the best contact area and inter-contact spacing for recording and over all shape of the structure. As per Edell et al. tapered tips were designed to minimize trauma to the tissue during insertion (7, 48). The gold material was chosen for its biocompatible and anti-inflammatory properties. The designing of the implant geometry was done using AutoCAD. The radial layout was chosen to optimize the resist coverage during the spin coating steps and did give excellent even coverage of all the

devices across the entire silicon wafer. The connector pads were designed to simplify the assembly process and to fit with snap contact flip connectors, allowing easy attachment and detachment of the devices. A negative mask design was done for polyimide layers and a positive mask was used for metal layer. Due to radial layout of the devices on the wafer and limitations of the conversion software used to convert CAD designs into the binary files the mask production software could understand, we were limited to either using negative masks for the metal layer or to reduce the number of devices to those laying on the primary axis. We tried both the approaches, but obtained the best results with the latter. Once the masks designs were successfully converted, chrome plated glass emulsion masks were easily produce using the standard lithography techniques (Appendix A).

Lithography processing of the devices had its own share of problems. Many of these manufacturing hurdles were overcome as discussed in the results section. To address problems with using polyimide HD4000 as a choice of material for the implantable device substrate, the problem of interfacial stress between polyimide and under laying silicon dioxide substrate needs to be resolved. Furthermore, the heat and mass transfer model suggests that the resulting profile of the polyimide surface is due to the uneven heat distribution to the polyimide substrate and therefore uneven mass transfer. Lastly, polyimide HD4000 is extremely sensitive to the processing environment and therefore may not be the ideal material for processing the cortical devices. Due to its sensitivity to the processing environment, especially humidity, often a residual film was left behind post processing sealing the contact sites and rendering the device non-functional. Reactive Ion oxygen plasma etches improved the interface,

but didn't always yield successful results. Less sensitive and more durable forms of polyimides are available, even though these may not be photodefinable and may require more steps in processing them into a specific shape. Nevertheless, the results we obtain by using the HD4000 were satisfactory. The functional devices were successfully implanted and excellent stimulus driven recordings were obtained.

We successfully manufactured several batches of the devices with average line widths of 7 μm and average contact site area of 1370 μm^2 . The overall thicknesses of the resulting devices were 15 μm on average at the plateau region towards the center of the polyimide surfaces. The electrochemical analysis of these devices also showed typical gold electrode profiles. The typical flat CV curves of the gold electrodes suggest a strong capacitive charge transfer behavior of the devices. Furthermore, peak current of 64 μA suggests that the devices would be very poor stimulating electrodes but excellent recording devices. An order of magnitude lower capacitive current yielded from the dummy connector pads shows that there is very little cross talk between two parallel traces running along the stem of the devices. There is a slight positive shift in the water window of the CV curves for the devices in comparison to gold wire CV and can be attributed to the additional insulation provided by the polyimide layers. The overall impedance of the functional polyimide devices at 1 kHz was 300k Ω , and showed a highly capacitive phase of 74 degrees. The magnitude values of the impedance were typical of those reported in silicon electrodes literatures (11, 25, 25, 29, 48-52). All the functional devices showed similar impedance profiles, and were an order of magnitude higher than that of gold wire impedance at all measured frequencies. The in-vivo electrochemistry showed similar results to in-vitro, suggesting very little changes in the

devices interfacial impedance profiles. There was a slight reduction in the peak CV currents recorded during in-vivo testing, which can be attributed to the different surrounding fluid properties than those of phosphate buffered saline used during in-vitro analysis. We were able to demonstrate the functionality of the devices under acute conditions in a rat animal model. The typical signal to noise ratio obtained was 1.2. Regardless, we obtained excellent post stimuli time histograms (PSTHs) measuring signals strongly driven by the sound stimuli. The raster plots and PSTHs showed a strong correlation at approximately 20 msec post stimuli, typical of primary auditory cortex. Furthermore, we demonstrated stability of the tissue-implant interface over a period of 1 hour. Lastly, we were also able to map out center frequencies for several of the recorded neurons, showing the devices to be an excellent tool for interfacing with neuronal tissues. The successful manufacturing of the polyimide devices with 40 μm x 40 μm contact sites, and the demonstration of its functionality, meets the requirements stated in the specific aim I.

Additionally, per specific aim II, we considered temporary enhancement of the mechanical stiffness of the polyimide to allow for more controlled insertion of the device into the cortical tissue. We used poly (glycolic acid) (PGA), to coat the surface of the device in order to achieve this objective. PGA is approved by FDA for its use in biodegradable sutures. Matsumoto et al. also suggested PGA-collagen composite material to be used as a dural substitute material (53). Furthermore, PGA has a glass transition temperature of 35 °C. This allowed us to regain some of the mechanical flexibility of the polyimide immediately after the implant. PGA slowly degrades over a period of several weeks (30, 31, and 36). In our study we demonstrated that nearly

100% of the PGA degraded within 1 week. We also established a protocol for melt coat processing of PGA (Appendix A). Results showed that the 1 mm³ of the PGA, while degrading in saline, produced a drop of approximately 0.3pH in the surrounding environment. Whereas coated PGA produced a similar drop in first 15 minutes of the experiment and then returned back to normal pH level of 7.4 within 6 hours. Also, in the latter case the surrounding medium was changed after each measurement to mimic diffusion and removal of the surrounding fluid typical in the body. Furthermore, we showed PGA coated devices enhanced the mechanical strength of the device 20 fold. PGA coated devices withstood 7.08 mN peak insertion force compared to 0.33mN of force at which uncoated polyimide device buckled. Using PGA coated devices we easily implanted the devices through the PIA covering. Successfully manufactured PGA coated devices fulfilled all the requirements stated in specific aim II.

Now, we will shift the focus of discussion to histology performed on polyimide and PGA coated devices addressing specific aim III. H&E staining provides an excellent tool for studying cell density, but due to the low biological response induced by our devices, it proved to be somewhat ineffective. Even though in some instances a narrow band of discoloration was observed in H&E stained slides, it was insufficient to easily quantify it. On the other hand GFAP staining proved easily quantifiable. There was an increase in GFAP expression from the baseline in both cases; uncoated polyimide and PGA coated devices. The mean increase in GFAP expression intensity for PI devices was 23 above the baseline value, whereas for PGA coated device were 31 and 62 for uncoated and coated sides respectively. Also, the distance of GFAP expression from the edge of the devices were measured to be 36 μ m, 16 μ m and 80 μ m for uncoated

polyimide devices, uncoated side of the PGA coated devices and coated side of the PGA coated devices respectively. The increase in gliosis around the PGA coating can be attributed to the drop in pH of the surrounding fluid during the degradation process. Nevertheless, these values are at the least 4-6 folds lower than those reported for silicon based implants, even when they are coated with anti-inflammatory and biocompatible materials such as Dexamethasone and Parylene-C (29, 47).

The scope of this thesis took into consideration several aspects of the manufacturing of neural prostheses and provided ample evidence to support the choices that were made. It considered two new materials, namely HD400 polyimide and short chain PGA polymers, as a possible choice of materials for neural interfaces. The results do show incremental benefits for employing these materials for the purpose of manufacturing neural prostheses. Even though this study only focused on HD-4000 polyimide, there are at least a dozen different types of polyimide that are being studied by other groups or could be studied in future work (3, 15, and 50). Also, in this study we plainly focused on short chain PGA polymers without consideration for pH control in the surrounding medium during degradation. In future work this should also be considered to enhance the tissue-implant interactions. Furthermore, incorporating stimulating electrodes alongside of these devices would also be the next logical step in the direction of device manufacturing and lithography.

In the scope of the thesis, we have also used several analytical techniques to assess several different parameters of the device functionality. Namely, we used PSTHs vs. time, which are not so often seen in neural interface literature, to study interfacial stability and indirectly monitor physiological changes at the interface in the time domain.

This technique was also employed by Chiganos et al. in our lab to monitor stroke progression (54-57). The GFAP intensity profiling was yet another tool not so commonly used in neural interface literature to measure the extent of gliosis, even though it is now found in recent literature. Lastly, the tissue-device interface should be more carefully studied using electrochemical methods as done by Kevin Otto's group for silicon devices (58).

REFERENCE LIST

- (1) Kandel ER, Schwartz JH, Jessell TM. Principles of neural science, 4th ed ed. New York: McGraw-Hill, Health Professions Division, 2000.
- (2) Nolte J. The Human brain: an introduction to its functional anatomy, fifth ed. St. Louis: Mosby: A harcourt Health Sciences Company, 2002.
- (3) Richardson RR, Jr., Miller JA, Reichert WM. Polyimides as biomaterials: preliminary biocompatibility testing. *Biomaterials* 1993 Jul;14:627-635.
- (4) HODGKIN AL, HUXLEY AF. A quantitative description of membrane current and its application to conduction and excitation in nerve. *J Physiol* 1952 Aug;117:500-544.
- (5) Rousche PJ, Petersen RS, Battiston S, Giannotta S, Diamond ME. Examination of the spatial and temporal distribution of sensory cortical activity using a 100-electrode array. *J Neurosci Methods* 1999 Aug 1;90:57-66.
- (6) Rousche PJ, Normann RA. Chronic recording capability of the Utah Intracortical Electrode Array in cat sensory cortex. *J Neurosci Methods* 1998 Jul 1;82:1-15.
- (7) Edell DJ, Toi VV, McNeil VM, Clark LD. Factors influencing the biocompatibility of insertable silicon microshafts in cerebral cortex. *IEEE Trans Biomed Eng* 1992 Jun;39:635-643.
- (8) Wise KD, Anderson DJ, Hetke JF, Kipke DR, Najafi K. Wireless Implantable Microsystems: High-Density Electronic Interfaces to the Nervous System. *Proceedings of IEEE* 2004 Jan;92:76-97.
- (9) Schmidt CE, Shastri VR, Vacanti JP, Langer R. Stimulation of neurite outgrowth using an electrically conducting polymer. *Proc Natl Acad Sci U S A* 1997 Aug 19;94:8948-8953.
- (10) Dobelle WH, Mladejovsky MG. Phosphenes produced by electrical stimulation of human occipital cortex, and their application to the development of a prosthesis for the blind. *J Physiol* 1974 Dec;243:553-576.
- (11) Rousche PJ, Pellinen DS, Pivin DP, Jr., Williams JC, Vetter RJ, Kipke DR. Flexible polyimide-based intracortical electrode arrays with bioactive capability. *IEEE Trans Biomed Eng* 2001 Mar;48:361-371.
- (12) Nicolelis MA, Ghazanfar AA, Faggin BM, Votaw S, Oliveira LM. Reconstructing the engram: simultaneous, multisite, many single neuron recordings. *Neuron* 1997 Apr;18:529-537.

- (13) Cui X, Lee VA, Raphael Y, et al. Surface modification of neural recording electrodes with conducting polymer/biomolecule blends. *J Biomed Mater Res* 2001 Aug;56:261-272.
- (14) Kipke DR, Vetter RJ, Williams JC, Hetke JF. Silicon-substrate intracortical microelectrode arrays for long-term recording of neuronal spike activity in cerebral cortex. *IEEE Trans Neural Syst Rehabil Eng* 2003 Jun;11:151-155.
- (15) Kanno M, Kawakami H, Nagaoka S, Kubota S. Biocompatibility of fluorinated polyimide. *J Biomed Mater Res* 2002 Apr;60:53-60.
- (16) Suzuki T, Mabuchi K, Takeuchi S. A 3D flexible parylene probe array for multichannel neural recording. *N. E., Conf. Proc.* 2003 154-156.
- (17) Takeuchi S, Ziegler D, Yoshida Y, Mabuchi K, Suzuki T. Parylene flexible neural probes integrated with microfluidic channels. *Lab Chip* 2005 May;5:519-523.
- (18) Ziegler D, Suzuki T, Takeuchi S. Fabrication of Flexible Neural Probes With Built-In Microfluidic Channels by Thermal Bonding of Parylene. *Microelectromechanical Systems, Journal of* 2006 Dec;15:1477-1482.
- (19) Tan J, Shen H, Carter KL, Saltzman WM. Controlling human polymorphonuclear leukocytes motility using microfabrication technology. *J Biomed Mater Res* 2000 Sep 15;51:694-702.
- (20) Satish L, Gandhi D, Das R, Rousche PJ. Analysis of In-vitro Neurite Extension for Neurotrophic Electrode Design. 2005 385-387.
- (21) Satish L, Gandhi D, Rousche PJ. Preliminary study of neurite outgrowth within polyimide microtubes. 2004 4306-4309.
- (22) Rousche PJ, Normann RA. Chronic intracortical microstimulation (ICMS) of cat sensory cortex using the Utah Intracortical Electrode Array. *IEEE Trans Rehabil Eng* 1999 Mar;7:56-68.
- (23) Campbell PK, Normann RA, Horch KW, Stensaas SS. A chronic intracortical electrode array: preliminary results. *J Biomed Mater Res* 1989 Aug;23:245-259.
- (24) Campbell PK, Jones KE, Normann RA. A 100 electrode intracortical array: Structural Variability. *Biomed Sci Instrum* 1990;161-166.
- (25) Normann RA, Campbell PK, Jones KE. A silicon based electrode array for intracortical stimulation: structural and electrical properties. 1989 939-940.
- (26) Stieglitz T, Meyer JU. Implantable microsystems. Polyimide-based neuroprostheses for interfacing nerves. *Med Device Technol* 1999 Jul;10:28-30.

- (27) Gandhi D, Rousche PJ, Das R, Saggere L, Krishnan S. Functionality Evaluation of Photo-definable Polyimide, Flexible Interface for the Central Nervous System. 2006 455-460.
- (28) Suzuki T, Ziegler D, Mabuchi K, Takeuchi S. Flexible neural probes with micro-fluidic channels for stable interface with the nervous system. *Conf Proc IEEE Eng Med Biol Soc* 2004;6:4057-4058.
- (29) Fofonoff TA, Martel SM, Hatsopoulos NG, Donoghue JP, Hunter IW. Microelectrode array fabrication by electrical discharge machining and chemical etching. *IEEE Trans Biomed Eng* 2004;51:890-895.
- (30) Stice PJ, Panitch A, Muthuswamy J. Improved viability of chronic neural implants using thin microelectrodes. 2003 1987-1989.
- (31) Stice PJ, Gilletti A., Panitch A, Muthuswamy J. Thin microelectrodes reduce GFAP expression in the implant site in rodent somatosensory cortex. *Journal of Neural Engineering* 2007;4:42-53.
- (32) Pietrzak WS, Verstynen ML, Sarver DR. Bioabsorbable fixation devices: status for the craniomaxillofacial surgeon. *J Craniofac Surg* 1997 Mar;8:92-96.
- (33) Stahelin AC, Weiler A, Rufenacht H, Hoffmann R, Geissmann A, Feinstein R. Clinical degradation and biocompatibility of different bioabsorbable interference screws: a report of six cases. *Arthroscopy* 1997 Apr;13:238-244.
- (34) Sittering M, Reitzel D, Dauner M, et al. Resorbable polyesters in cartilage engineering: affinity and biocompatibility of polymer fiber structures to chondrocytes. *J Biomed Mater Res* 1996;33:57-63.
- (35) Belkas JS, Shoichet MS, Midha R. Peripheral nerve regeneration through guidance tubes. *Neurol Res* 2004 Mar;26:151-160.
- (36) Goupil D, Ratner BD, Hoffman AS, Schoen FJ, Lemons JE. Sutures. In: New York AP, ed. *Biomaterials Science: An Introduction to Materials in Medicine* 1996:356-360.
- (37) Middleton JC, Tipton AJ. Synthetic biodegradable polymers as orthopedic devices. *Biomaterials* 2000 Dec;21:2335-2346.
- (38) Daniels AU, Chang MK, Andriano KP. Mechanical properties of biodegradable polymers and composites proposed for internal fixation of bone. *J Appl Biomater* 1990;1:57-78.
- (39) Frost, Sullivan. Chap 10. U.S. Absorbable and Erodible Biomaterials Products Markets 1995.

- (40) Das R, Gandhi D, Krishnan S, Saggere L, Rousche PJ. A benchtop system to assess cortical neural interface micromechanics. *IEEE Trans Biomed Eng* 2007 Jun;54:1089-1096.
- (41) Barrows TH. Degradable Implant Materials: A Review of Synthetic Absorbable Polymers and their Applications. *Clinical Materials* 1986;1:233-257.
- (42) Gilding DK, Reed AM. Biodegradable Polymers for Use in Surgery—Polyglycolic/Poly(lactic acid) Homo- and Copolymers. *Polymer* 1979;1459-1484.
- (43) Kohn J, Langer R, Ratner BD, Hoffman AS, Schoen FJ, Lemons JE. Bioresorbable and Bioerodible Materials. *Biomaterials Science: An Introduction to Materials in Medicine*, New York, Academic Press ed 1996:64-72.
- (44) Shalaby SW. *Biomedical Polymers, Designed to Degrade Systems*. New York: 1994.
- (45) Szarowski DH, Anderser MD, Retterer S, et al. Brain Responses to Micro-machined Silicon Devices. *Brain Research* 2003;23-35.
- (46) Turner JN, Shain W, Szarowski DH, et al. Cerebral Astrocyte Response to Micromachined Silicon Implants. *Experimental Neurology* 1999;33-49.
- (47) Zhong Y, Bellamkonda RV. Dexamethasone-coated neural probes elicit attenuated inflammatory response and neuronal loss compared to uncoated neural probes. *Brain Res* 2007 May 7;1148:15-27.
- (48) Edell DJ, McNeil VM, Clark LD. Microfabrication technology for development of chronic neural information transducers. 1986 180-183.
- (49) Campbell PK, Jones KE, Huber RJ, Horch KW, Normann RA. A silicon-based, three-dimensional neural interface: manufacturing processes for an intracortical electrode array. *IEEE Trans Biomed Eng* 1991 Aug;38:758-768.
- (50) Iijima M, Takahashi Y. Electrical, thermal and mechanical properties of polyimide thin films prepared by high temperature vapor deposition polymerization. *High Performance Polymers* 1993;3:229-237.
- (51) Weiland J., Humayun M., Anderson D. Electrical Properties for Iridium Oxide Versus Titanium Nitride Stimulating Electrodes. *IEEE Tran Bio Eng* December 2002;49:1574-1579.
- (52) Lee I., Choo M, Choi K., Whang C., Lee Y. Characterization of iridium film as a stimulating neural electrode. *Biomaterials* 2002;23:2375-2380.

- (53) Matsumoto K., Nakamura T., Fukuda S., Sekina T., Ueda H., Shimizu Y. A Gelatin Coated Collagen-Polyglycolic Acid composite Membrane as a Dural Substitute. *ASAIO Journal* 2001;47:641-645.
- (54) Chiganos TC, Jensen WJ, Rousche PJ. Characterization of auditory cortex responses after photothrombotic infarction. 2005.
- (55) Chiganos TC, Jensen WJ, Rousche PJ. Comparative electrophysiology within the core and penumbra regions after focal ischemic stroke. 2006.
- (56) Chiganos TC, Jensen WJ, Rousche PJ. Electrophysiological response dynamics during focal cortical infarction. *Journal of Neural Engineering* 2006;3:L15-L22.
- (57) Jensen WJ, Chiganos TC, Rousche PJ. A method ofr monitoring intra-cortical motor cortex responses in an animal model of ischemic stroke. 2006.
- (58) Otto K., Johnson M., Kipke DR. Voltage Pulses Change Neural Interface Properties and Improve Unit Recordings with Chronically Implanted Microelectrodes. *IEEE Tran Bio Eng* 2006;53:333-340.

APPENDIX A

Protocol for Polyimide (PI) Device Processing:

- 1) Begin with 4 inch Silicon wafers.
- 2) Clean the Silicon wafers with PIRANHA solution of $\text{H}_2\text{O}_2 : \text{H}_2\text{SO}_4$ (1:3) for 20 minutes.
- 3) Thermal Oxidation of wafers at 1000 °C for 15 minutes. *See Oxidation Protocol.*
- 4) Clean the Silicon wafers again with PIRANHA solution of $\text{H}_2\text{O}_2 : \text{H}_2\text{SO}_4$ (1:3) for 20 minutes.
- 5) Puddle spin deposit POLYIMIDE (PI) at 1500 rpm for 1 minute on the Silicon wafers.
- 6) Soft bake the above prepped PI-wafer for : 100 seconds at 85 °C and
100 seconds at 95 °C
- 7) Expose the PI-wafer using MASK 1 for 15-16 seconds.
 - a. PI requires exposure levels of 300 mJ/cm^2
 - b. MA6 provides 365nm UV light intensity of 20 mJ/cm^2 seconds
 - c. i.e. $300/20 = 15$ seconds of exposure time
- 8) Post exposure bake the PI-wafer for: 100 seconds at 85 °C and
100 seconds at 95 °C
- 9) Develop the PI-wafers using PA-400D developer solution (obtained from HD Microsystems) for 4-5 minutes.
- 10) Rinse the PI-wafers using PA-400R rinse solution (obtained from HD Microsystems) for ~1 minute.
- 11) Air dry the PI-wafers using nitrogen gun for ~20 seconds. Note: no water.
- 12) Cure the bottom layer of PI-wafer at 375 °C for 60 minutes.
- 13) Expose the PI-wafer to oxygen plasma for 2.5 min using Reactive Ion Etching (RIE).
- 14) E-beam deposit metal (Au/Cr) using varian. *See Varian Protocol.*
- 15) Pattern metal with MASK 2 using S1818 photoresist. *See Photoresist processing Protocol.*
- 16) Repeat steps 5-13. Use MASK 3 for step 7, instead.
- 17) Lift off devices by etching underline oxide layer with HYDROFLUORIC ACID.
- 18) Rinse the devices with DI water and store them in a sterile pouch.

Oxidation Protocol:

1. Replace water in a flask with new DI water
2. Switch on Variac, power supply to 130V.
3. Wait till water temperature reads 100 °C
4. Reduce the variac setting to 90V
5. Program the oxidation furnace to increase temperature from 700 °C (idle temperature) to 1000 °C at the rate of 10 °C/min
6. Soak the wafer in water vapor stream at 1000 °C for 15 min, to produce 1um thick oxide layer.
7. Allow the oxidation furnace to return to its idle temperature at the same rate.
8. Remove the wafer

Varian e-beam metal deposition Protocol:

1. Open N₂ valve
2. Re-pressurize the chamber to atm.
3. Place your wafer onto the planetary facing downwards
4. Turn off N₂ valve
5. Place the metal in the container located in the center of the system
6. Seal the chamber and pressurize the system
7. Enter density values for appropriate metals. (7.2g/cc for gold)
8. Power on the e-beam source
9. Set electron beam current to appropriate evaporation conditions
10. Monitor deposition rate, and maintain approximate rate of 3-4Å/s
11. Repeat steps 1-6 to remove the sample and pressurize the system

S1818-Positive Photoresist processing Protocol:

1. Dehydrate the wafer at 110 °C for 20 min
2. Coat the substrate with primer for 10 sec and then spin-off excess for 10 sec.
3. Puddle spin deposit S1818 at 1500 RPM for 30 sec to achieve ~2um thick coating
4. Soft bake at 110 °C for 3 min
5. Expose using MASK 2 for 6 sec.
6. Develop using develop solution (351:DI – 1:4) for approximately 40 sec
7. Rinse in DI water cascade three times for 5 min each.
8. Etch underlying metal using Appropriate etchant.
9. Strip of developed photoresist using 1112A remover by soaking the wafer in it for 30-40 min at room temperature raise temperature to 40 °C is necessary, but the upper limit of the temperature must be carefully controlled.

Coating the PGA on to an Electrode:

1. Start with Polyimide electrode
2. Melt 0.3g of PGA powder in a glass Petri dish at 210-220°C (Be careful not to over heat, because at about 250°C PGA degrades.)
3. Dip the electrode at a shallow angle to the surface so that only one side is coated.
4. Repeat if a thicker coating is needed.

APPENDIX B

Histology procedures

- Fifteen days post-implant animals were perfused for tissue preparation:
 1. Give a dosage KXA anesthesia ($0.2 \text{ ml } 100 \text{ g}^{-1}$)
 2. Perfusion of 0.9% saline solution
 3. Perfusion of 10% formalin solution
 4. Extract the brain tissue
 5. Store in the formalin fixative
 6. Section the tissue to separate the implanted areas.
 7. Dehydrate and fix the tissue:
 - a. 70% ethanol (> 4 hours)
 - b. 95% ethanol (4 hours)
 - c. 100% n-butanol (2x12 hours)
 - d. Equal parts of n-butanol and toluene (12 hours)
 - e. Toluene (12 hours)
 - f. Paraffin (24 hours)
 8. Section paraffin embedded tissue serially at an 8 μm thickness, cut perpendicular to the device implant.
- Sections were taken to an implant depth of 2-3mm to obtain a significant amount of data for qualitative analysis.
- Free floating sections were mounted for hematoxylin and eosin (H&E) and immunochemistry staining.

Immunochemistry GFAP Protocol for Paraffin Fixed Sections

1. Deparaffinize sections in xylene (5 min)
2. Hydrate with 100% ethanol (3 min)
3. Hydrate with 95% ethanol (1 min)
4. Rinse in tap water
5. Epitope Retrieval
 - a. Briefly, pre-heat steamer or water bath with staining dish containing 0.1 M Citrate Buffer (pH 6.0) until temperature reaches 95-100 °C.
 - b. Immerse slides in the staining dish and place the lid loosely on the staining dish (20 min)
 - c. Place the staining dish at room temperature and allow the slides to cool (20 min)
 - d. Let slides reach temp. equilibrium in PBS (10 min) and let sit overnight at 4°C
6. Primary Antibody
 - a. Incubate sections in humidity chamber with (50-100ml) Rabbit Anti-Cow GFAP (DakoCytomation, Cat# Z0334) diluted 1:500 in primary antibody dilution containing serum block (1 hour)

- b. Rinse in PBS (30 min)
- 7. Secondary Antibody
 - a. Incubate sections in humidity chamber with Goat Anti-Rabbit secondary diluted (1 hour)
 - b. Rinse in PBS (30 min)
- 8. Detection
 - a. Incubate sections with ABC solution in humidity chamber (1 hour)
 - b. Rinse in PBS (30 min)
- 9. Chromogen/Substrate
 - a. Incubate sections in nickel intensified DAB substrate solution (7min)
 - b. Rinse in PBS briefly.
 - c. Dehydrate through:
 - i. 70% ethanol (3 min)
 - ii. 95% ethanol (3 min)
 - iii. 100% ethanol (3 min)
 - d. Clear in xylene (5 min)
 - e. Coverslip with permanent mounting medium.

APPENDIX C

Page Intentionally Left Blank

FORM A
Protocol for Animal Use
Version 3.1

Office for the Protection of Research Subjects (OPRS)
Animal Care Committee (ACC)

1737 West Polk Street (MC 672)
 201 Administrative Office Building
 Chicago, IL 60612
 Phone: 312.996.1972 Fax: 312.996.9088
 www.research.uic.edu

PLEASE TYPE THIS FORM

If this protocol is a resubmission, which protocol(s) is it intended to replace: Old ACC Protocol No.(s):														
DATE APPLICATION COMPLETED: 11/30/2004		ACC Protocol No. A												
1. PROJECT TITLE: (limit to 60 characters) Electrophysiologic Response Dynamics of Cortical Infarction														
2. PRINCIPAL INVESTIGATOR: <table style="width: 100%;"> <tr> <td style="width: 33%;">Name (Last, First): Rousche, Patrick</td> <td style="width: 16%;">Work Phone Number: 312 9962333</td> <td style="width: 16%;">Fax Number: 312 9965921</td> <td style="width: 35%;">Emergency Phone Number: 630 8053910</td> </tr> <tr> <td>Department Affiliation: Bioengineering</td> <td colspan="2">Mailing Address¹ : Bioengineering (MC 063)</td> <td>Choose One, if Applicable: <input type="checkbox"/> New Address - Change for all protocols <input type="checkbox"/> Secondary Address - Use this protocol only </td> </tr> <tr> <td>E-mail Address: rousche@uic.edu</td> <td colspan="3"></td> </tr> </table>			Name (Last, First): Rousche, Patrick	Work Phone Number: 312 9962333	Fax Number: 312 9965921	Emergency Phone Number: 630 8053910	Department Affiliation: Bioengineering	Mailing Address ¹ : Bioengineering (MC 063)		Choose One, if Applicable: <input type="checkbox"/> New Address - Change for all protocols <input type="checkbox"/> Secondary Address - Use this protocol only	E-mail Address: rousche@uic.edu			
Name (Last, First): Rousche, Patrick	Work Phone Number: 312 9962333	Fax Number: 312 9965921	Emergency Phone Number: 630 8053910											
Department Affiliation: Bioengineering	Mailing Address ¹ : Bioengineering (MC 063)		Choose One, if Applicable: <input type="checkbox"/> New Address - Change for all protocols <input type="checkbox"/> Secondary Address - Use this protocol only											
E-mail Address: rousche@uic.edu														
3. <input type="checkbox"/> CO-INVESTIGATOR <input checked="" type="checkbox"/> OTHER PROJECT STAFF (list only those to be contacted in emergency) Name (Last, First): Chiganos, Terry Campus Phone Number: 312 9969465 Fax Number: 312 9965921 Emergency Phone Number: 312 296-4268 Department Affiliation: Bioengineering E-mail Address: tchiga1@ioc.edu Mailing Address ¹ : Bioengineering (MC 063) Choose One, if Applicable: <input type="checkbox"/> New Address - Change for all protocols <input type="checkbox"/> Secondary Address - Use this protocol only Copy on all Correspondence? <input checked="" type="checkbox"/> Yes <input type="checkbox"/> No Role on Protocol ² 1) Scientist	<input checked="" type="checkbox"/> CO-INVESTIGATOR <input checked="" type="checkbox"/> OTHER PROJECT STAFF (list only those to be contacted in emergency) Name (Last, First): Jensen, Winnie Campus Phone Number: 312 9969465 Fax Number: 312 9965921 Emergency Phone Number: 773 5014140 Department Affiliation: Bioengineering E-mail Address: wj@hst.aau.dk Mailing Address ¹ : Bioengineering (MC 063) Choose One, if Applicable: <input type="checkbox"/> New Address - Change for all protocols <input type="checkbox"/> Secondary Address - Use this protocol only Copy on all Correspondence? <input type="checkbox"/> Yes <input checked="" type="checkbox"/> No Role on Protocol ² 1) Scientist	<input type="checkbox"/> CO-INVESTIGATOR <input type="checkbox"/> OTHER PROJECT STAFF (list only those to be contacted in emergency) Name (Last, First): Campus Phone Number: Fax Number: Emergency Phone Number: Department Affiliation: E-mail Address: Mailing Address ¹ : Choose One, if Applicable: <input type="checkbox"/> New Address - Change for all protocols <input type="checkbox"/> Secondary Address - Use this protocol only Copy on all Correspondence? <input type="checkbox"/> Yes <input type="checkbox"/> No Role on Protocol ²												

¹ All ACC correspondence will be sent to this address. For on campus investigators use Department and Mail Code. For off campus investigators provide complete mailing address.

² Indicate specific role on protocol by number: 1) Scientist* - will perform experiments with animals (includes Co-PIs, Post-docs, graduate/undergraduate students and research technicians), 2) Consultant - will not be directly involved in animal studies, 3) Research Coordinator - will not be directly involved in animal studies. * All personnel listed as scientists must be on Appendix 3.

4. Number of Years Requested for Protocol: <input type="checkbox"/> 1 yr <input type="checkbox"/> 2 yrs <input checked="" type="checkbox"/> 3 yrs					
5. Protocol will become effective and may be initiated on the date that final clarifications are reviewed and approved					
6. Funding Support³ (a must be completed for all protocols; b, d & e, must be completed for each external funding source supported by this protocol: c may be left blank, if unknown)					
a. Funding Agency (e.g., NIH, foundations, departmental, etc.): Department of Bioengineering and Department of Neurosurgery					
b. Title of Funding Proposal: CAREER: Intellectual Infrastructure and Critical Enabling Technology Development for Advanced Neural Engineering Applications					
c. Number Assigned by Funding Agency: BES- 0348145			d. Proposal Approval Form Number: 04-1-176		
e. Funding Status:		Funded: <input checked="" type="checkbox"/>	Pending: <input type="checkbox"/>	Not Submitted Yet: <input type="checkbox"/>	
7. Animals					
	Species/Strain	Sex	Total No. Requested	Age or Weight	Use ⁴
a.	<u>Rat/Sprague-Dawley</u>	M	90	44-48 Days	1
b.					
c.					
d.					
e.					
f.					
g.					
h.					

³ If more than one funding source will be supporting this ACC protocol, complete Appendix 4. All funding sources using animals on this ACC protocol must be reported to the ACC.

⁴ Indicate uses of animals on protocol by number: 1) Experimental 2) Breeders 3) Inappropriate genotype 4) Other - specify. Only one use may be indicated per line. If the same animal model has multiple uses, enter on separate lines.

8. Special Requirements

a. All rodents purchased should be specific pathogen free (SPF). <i>Should investigators require non-SPF rodents, contact BRL veterinary staff (312-996-7040) to discuss purchasing needs.</i>		
b. Where will animals be housed?	Room 124	Building BRL
c. Where will animals be used?	Room B20	Building NPI, 801 S Wood St
<i>Will animals be maintained in this room outside of the BRL (or an approved satellite facility) for more than 12 hours?</i> <input type="checkbox"/> Yes <input checked="" type="checkbox"/> No		
d. For protocols involving nonhuman primates, check all parts of the UIC Environmental Enrichment Plan in which animals will be exempt from participating and justify below the reason(s) for the animals not to participate in that particular portion of the plan. <i>For further information on the Environmental Enrichment Plan, contact BRL veterinary staff (312-996-7040).</i>		
<div style="display: flex; flex-wrap: wrap;"> <div style="width: 50%;"><input type="checkbox"/> Social contact through mesh screen</div> <div style="width: 50%;"><input type="checkbox"/> Food supplements (nuts, fruit, vegetables, etc.)</div> <div style="width: 50%;"><input type="checkbox"/> Social contact through pair or group housing</div> <div style="width: 50%;"><input type="checkbox"/> Manipulable objects (chew toys, branches, mirrors, etc.)</div> </div>		
e. Special instructions for maintenance or purchase. Note: if your project involves the maintenance of a breeding colony, complete the appropriate Appendix 1. Animals who undergo survival surgery may be housed individually to facilitate the recovery process.		
f. If using rodents, will animals be housed in wire-bottom cages? <input type="checkbox"/> Yes <input checked="" type="checkbox"/> No If yes, justify use of wire-bottom caging, indicate duration on wire-bottom caging and describe monitoring program (See UIC ACC Guidelines on use of wire-bottom caging for Rodents http://www.research.uic.edu/protocolreview/acc/policies/index.shtml).		

9. Use of Compounds, Organisms, Biologicals, Anesthetic Gases, Recombinant DNA, and Medical Materials

- a. Hazardous Materials- Are any of the following being used in vivo? If you indicate 'yes' for any of the substances below, you must complete and attach Appendix 2.

Specify compound or organism

Carcinogens	<input type="checkbox"/> Yes	<input checked="" type="checkbox"/> No
Biohazard	<input type="checkbox"/> Yes	<input checked="" type="checkbox"/> No
(IBC Approval No. and Biosafety level)		
Chemical hazards	<input type="checkbox"/> Yes	<input checked="" type="checkbox"/> No

Radioisotopes (RPN Approval No.)

☐ Yes

☒ No

Recombinant DNA (IBC Approval No. and Biosafety level)

☐ Yes

☒ No

NOTE: *Bloodborne pathogen training is required for all use of human cells or tissues. Contact EHSO at 312-996-7411 or www.uic.edu/depts/envh/ for additional information on training.*

9. Use of Compounds Organisms, Biologicals, Anesthetic Gases, Recombinant DNA, and Medical Materials (continued)

b. Murine Biologicals: Are murine biologicals (tumor lines, serum, cell lines, etc.) being used in animals that will have to be housed in animal facilities after administration?

☐ Yes

☒ No

List specific biological(s):

If using murine biologics, please contact the BRL veterinary staff at 312-996-1217 for additional information.

c. Anesthetic Gases

1. Are anesthetic gases being used outside the Biologic Resources Laboratory's surgical facility?

☐ Yes

☒ No

Agent:

2. Describe scavenging system (refer to Guidelines on the Use of Inhalation Anesthetics for Laboratory Animals [<http://www.research.uic.edu/protocolreview/acc/policies/index.shtml>])

d. Medical Materials

1. Will expired medical materials such as drugs, fluids, and sutures be used in the protocol activity?

☒ Yes

☐ No

If "Yes", indicate the type of expired material to be used, the type of project it will be used in (acute vs. chronic procedure) and justify the usage (refer to UIC Policy on the Use of Expired Medical Materials [<http://www.research.uic.edu/protocolreview/acc/policies/index.shtml>]).

Expired medical materials will only be used in non-survival, acute surgery. Such materials include, 1) suture and 2) fluids (saline for irrigation/injection, deionized water).

NOTE: No expired antibiotics, analgesics or anesthetic drugs will be used for either survival or non-survival surgeries.

2. Will non-pharmaceutical grade medications such as antibiotics, anesthetics, or analgesics be used in the protocol activity? Answer "YES" if an acceptable veterinary or human pharmaceutical-grade medication is available and not being used and "NO" if all medication is pharmaceutical grade or the medication being administered is a test compound for which there is no pharmaceutical-grade available.

☐ Yes ☒ No

If "Yes", indicate the type of medication and justify usage (refer to UIC Policy on the Use of Non-Pharmaceutical Grade Compounds [<http://www.research.uic.edu/protocolreview/acc/policies/index.shtml>]).

10. Project

- a. Purpose of the research/teaching plan: In layperson's language, describe the overall purpose of the plan in a few sentences.

Our present ability to treat and rehabilitate stroke patients is limited by our inadequate knowledge of the disease process. The proposed experiments are designed to study the electrophysiologic changes in the brain that are associated with cortical stroke. We hypothesize that neurons within the zone of cell death (infarction) and in the surrounding cortex will exhibit demonstrable changes in function as part of the stroke recovery process. Studying the basic electrophysiological mechanisms of neuronal recovery and adaptation following stroke may yield potential therapeutic strategies for acute stroke patients.

- b. Scientific background: Describe the scientific background of the research/teaching plan.

Current advancements in microwire technology allow for the continuous observation of cortical neurons after stroke. The ability to monitor the electrophysiologic response of cortical neurons during and following ischemia will undoubtedly yield constructive information about neuronal plasticity, cortical reorganization and inter-hemispherical communication. Understanding the basic electrophysiologic characteristics of the cortical response to ischemia will elucidate potential therapeutic mechanisms designed to inhibit permanent damage of the cortex and/or accelerate the subsequent healing response. Significant research has described the chemical changes of neurons after stroke such as neurotransmitter and receptor downregulation and the intracellular mechanism by which neurons cease to respond. Several clinical trials have failed to substantiate the therapeutic effectiveness of drugs designed to halt the mechanisms of neuronal damage after stroke. Empirical observation of the electrophysiologic response, however, may offer new strategies to combat ischemic damage such as direct electrical stimulation of the cortex or the development of evidenced-based rehabilitation programs.

We aim to answer two major questions: 1) What is the dynamic electrophysiologic profile of a cortical neuron during and subsequent to prolonged ischemia? and, 2) How do the electrical response properties of peri-infarct neurons change as a result of plasticity during the recovery/rehabilitation process?

We aim to characterize the in vivo electrophysiologic response to acute cerebral infarction. The proposed study will employ novel microelectrode technology developed for chronic cortical prosthetic devices to continuously monitor electrophysiologic activity during and subsequent to prolonged cortical ischemia. Based on previous studies of neuronal plasticity and inter-hemisphere diaschisis after stroke, neurons within the corresponding contralateral region will likely exhibit demonstrable changes in function in addition to those within and surrounding the infarct zone. The time course of electrophysiologic deterioration will ultimately determine the treatment window during which neurons may still be salvaged. Furthermore, understanding the time course of the plastic response will identify the optimal time intervals for intervention and augmentation of the constructive plasticity.

c. Rationale for using animals: What is the rationale for using animals in this protocol? Include an explanation of why alternatives to the use of animals, such as in vitro methods, computer models, or cell culture are not appropriate.

The animal species used exclusively in this research proposal is the Sprague Dawley rat (male). Although human data regarding the dynamic cortical response to ischemic damage may yield a comprehensive, clinically relevant understanding of the stroke process, there are no ethical means by which to obtain preliminary data.. The technology for safely recording from the human brain using multi-channel electrode arrays is not currently available. Due to the similarities between the human and rat cerebral cortex with respect to the internal vascular structure and cellular organization, rats provide a means of consistently reproducing cerebral infarctions and are an excellent substitute. While mathematical models and in vitro cell culture arrays are capable of assessing responses from single neurons in the brain, no models accurately mimic the complex behavior of larger neural networks. Tissue cultures are very crude representations of the highly complex neuronal structure of the brain and do not account for the constant architectural remodeling and plasticity of the cortex. The dynamic response to stroke is dependent upon lateral connections within the ipsilateral cortex and projections to corresponding cortical regions of the contralateral hemisphere. The entire central nervous system, therefore, must remain intact to study the effects of cerebral infarctions and the recovery process. The size and organization of the rat brain provide the ideal substrate for such investigation.

d. Justification of species/strain: What are the scientific reasons for selecting the species/strain for the proposed study?

Sprague-Dawley rats are chosen for several reasons: 1) rats have exquisitely detailed sensory and motor brain areas with many of the same features as found in humans and non-human primates, 2) rats are easy to care for and require minimal housing space, 3) rats have exhibited a consistent tolerance to brain surgery (the animals often recover in 1-2 days), and 4) rats are the least sentient animals with the sufficient dexterity, size and maneuverability to complete the proposed experiments.

10. Project (continued)

e. Study Design: Describe in detail your study design involving the use of experimental animals. Details should include as appropriate, anesthetics/analgesics to be used, procedures to be performed, post-procedural care, duration of experiment including method of euthanasia, study endpoints, etc. It is not necessary to include a detailed surgical description in this section (see Form B, item 6); however, an indication of the procedure in the context of the study design (e.g., type of surgery and when it will occur) should be included in this section. *Attach separate sheet(s) as necessary, but full text of grant applications and/or detailed descriptions of laboratory procedures that do not directly involve a living animal are not appropriate.*

See attached

10. Project (continued)

f. Justification of numbers: Provide a justification for the number of animals (per group and total) to be used in the proposed study. Investigators are **strongly** encouraged to include a table or flow chart if large numbers of animals or multiple groups will be used. If the study involves a breeding colony, then completion of Appendix 1 is sufficient justification of breeders and animals of an inappropriate genotype. In such a case, justify the experimental animals only in this section.

Experimental design goals commonly reflect one of the following four categories. The respective information for justification of the number of animals should be supplied accordingly.

- (1) **Data for statistical analysis:** If numbers are chosen with the intent of obtaining statistically analyzable data, the most objective tool for justification is usually a power analysis to determine sample size. When groups are compared, the goal of conducting a power analysis is to determine the appropriate number of animals per group to ensure a specific chance of detecting a specific difference. The chance, or probability, is the statistical power. For statistical justification using a power analysis, the following information will be expected:
 - a) Statistical test/design used and, if applicable, whether the test is one- or two-sided. Note that one-sided tests are usually not justified.
 - b) Effect size, or equivalent information (e.g., the size of the difference of interest between population means relative to the population standard deviations)
 - c) Alpha level (significance, or "p" value; typically 0.05).
 - d) Power level used in the analysis (typically 60-80%).
 - e) Sample size determined from the power analysis (per group and total per experiment).
 - f) Complete reference to the method used for power analysis (e.g., book, software, etc.).
- (2) **The need to obtain a certain amount of tissue, protein, etc. for in vitro analyses:** The justification of the number of animals must provide a calculation based on the amount of sample (e.g., # cells) obtained per animal, the amount of sample needed for in vitro analyses, and the number and types of in vitro analyses that will be examined.
- (3) **Pilot Studies:** If animal numbers are requested for the purposes of conducting a pilot study, the following information will be expected:
 - a) Main outcome measure being evaluated (e.g., reduction in tumor size)
 - b) The definition of success (e.g., a 50% reduction in tumor size in 3 animals) that would indicate that the study should be followed up by a full study.

*** The pilot study category should not be used to circumvent performing a power analysis where appropriate. If the Committee believes that the number of animals requested for a pilot study may reasonably be sufficient for statistical analysis, a request to supply a power analysis may delay approval of the protocol.*

- (4) **Contact or directed work:** If the number of animals is set by regulations or the funding agency, a statement to that effect and supporting reference is an adequate justification.

Exceptions to these categories must be clearly described. For more information, please refer to the ACC web site under FAQs (<http://www.research.uic.edu/protocolreview/acc/index.shtml>) or the Chapter 3 of the UIC Investigator's Manual (http://www.brl.uic.edu/ANIMAL_USERS_MANUAL/chapter3/ch3.htm) for additional information. *Attach separate sheet(s) as necessary.*

See attached

- g. Personnel and qualifications: Complete Appendix 3 and attach for all protocols.

11. Disposition of Sick or Dead Animals**Sick Animals**

- ☒ Call investigator
☐ Sacrifice
☒ Veterinarian to treat
☐ Other (specify)

Dead Animals

- ☒ Call investigator
☐ Discard
☒ Save, freeze
☐ Necropsy
☐ Refrigerate
☐ Other (specify)

12. Euthanasia*

a. List by species all methods to be used; where appropriate, include dose and route of administration. ** If any methods other than those classified as Acceptable are to be used, Question 12b must also be completed. For a detailed explanation, refer to item VIII, C of the UIC Animal Care Policy (<http://www.research.uic.edu/protocolreview/acc/policies/index.shtml>).*

Animals will be prematurely euthanized under the following circumstances:

- 1) If animals do not begin a return to the normal state within 7 days following survival surgery (1-2 days of recovery time is considered normal)
- 2) If the acrylic/connector mound becomes dislodged (rare occurrence) or if the animals show obvious physical stress in response to the implant (e.g. excessive blood or pus discharge from the wound site, excessive scratching and/or physical manipulation of the implant area)
- 3) If the animals is several affected by the stroke (i.e. unable to ambulate, reach food or water)

Assuming no complications compromise the surgery (see above), the animals will be sacrificed when the full complement of electrophysiological testing is complete or the implanted electrodes fail to produce satisfactory signals. The length of the post-infarction electrophysiological testing is primarily limited by the viability of the electrode implant. To describe long-term changes after stroke, recordings from chronic implant animals will be made for as long as the implant is functional. If the brain signals no longer indicate that reorganization is occurring (i.e. the PSTHs stabilize), the experiment will be terminated and the animal will be sacrificed. The time period for post-infarction recordings is dependent upon the time scale for plasticity which currently is unknown.

The primary euthanasia agent will be sodium pentobarbital. We request permission to use injection of sodium pentobarbital as the euthanasia agent for sacrifice in the PI's laboratory (it is not possible to accurately estimate the exact number of animals to be euthanized using this method) for all animals that undergo acute procedures. A lethal dose of sodium pentobarbital (1-2 ml, NEMBUTAL 50mg/ml) will be administered via IV, IP or direct cardiac puncture only to animals under heavy anesthesia. Animals will only be heavily anesthetized for direct cardiac administration of sodium pentobarbital. The CO2 method of euthanasia will be performed using the dedicated equipment located at the BRL for animals that need to be immediately sacrificed for any of the above outlined reasons. Both euthanasia agents are listed as acceptable agents in the AVMA (American Veterinary Medical Association) report on euthanasia and the 'Euthanasia Policy' of the Animal Care Committee at University of Illinois at Chicago,

Any animals scheduled for histological examination of implanted brain tissue will be perfused through the heart with saline followed by formaldehyde fixative. Prior to perfusion the animal will be heavily anesthetized using a double bolus injection of the normal 10:1 Ketamine (50 mg) / Xylazine (5 mg) (0.2 ml/100 gr body weight).

b. Describe and justify the method of euthanasia if it is not classified as acceptable by the American Veterinary Medical Association. (Note: Cervical dislocation without sedation requires scientific justification).

13. Describe and justify the disposition of animals other than by euthanasia, include the use of animals in additional experimental studies.

We request permission to perform acute, non-survival surgery on animals that have already been instrumented with a chronic brain implant.

Justification: The non-survival surgery presents us with several advantages that will optimize the use of each animals and ultimately decrease the total number of animals needed to produce sufficient data. Currently, the animals are sacrificed after the implanted cortical electrode fails. The data yield per animal can be doubled by performing one final acute electrode implant/infarction on the remaining undisturbed hemisphere. Although the final non-survival procedure is technically a second surgery, the animals will be sacrificed immediately following the acute surgery. Additionally, survival surgeries also allow further surgical training of new personnel.

14. Potential for Pain or Distress

a. Would the procedures described in this protocol and/or their consequences potentially produce more than slight or momentary pain or distress if performed in an unanesthetized animal? (See the definition of potential pain and distress in the UIC Animal Use Protocol Instructions- <http://www.research.uic.edu/protocolreview/acc/policies/index.shtml>).

☒ Yes ☐ No

b. If there is a potential for pain or distress, will anesthetics, analgesics, or tranquilizers be used?

☒ Yes ☐ No

c. Surgery

☒ Yes ☐ No

If "Yes" is checked in any part of item 14, then item 15 and Form B MUST be completed before starting this project. For procedures and/or their consequences that only produce slight or momentary pain or distress, complete Form B, item 3.

15. Justification of Potentially Painful/Distressful Procedures and Alternative Search

a. LIST ALL the potentially painful/distressful procedure(s) described under A10e and PROVIDE A JUSTIFICATION for their use.

(a) Surgical electrode implant.

Justification: The described experiments using electrode implants in sensory and motor cortex of rats have no alternative techniques available. The complexity of the mammalian nervous system often precludes the use of computer models. While mathematical models are helpful in assessing responses from single neurons in the brain, there are currently no available models for larger neural networks. Tissue cultures are very crude representations of the highly complex neuronal structure in the brain. Furthermore, neither mathematical models nor tissue cultures are able to mimic neuronal processes during sensation and thus are not applicable to these experiments. The best way to study sensory-motor responses and pathways in the brain and periphery is to perform the experiments in an awake, behaving animal model. Rats are the least sentient animals capable of performing complex behavioral tasks and rats have proved to be very robust animals. The PI has currently implanted more than 100 rats - the complications are few and most rats recover within 24-48 hours. Medline was consulted for possible alternatives to electrode implantation and to avoid duplicating previous work. The results are presented in the table below. Please note that the search terms have been limited to the 'title/abstract' category to ensure that only the most relevant papers are listed.

(b) Cerebral Infarction

Justification: Since the aim of the study is to characterize cortical changes after stroke, the cerebral infarction is obviously necessary. The locations of cerebral infarction are chosen to minimize functional loss after surgery.

b. Provide a Literature Search supporting that appropriate alternatives such as less sentient animal models, computer models, tissue cultures, and/or refinement of techniques were not available to the project. Refer to the definition of alternative techniques in the UIC Animal Use Protocol Instructions.

Database Used	Search Terms	Date of Search	Period of Years of Search	Number of Relevant References	Were alternatives found?
Medline (a)	rat, electrode, cortex	11/16/2004	1975-2004	275	No
Medline (b)	photothrombosis	11/29/2004	1970 -	88	No
Medline (c)	stroke, plasticity, electrode, cortex	11/29/2004	1970 -	6	No

c. If alternatives were found, justify why they are not being used. Additional relevant sources that may be supportive of your effort are scientific meetings, scientific discussions, consultation with veterinary staff, and federal law or other legal guidelines.

Assurances

1. *The Principal Investigator assures that the personnel listed in Appendix 3 have the appropriate experience and/or training to conduct the procedure(s) described in this protocol or will receive appropriate training prior to initiation of the project. The addition of new personnel to this protocol requires that a modification be submitted to OPRS listing the individual(s) and their respective experience/training prior to initiation of work with animals.*

Principal Investigator/Responsible Faculty Member*

Date

2. *This project does not unnecessarily duplicate previous experiments and will be performed in conformance with the UIC Animal Care and Use Policies.*

Principal Investigator/Responsible Faculty Member*

Date

3. *The Principal Investigator is responsible for informing all personnel listed in Appendix 3 of the institution's Occupational Health Program for Personnel Caring For or Using Laboratory Animals prior to initiation of the project. The Principal Investigator is also responsible for making sure that each person listed in Appendix 3 is included in the program in a manner consistent with their category of animal contact. A copy of the program will be sent to each Principal Investigator with their letter of approval and with each addition of personnel.*

Principal Investigator/Responsible Faculty Member*

Date

4. *The Principal Investigator assures that this protocol describes all animal models and all animal procedures that are proposed in the funding sources listed in Form A, item 6 and Appendix 4. The addition of a new funding source requires that a modification be submitted to OPRS adding the funding source(s) to the protocol and requires completion of Appendix 4 prior to the acceptance of award from new funding source.*

Principal Investigator/Responsible Faculty Member*

Date

Are you a UIC faculty member? ☐ Yes ☐ No

**If the PI for this protocol is not a member of the UIC faculty, a responsible faculty member must be listed as co-investigator in Form A, item 3, and sign Assurances 1, 2, 3, and 4, in addition to PI.*

Department Head Signature

As department head, I acknowledge that this research and/or teaching protocol is consistent with the standards set by our department.

Signature of Department Head

Date

Printed Name of Department Head

The UIC Animal Users Manual is available at http://www.brl.uic.edu/ANIMAL_USERS_MANUAL/index.html.

The UIC ACC Policies and Guidelines are available at <http://www.research.uic.edu/protocolreview/acc/policies/index.shtml>

Devang Gandhi

PROFESSIONAL PROFILE

- ❖ Experienced researcher who has submitted scientific publications, and has given presentations in academic preceedings
- ❖ Expertise in Matlab having to develop several neural simulation and signal/image analysis tools with GUI interfaces
- ❖ Designed and implemented threshold detection algorithms for neural signal analysis, and MRI image analysis to reconstruct 3D activation map.
- ❖ Skilled in Autocad 14, Pspice, Ansys, and proficient knowledge of Scripting Languages – Java Scripting, Expect scripting and CGI/perl scripting for developing web based interfaces.

EDUCATION

- ❖ **PhD Bioengineering**
University of Illinois, Chicago, IL
Concentration: Neural Engineering
Thesis: “Microfabrication and assessment of Polyimide based neural-interface array”
- ❖ **B.S. Electrical Engineering**
Purdue University, West Lafayette, IN
Concentration: Biomedical Engineering

PROFESIONAL EXPERIENCE

Research Engineer, SmartSignal Corporation, Lisle, IL

- ❖ Research and development in Artificial Intelligence: Prognostics

Graduate Research Assistant, Neural Engineering Applications Laboratory, Chicago, IL

- ❖ Design, Development and Investigation of implantation technique, as well as material and function properties of the Polyimide neural interface in a rat animal model.
- ❖ Cad based design of multi-layer microstructures for neural-interface array
- ❖ Ansys based 2D and 3D simulations of process in development protocol as well as stress analysis of insertion application to understand and enhance the array design
- ❖ Microfabrication using polymer micro-fabrication technology in a class 100 cleanroom

Teaching Assistant, Department of Bioengineering (UIC), Chicago, IL

- ❖ Several courses ranging from Freshmen level to graduate level
- ❖ Developed and implemented a Lab module for Biosensing lab and a Neural Engineering Research Training tool in Matlab for Graduate level Neural Coding coursework.
- ❖ Developed and implemented a freshmen level Matlab course.

Lead Engineer, Motorola Corporation, Arlington Heights, IL

- ❖ Developed Java based script to Decode and Analyze RADIUS messaging
- ❖ Implemented Java based and C/C++ based Algorithm for data analysis and Input mapping
- ❖ Assist in developing Feature Requirement Documentation.
- ❖ Resolving product defects by working with vendors.

EXTRACULLICULAR ACTIVITIES AND HONORS

Teaching Assistant of the Year Award, University of Illinois at Chicago (UIC), Chicago, IL

- ❖ Awarded annually to a teaching assistant that shows extraordinary ability in classroom activities

Ambassador Leadership Award, Purdue University, Lafayette, IN

- ❖ Awarded annually to a representative of dormitory student body.

National Honors Society, Hoffman Estates High School, Hoffman Estates, IL

- ❖ Was invited to join the national competitive organization that represents high scholastic achievement

Robotics Award, Chicago BEST robotics, Chicago, IL

- ❖ Secured 3rd place as team leader of a robotics group

Member, Society of Hispanic Professional Engineers, West Lafayette, IN

Member, Biomedical Engineering Society, West Lafayette, IN

PUBLICATIONS AND PRESENTATIONS

- ❖ **PowerPoint Presentation: D. Gandhi**, T. Valyi-Nagy, and P.J. Rousche, "Histological Assessment of Immuno-Compatibility of Polyimide Based Implantable Microelectrode Arrays," BMES 2007.
- ❖ **Journal Publication: R. Das, D. Gandhi**, S. Krishnan, L. Saggere, and P.J. Rousche, "A Benchtop System to Assess Cortical Neural Interface Micromechanics," IEEE Trans. On Biomed. Eng., v45(6), pp. 1089-1096, June 2007.
- ❖ **Poster Presentation: D. Gandhi**, R. Das, and P.J. Rousche, "PGA Coated, Enhanced Polyimide-Based Microelectrode Arrays for Cortical Stimulation and Recording," BMES 2006.
- ❖ **PowerPoint Presentation: D. Gandhi**, R. Das, S. Krishnan, L. Saggere, and P.J. Rousche, "Functionality Evaluation of Photo-definable Polyimide, Flexible Interface for the Central Nervous System," 1st IEEE/RAS-EMBS International Conference on BioRob., pp.455-460, Feb. 2006.
- ❖ **Poster Presentation: D. Gandhi**, R. Das, and P.J. Rousche, "New Photodefinable, Polyimide-Based Microelectrode Arrays for Cortical Stimulation and Recording," BMES 2005.
- ❖ **Poster Presentation: L. Satish, D. Gandhi**, R. Das, and P.J. Rousche, "Analysis of In-Vitro Neurite Extension for Neurotrophic Electrode Design," 2nd International IEEE EMBS Conference on Neural Engineering, Conference Proceedings, pp. 385-387, March 2005.
- ❖ **NSF-REU Program (UIC): K. L. Harrigan, A. Chowdhury, D. Gandhi**, R. Das, and P.J. Rousche, "Electrochemical Characterization of Microelectrodes for use in Cortical Tissue," 2005
- ❖ **NSF-REU Program (UIC): A. Chowdhury, K. L. Harrigan, D. Gandhi**, R. Das, and P.J. Rousche, "Mechanical Characterization of Microelectrodes: Used for Auditory Cortical Prosthesis," 2005
- ❖ **Poster Presentation: L. Satish, D. Gandhi**, and P.J. Rousche, "Preliminary Study of Neurite Outgrowth Within Polyimide Microtubes," 26th Annual International Conference of the IEEE on Engineering in Medicine and Biology Society, IEMBS, v6, pp. 4306-4309, Sept. 2004.